Thermal Fields during Welding and their Analogues

by

James P. Carrick

CONTAINS

PULLOUTS

Acknowledgements

This work was originally sponsored by the Science Research Council and subsequently by the University Court of the University of Glasgow. For their support and for the facilities provided by the University, I am very grateful.

I shall always be indebted to Professor J.D. Robson and to Dr. D.F. McNamee for their attention and guidance throughout the project. For the technical services and facilities, I am grateful to Mr. I.D. Cameron and, for the long hours of effort on my behalf, to Mr. C. Mathieson and Mr. J. Barrowman on whose skill and experience I depended for the construction of the test rig and equipment. I am very grateful also to Mr. R. Fletcher for his expert assistance and invaluable advice in the preparation of the plates contained in the text and to Misses E. Miller and A. MacLeod for undertaking and completing so skilfully, the typing of the text.

There are many to whom I am indebted and to whom I must apologise for omitting from this brief statement but I must finally mention the sacrifices made and encouragement given by my wife, Allison. I cannot express sufficiently my gratitude to her.

SUMMARY

To avoid the problems associated with specifying the exact nature of the heat input from welding arcs, an analogue model is proposed which simulates the quasi-static thermal field produced around the isothermal contour of the molten weld pool boundary during the welding of thin plate. The design of an electrical analogue based directly on Rosenthal's equation (1) governing the quasi-static heat flow about a moving source is shown to be impractical although this approach identifies the physical significance of the two parameter ratios $\frac{v}{\alpha}$ and $\frac{q}{k}$.

To overcome the difficulties associated with the direct analogue, a simple transformation of Rosenthal's equation is employed and the design of an indirect or ϕ field analogue of this transformed equation is developed. The details of the construction and commissioning of such an analogue are reported.

The application of this analogue to studying the quasi-static thermal field is tested by comparing analogue predicted and experimentally measured temperature histories of points in the HAZ for a range of autogenous TIG melt runs on thin mild steel plate. The experimental results are obtained from a purpose built automatic welding rig which incorporates a facility for determining the shape of the molten weld pool during welding.

The results from these comparative tests show a good agreement between predicted and measured temperature histories and the application of the ϕ field analogue to studying the thermal field during welding is discussed.

CONTENTS

Conclusion / over

CHAPTER I

INTRODUCTION

In an attempt to gain a more fundamental understanding of the welding process and of its effect on the parent metal, a considerable effort has been devoted to studying the thermal field in the parent metal during welding. The temperature distribution in the welded material is one intensive property of the system which can be measured and hence studied. It is this change in temperature which is a primary cause of the micro-structural changes which can occur in the welded joint. Since the temperature effect is greatest in the region closest to the weld itself, i.e. the heat affected zone (HAZ), and can give rise to severe problems of hardening and subsequent failure particularly in the welding of high strength steels, it is of considerable practical importance to be able to predict temperature histories in the HAZ during welding.

This study concerns itself particularly with the thermal field in the HAZ during welding and the techniques which are available for predicting and studying this field.

1.1) Fundamental Considerations and Background

To study the heat flow during welding, it is necessary to consider the transfer of energy from a highly localised moving source, e.g. an electric arc, to the parent material and the subsequent diffusion of this energy through the material. The first significant attempt to model this process was made by

Rosenthal (1)* in a new classic paper. In this model, the energy source is considered to be concentrated in a point in three dimensional (3-D) cases or a line in two dimensional (2-D) cases. The resulting temperature distribution in the parent material is then given by the solution to Fourier's equation of heat conduction in an isotropic medium with constant properties. This has the form

$$\nabla^2 T = \frac{1}{\alpha} \cdot \frac{\partial T}{\partial t} \qquad (1.1)$$

where α is the thermal diffusivity of the parent material (assumed constant).

It is, however, an observable fact that, provided the welding conditions and geometry remain constant, the temperature field relative to the moving source quickly becomes constant after the start of a weld. To account for this "quasi-stationary" effect, Rosenthal defined new co-ordinates with the origin at the source and then considered that, with respect to these co-ordinates, $\frac{\partial T}{\partial t} = 0$. If the welding speed is v in the x-direction (see Fig. 1.1), Fourier's equation, with this co-ordinate transformation and setting $\frac{\partial T}{\partial t} = 0$, becomes

$$\nabla^2 T + \frac{v}{\alpha} \cdot \frac{\partial T}{\partial x} = 0 \qquad (1.2)$$

In this work, this equation will be referred to as "Rosenthal's equation" and any potential field distribution governed by this equation will be termed a "Rosenthal field".

* Numbers in parenthesis refer to the list of references

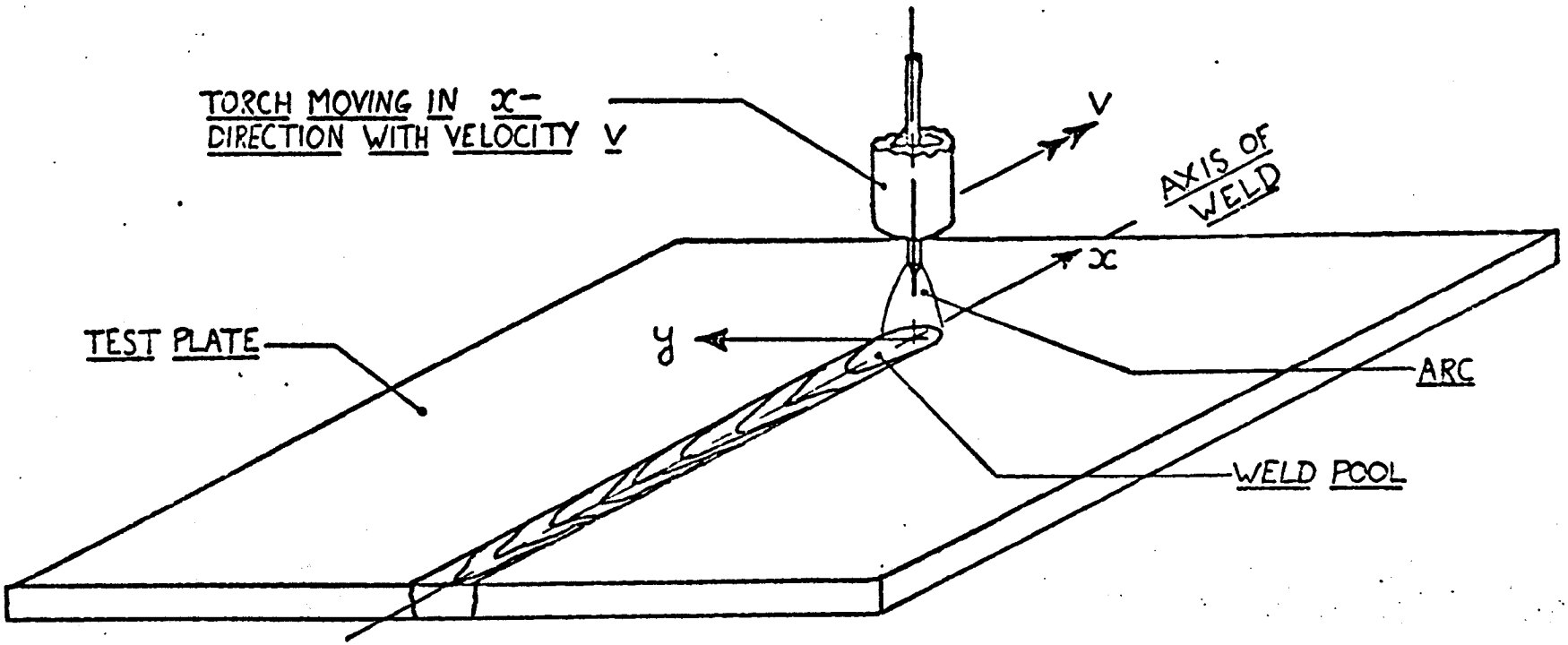

FIG 1·1 THE ROSENTHAL CO-ORDINATE SYSTEM

Using the point source model, Rosenthal produced analytical solutions of equation 1.2 for various geometries. A useful simplification for the 2-D case of a single pass butt weld on thin plate was made by Wells (2) who related the maximum width of any isotherm to the welding heat input. Such analysis based on Rosenthal's point source model was subsequently referred to in the literature as the "Rosenthal-Wells Theory". In a very useful paper, Myers et al (3) compared the experimental results of a number of researchers, notably Christensen et al (4), with the Rosenthal-Wells Theory. Briefly, their findings were that the theory gave reasonable agreement at points beyond the HAZ and at low to medium welding speeds. For points close to the molten zone and at high welding speeds the theory proved to be inadequate. The HAZ is, of course, the zone in which it is most necessary to have an accurate knowledge of the thermal field. The reasons for these discrepancies are to be found in the basic assumptions of the Rosenthal-Wells Theory.

In his model of welding, Rosenthal made the following assumptions:

i) the energy source is concentrated in a point (or line) and there are no other sources

ii) the parent material experiences no change of phase and its thermal properties (i.e. thermal conductivity, specific heat and density) remain constant with temperature.

iii) quasi-static conditions exist i.e. the temperature distribution with respect to the source remains constant.

iv) /over

iv) the conducting medium is infinitely large.

However, as has been suggested (3) the justification for these assumptions is not that they are representative of actual welding conditions but that they make it possible to find analytical solutions for the equations. In fact, the major deficiences in the model are contained in the first two assumptions. In practice, welding arcs are somewhat diffuse and although the physics of the arc is not completely understood, experimental evidence (5,6) suggests that the heat input to the workpiece in many arc processes passes through an area approximately the same as the surface area of the molten pool. While, as Wells (2) correctly says, "the remote temperature distribution may be independent of the purely local distribution of the source", the temperature distribution in the HAZ will certainly depend on the diffuse nature of the source.

Furthermore, since the energy transferred by the arc to the workpiece cannot be measured directly, nor is it simply related to the arc voltage and current, an estimate of "arc efficiency" has to be made. It has been the accepted practice to define this efficiency as the ratio of the heat input to the weld to the "available energy" at the electrode i.e. the volt-amps supplied to the electrode. To obtain estimates of the heat input to the weld; various calorimetric techniques have been used (4,5,7). Unfortunately, not only does the arc efficiency thus defined vary for different welding processes as may be expected, it is also a function of other welding variables e.g. arc height, welding speed, properties of the parent material etc. which are determined for a particular weld, not just the type of weld.

The behaviour of the arc is also dependent on the diffusion of parent metal ions from the molten pool into the arc stream (6). This diffusion is obviously dependent upon the surface temperature of the molten pool. The calorimetric techniques typically require the continuous cooling of the parent metal which inevitably reduces the molten pool temperature if, indeed, any melting takes place at all. Thus, arc efficiencies estimated using such methods are not representative of arcs found in actual welding practice.

By definition, the welding process also involves the melting and re-solidification of the parent material. The Rosenthal-Wells Theory takes no account of this and it is, therefore, not surprising that the shape of the melting point isotherm predicted by theory bears little relation to molten pool shapes experienced in practice (5,8,9). Indeed, there is some experimental evidence (10,11) that indicates that the factors affecting pool shape are equally as complex as those influencing arc heat transfer.

1.2) The Pool-Shape Model

Recognising these complexities, Apps and Milner (9) suggested that a more successful approach to predicting the thermal field, particularly in the HAZ, may be made if the energy source were considered to be the molten pool itself. There are very significant advantages in adopting this approach. If it is assumed that all the energy transferred from the arc passes into the molten pool, then the thermal field in the surrounding material must be governed by the conduction of heat through the pool boundary into the surrounding solid material. Therefore, the necessity for accounting for both the heat transfer from the arc and the interactions in the molten pool would be removed. Furthermore, as the

shape of molten pool can be determined experimentally (5.9) and as the molten/solid interface at the pool boundary is at the melting point of the material, the pool boundary provides a mathematically definable boundary condition.

This approach was not further pursued until Tanbakuchi (12) produced finite difference solutions of Rosenthal's equation, modified to account for the variation in thermal properties with temperature, with the pool boundary as a defined boundary condition. Tanbakuchi achieved considerable success with this approach in that he was able to predict temperature in the HAZ for thin plate much more accurately than had been previously possible using Rosenthal-Wells Theory. (This refernece also includes an excellent survey of the related literature up to 1967).

Since the dependence of the pool shape on the welding parameters is not completely understood, it is not possible to non-dimensionalise the pool shapes and the associated thermal fields for a broad spectrum of welding conditions as was possible with Rosenthal's point source model. Using the pool shape as the basis for the heat flow analysis therefore requires that the analysis be repeated for each pool shape considered. This necessity to repeat the analysis for each pool shape does not, of course, invalidate the pool shape model or the numerical analysis but it does make any such heat flow investigation expensive especially as the numerical analysis requires a large memory storage digital computer.

To overcome this drawback and to enable the advantages of the pool shape model to be more readily exploited, it was felt that there might be a significant advantage in adopting an analogue rather than

digital approach to the analysis. In studying, for example, the thermal fields associated with a large number of welds, it was felt that any significant trends could be identified more readily and at less cost using an analogue approach and that specific cases could then be identified for a more detailed numerical analysis. In this way, the pool shape model could be more generally applied and its inherent advantages fully exploited. By its nature, an analogue approach might also be expected to promote a greater physical understanding of the processes involved in the heat flow during welding.

The first attempt to employ analogue techniques to the study of welding heat flow was made in 1973 by Boughton (13), working at the British Welding Institute. To study the relation between weld penetration and arc heat input, Boughton constructed a simple electrical network analogue of Fourier's equation. This was used to predict the transient thermal processes occurring at the fusion front of the weld pool, particularly at the start of a weld before quasi-static conditions were reached. In this way, Boughton was able to predict the heat input required to ensure uniform penetration at the start of a weld. This was a remarkable result considering the simplicity of his model. Unfortunately, he was still unable to relate overall pool geometry to the welding parameters and, consequently, it was not possible using his analogue to study, in any detail, the thermal field in the HAZ, even assuming quasi-static conditions.

However, employing the pool shape model does, as already stated, circumvent the problem of predicting pool geometry. Furthermore, for quasi-static conditions, only a steady state analogue of Rosenthal's equation would be required. Analogue techniques for studying heat flow

problems are already well established (14, 15). While these techniques generally relate to Laplacian fields i.e. fields whose governing equation is given by

$$\nabla^2 T = 0 \qquad (1.3)$$

it was felt intuitively that, as the quasi-static Rosenthal field is really only a particular case of Laplace's equation, it would be possible to modify one of these techniques of Laplacian fields to permit the analysis of Rosenthal fields and, hence, the analysis of thermal fields during welding.

It was, therefore, decided to initiate a project to study the viability of this alternative approach and, in particular, to

a) investigate the fundamental characteristics of Rosenthal fields and how these relate to similar Laplacian fields.

b) design and construct a 2-D analogue on which the curvilinear shape of 2-D weld pools could be imposed as a boundary condition and which would predict the thermal field in the surrounding material.

c) design and construct a welding facility to provide experimental data on pool shapes and associated temperature histories in the HAZ in order that a comparison might be made with analogue predicted temperatur histories.

These three objectives and the conclusions drawn as a result of their implementation comprise the subject matter of the following chapters.

CHAPTER 2

PROPERTIES OF ROSENTHAL FIELDS

It is of interest to study the nature of the solutions to similar problems governed respectively by the equations of Rosenthal and Fourier. The mathematics of Fourier's equation is, of course, extremely well documented and techniques for its solution readily available. Should it be possible to relate the solutions of Rosenthal problems to those of similar Fourier problems, then it would certainly be possible to relate the solutions of quasi-static Rosenthal field problems to the solutions of corresponding Laplacian field problems (i.e. steady-state Fourier). The most appropriate technique available for the solution of Laplacian field problems could then be applied to the welding heat flow problem which is basically governed by the quasi-static Rosenthal equation 1.2.

However, since this discussion is intended to be general in nature, the quasi-static condition will not be enforced i.e. although it does not relate specifically to the welding problem, the time dependent form of Rosenthal's equation

$$\nabla^2 T + \frac{v}{\alpha} \cdot \frac{\partial T}{\partial x} = \frac{1}{\alpha} \cdot \frac{\partial T}{\partial t} \qquad (2.1)$$

will be considered as more general comparisons can then be made with Fourier's equation

$$\nabla^2 T = \frac{1}{\alpha} \cdot \frac{\partial T}{\partial t} \qquad (2.2)$$

For simplicity, the general solutions to linear boundary value problems will be obtained for the 1-D forms of equations 2.1 and 2.2.

2.1) The 1-D Solutions

The 1-D form of equation 2.1 is simply

$$\frac{\partial^2 T}{\partial x^2} + \frac{v}{\alpha} \cdot \frac{\partial T}{\partial x} = \frac{1}{\alpha} \cdot \frac{\partial T}{\partial t} \qquad (2.3)$$

This is a linear partial differential equation and provided any boundary conditions are also linear, a general solution of equation 2.3 may be sought by separating the variables.

Assume that $T(x,t)$ may be written as

$$T(x,t) = X(x).\Omega(t) \qquad (2.4)$$

Substituting for $T(x,t)$ in equation 2.3 and re-arranging gives

$$\frac{1}{X(x)}\left[\frac{\partial^2 X}{\partial x^2} + \frac{v}{\alpha} \cdot \frac{\partial X}{\partial x}\right] = \frac{1}{\alpha\Omega(t)} \cdot \frac{\partial \Omega}{\partial t}$$
$$= -\lambda^2$$

where λ is the separation constant.

This gives the separated equations

$$\frac{\partial^2 X}{\partial x^2} + \frac{v}{\alpha} \cdot \frac{\partial X}{\partial x} + \lambda^2 X(x) = 0 \qquad (2.5)$$

and

$$\frac{\partial \Omega}{\partial t} + \alpha\lambda^2 \Omega(t) = 0 \qquad (2.6)$$

The solutions of equation 2.5 define the eigenvectors of the system and the values of λ, definable when particular boundary conditions are known, are the corresponding eigenvalues. The solutions of equation 2.5 are of the form

$$X(x) = e^{-\frac{v}{2\alpha}.x}\left[A\cos\gamma x + B\sin\gamma x\right] \qquad (2.7)$$

where A and B are undetermined constants and λ is related to γ by

$$\lambda^2 = \gamma^2 + \left(\frac{v}{2\alpha}\right)^2 \qquad (2.8)$$

Since there are an infinite number of constants which can be used in equation 2.7 and for it still to be a solution of equation 2.5, the sum of all such solutions is also a solution. The general solution may, therefore, be written as

$$X(x) = e^{\frac{-v}{2\alpha}.x} \sum_{n=o}^{\infty} (A_n \cos \gamma_n x + B_n \sin \gamma_n x) \qquad (2.9)$$

The corresponding solution to equation 2.6 is given by

$$\Omega(t) = \sum_{n=o}^{\infty} \Omega_n e^{-\alpha \lambda_n^2 t}$$

$$= \sum_{n=o}^{\alpha} \Omega_n e^{-\alpha\left[\left(\frac{v}{2\alpha}\right)^2 + \gamma_n^2\right] t} \qquad (2.10)$$

where Ω_n are constants determined by the initial conditions.

Combining equations 2.9 and 2.10 with equation 2.4 gives the general solution

$$T(x,t) = e^{\frac{-v}{2\alpha}.x} \cdot \sum_{n=o}^{\infty} (A_n \cos \gamma_n x + B_n \sin \gamma_n x)\Omega_n . e^{-\left[\frac{v}{2\alpha}^2 + \gamma_n^2\right].t}$$

$$= e^{-(\frac{v}{2\alpha})(x + \frac{v}{2}.t)} \cdot \sum_{n=o}^{\infty} (A_n' \cos \gamma_n x + B_n' \sin \gamma_n x).e^{-\alpha \gamma_n^2 t} \qquad (2.11)$$

It should be appreciated that the constants A_n' and B_n' are dependent on both the initial and boundary conditions but the coefficient γ_n is dependent solely upon the boundary conditions.

In a similar way, consider the 1-D form of Fourier's equation

$$\frac{\partial^2 T}{\partial x^2} = \frac{1}{\alpha} \cdot \frac{\partial T}{\partial t} \qquad (2.12)$$

Again, separating the variables by writing

$$T(x,t) = X(x).\Omega(t) \qquad (2.13)$$

and substituting in equation 2.12 yields, the separated equations

$$\frac{\partial^2 X}{\partial x^2} + \gamma^2 X(x) = 0 \qquad (2.14)$$

and

$$\frac{\partial \Omega}{\partial t} + \alpha\gamma^2 \Omega(t) = 0 \qquad (2.15)$$

where γ is the separation constant. The eigenvectors of this system are then given by the general solution of equation 2.14.

i.e. $$X(x) = \sum_{n=0}^{\infty} (A_n \cos \gamma_n x + B_n \sin \gamma_n x) \qquad (2.16)$$

where A_n and B_n are undetermined constants and the values of γ_n are eigenvalues.

The solution of equation 2.15 is again given by

$$\Omega(t) = \sum_{n=0}^{\infty} \Omega_n e^{-\alpha \gamma_n^2 t} \qquad (2.17)$$

where Ω_n are constants determined by the initial conditions.

Combining equations 2.16 and 2.17 and substituting in equation 2.13 yields the general solution of the Fourier system

$$T(x,t) = \sum_{n=0}^{\infty} (A_n' \cos \gamma_n x + B_n' \sin \gamma_n x) e^{-\alpha \gamma_n^2 t} \qquad (2.18)$$

2.2) A Discussion on Modal Characteristics

A comparison can now be made with the solution for the corresponding Rosenthal system given by equation 2.11. Provided the same initial and boundary conditions apply to both systems, the following points can be noted.

i) There is a simple relationshop between the eigenvectors of the two systems. If the eigenvector of the Fourier system is given by $V_n(x)$, then the corresponding eigenvector of the Rosenthal system $R_n(x)$ is given by

$$R_n(x) = e^{-\frac{v}{2\alpha}\cdot x} \cdot V_n(x) \qquad (2.19)$$

(c.f. equations 2.9 and 2.16).

This relationship is generally true irrespective of the particular eigenvector (value of n) considered.

ii) A corresponding relationship exists between the eigenvalues of the two systems. If the eigenvalue of the Fourier system is given by γ_n, then the corresponding eigenvalue of the Rosenthal system λ_n is given by

$$\lambda_n^2 = \left(\frac{v}{2\alpha}\right)^2 + (\gamma_n)^2 \qquad (2.20)$$

This relationship is also generally true irrespective of the particular eigenvalue (value of n) considered.

iii) Although the eigenvalues of the two systems are related but different, the trigonometric coefficients γ_n appearing in both solutions are identical provided the same boundary conditions apply to both systems. It must be emphasised that, in itself, γ_n is an eigenvalue only of the Fourier system.

iv) Although it would appear that there is a simple relationship between the two solutions (equations 2.11 and 2.18), this will not, in general, be true. For the same boundary and initial conditions, the values of the constants A_n' and B_n' will be different in the two solutions. Both these solutions are mathematical expressions of the fact that, at any time, the potential distribution T(x,t) is a linear combination of the eigenvectors. Since the eigenvectors of the two systems are different, their combination (defined by A_n' and B_n') to describe one potential distribution (e.g. the initial condition) must also be different. It is worth noting, however, that a relationship between the values of A_n' and B_n' for the two systems will exist but that it will be dependent upon the relationship between the eigenvalues (and hence on n).

v) While the above discussion has been restricted to a 1-D analysis, these conclusions would apply equally to 2 and 3-D systems.

It would, therefore, seem that, while a relationship does exist between potential distributions governed by Rosenthal's and Fourier's equation, this relationship is not simple i.e. there does not appear to be any single factor or transformation which can be applied to a solution of Fourier's equation in order to change it into a solution of Rosenthal's equation for the same boundary conditions.

However, it is very significant that the eigenvectors and eigenvalues of the two systems are simple related. These modal characteristics are the fundamental units of which a complete solution is constructed. Although this discussion included, for

generality, time dependence, the solutions to steady state problems are, in general, a combination of the same eigenvectors in a similar way. Now, it is obvious that the eigenvalues of a particular system are dependent upon the basic governing equation and the boundary conditions. If, in some way, the basic governing equation was changed while keeping the boundary conditions constant, then the eigenvalues of the system would also be changed accordingly. For example, equation 2.12 defines Fourier's equation in a 1-D, isotropic, homogeneous medium. If the conductivity were allowed to vary within the medium (i.e. non-homogeneous), the governing equation would become

$$\frac{\partial}{\partial x}\left[k(x).\frac{\partial T}{\partial x}\right] = \rho c.\frac{\partial T}{\partial t} \qquad (2.21)$$

where $k(x)$ is the conductivity of the medium, ρ its density and c its specific heat, and the eigenvalues of this system would no longer be defined by equation 2.16. The precise nature of the eigenvalues would, of course, depend upon $k(x)$.

Since there is such a simple relationship between the eigenvalues of the Rosenthal and Fourier systems, it is possible that a particular $k(x)$ exists which would give equation 2.21 the same form as Rosenthal's equation. The variable conductivity Fourier system would then be a direct analogue of the Rosenthal system. Such a $k(x)$ does exist and the application of this analogue principle to the welding problem is discussed in the next chapter.

Footnote

The preceding discussion raises another question of some interest in

that it is not clearly understood how the eigenvectors of an originally uniform system are affected when one of the properties (e.g. conductivity) of that system is allowed to vary. This was also investigated by the author in relation to the longitudinal vibrations of some variable cross-section beams and is reported in Appendix 1.

CHAPTER 3

DIRECT ANALOGUES

3.1) The Analogue Principle

The equation governing the time dependent potential distribution in an isotropic but non-homogeneous conducting medium can more generally be written as

$$\text{div } k.\ \text{grad } T \quad = \quad \rho c.\ \frac{\partial T}{\partial t} \tag{3.1}$$

where ρ and c are not necessarily constant. If the conductivity k is a function of x alone, the above equation in Cartesian co-ordinates reduces to

$$\nabla^2 T + \frac{1}{k}.\frac{\partial k}{\partial x}.\frac{\partial T}{\partial x} \quad = \quad \frac{1}{\alpha}.\frac{\partial T}{\partial t} \tag{3.2}$$

where $\alpha = \frac{k}{\rho c}$

Comparing this equation with the general form of Rosenthal's equation (equation 2.1) shows that the two equations have the same form if and only if

$$\frac{1}{k}.\frac{\partial k}{\partial x} \quad = \quad \frac{v}{\alpha} \tag{3.3}$$

and provided α in equation 3.2 is constant. The solution to equation 3.3 is simply

$$k \quad = \quad k_o e^{\frac{v.x}{\alpha}} \tag{3.4}$$

where k_o is an arbitrary constant.

Thus, the effect of moving axes in a homogeneous medium on the form of the basic governing equation (i.e. Rosenthal's co-ordinate

transformation of Fourier's equation) is exactly equivalent to the effect of an exponential variation in conductivity defined by equation 3.4.

It should be noted that this equivalence is only complete if α in equation 3.2 is constant i.e. $\rho c = e^{+\frac{v}{\alpha}.x}$. For steady state conditions, this further restriction is not required.

It is precisely this equivalence which indicates the possibility of using a simple analogue to obtain solutions of Rosenthal's equation. The analogue would have equation 3.2 as its governing equation (with stationary axes) with the analogue conductivity varying in the exponential manner defined by equation 3.4.

It must also be emphasised that although this analogue principle has been developed for thermal diffusion, any potential field governed by an equation similar to equation 3.2 could also serve as an analogue provided the field property analogous to conductivity could be varied in the same exponential manner.

3.2) Analogue Solutions of Rosenthal's Point Source Model of Welding

To illustrate how this principle may be employed, its application to the heat flow in welding will be discussed with particular reference to the point source model proposed by Rosenthal. Since the object of the project was to study 2-D fields, only the 2-D form of Rosenthal's quasi-static equation will be considered.

i.e. $$\frac{\partial^2 T}{\partial x^2} + \frac{\partial^2 T}{\partial y^2} + \frac{v}{\alpha} \cdot \frac{\partial T}{\partial x} = 0 \qquad (3.5)$$

Rosenthal defined the source of heat (in this case a line source) as

$$q \longrightarrow 2\pi rk. \frac{\partial T}{\partial r} \qquad \text{as} \qquad r \longrightarrow o$$

where $r = (x^2 + y^2)^{\frac{1}{2}}$

Owing to the variety of materials which are welded, and the corresponding variety of welding parameters, it is useful to non-dimensionalise the independent variables in equation 3.5. This can conveniently be achieved by introducing the non-dimensional variables,

$$\phi = \frac{v}{\alpha}.x \qquad \text{and} \qquad \psi = \frac{v}{\alpha}.y$$

With these transformations equation 3.5 becomes

$$\frac{\partial^2 T}{\partial \phi^2} + \frac{\partial^2 T}{\partial \psi^2} + \frac{\partial T}{\partial \phi} = 0 \qquad (3.6)$$

with the source re-defined as

$$\frac{q}{k} \longrightarrow 2\pi R.\frac{\partial T}{\partial R} \qquad \text{as} \qquad R \longrightarrow 0 \qquad (3.7)$$

where $R = (\phi^2 + \psi^2)^{\frac{1}{2}}$

Considering now the principle developed above, it can readily be shown that equation 3.6 is also the governing equation for the steady state potential distribution in an isotropic but non-homogeneous medium where the variation in conductivity is defined by

$$k = k_o e^{\phi} \qquad (3.8)$$

Let it be accepted that a potential field having this variation in conductivity (or similar property) could be constructed. Such a field would then be an analogue of the welding heat flow problem defined above and could be used to provide solutions of this problem. Some aspects of the solutions obtainable from such an analogue will now be considered with specific reference to the point source model defined by Rosenthal.

Firstly, no specification has been made as to the type of potential field (e.g. electric, magnetic, fluid, thermal, etc.) or to the range and value of the analogue space variables. These are obviously determinable from practical considerations. For the purpose of this discussion, however, the analogue space variables will be considered identical to the variables $\emptyset$ and Ψ. It will also be assumed that the analogue potential V (whatever it is) at any point in the field can be readily measured and that the relation between V and the welding heat flow temperature T has been established. This relationship would be defined when the design details of the analogue are determined but it would have the simple form

$$V = a.T \qquad (3.9)$$

where a is a constant.

It will also be noticed that although the variation in analogue conductivity must be defined by equation 3.8, the actual value of k_o appears to be arbitrary. It does, however, become fixed once the location of the origin is decided.

Now, the potential distribution on the analogue field $V(\phi, \psi)$ is governed by

$$\frac{\partial^2 V}{\partial \phi^2} + \frac{\partial^2 V}{\partial \psi^2} + \frac{\partial V}{\partial \phi} = 0 \qquad (3.10)$$

and the corresponding source condition must have the form

$$\frac{Q}{k_o} \longrightarrow 2\pi R. \frac{\partial V}{\partial R} \qquad \text{as} \qquad R \longrightarrow 0 \qquad (3.11)$$

where Q is the strength of the analogue source. For the analogue to represent exactly the heat flow problem, it is necessary that the source conditions should also be made equivalent. Since $V = aT$, substitution in equation 3.11 gives

$$\frac{Q}{ak_o} \longrightarrow 2\pi R \frac{\partial T}{\partial R} \qquad \text{as} \qquad R \longrightarrow 0$$

and comparison with the actual source condition (equation 3.7) demands that

$$\frac{Q}{ak_o} = \frac{q}{k} \qquad (3.12)$$

Since both q and k are known for particular welding conditions and since k_o is fixed for a particular location of the origin on the analogue field and 'a' is defined as above, then the strength Q of the analogue source is determined from equation 3.12.

A second boundary condition is, of course, necessary to completely define the heat flow problem. Whatever its nature, however, it could be related to a corresponding condition on the analogue field by a procedure similar to the above.

Thus, the problem can be readily set up on such an analogue.

It now remains to discuss how the potential distribution on the analogue field could be interpreted in terms of the actual temperature distribution.

Firstly, the analogue potential is directly proportional to temperature, being defined by equation 3.9. Secondly, since $\phi = \frac{v}{\alpha}.x$ and $\psi = \frac{v}{\alpha}.y$, the ratio $\frac{v}{\alpha}$ acts as a scale factor between the real and analogue fields. Furthermore, if a solution is desired to a problem having different values of $\frac{v}{\alpha}$ and $\frac{q}{k}$, there is no necessity to re-determine the potential distribution (always provided the second boundary condition remains the same). A change in $\frac{v}{\alpha}$ will only require a change in scaling. Re-writing equation 3.12 as

$$a = \left(\frac{Q}{k_o}\right)\left(\frac{k}{q}\right) \qquad (3.13)$$

it can be seen that if $\frac{Q}{k_o}$ is kept constant, 'a' is inversely proportional to $\frac{q}{k}$ and, hence, a change in $\frac{q}{k}$ is simply reflectedin a change in the relation between analogue potential and temperature given by equation 3.9. Thus, such an analogue has the interesting property that it will provide general solutions of point source models subject only to the practical limitations of the analogue. The interpretation of the general analogue solution for particular values of v, α, q and k will, of coûrse, produce unique solutions as is required by potential theory.

Another point of interest arises from the fact that the choice of k_o on the analogue is arbitrary. This implies that the origin on the analogue can be chosen with complete freedom. That is, if the origin is chosen at $\phi = \beta$, $\psi = 0$, then the variables must

be changed to $\phi' = \phi - \beta$, $\psi = \psi$, yielding the same governing equation as before. However, in this case, since

$$k = k_o e^{\phi}$$

the variation in conductivity must be re-defined as

$$k = k'_o e^{\phi'}$$

where

$$k'_o = k_o e^{\beta}$$

It must be emphasised, however, that the same potential distribution would be obtained with the source situated at $\phi = 0$ compared with $\phi = \beta$ provided the ratio $\frac{Q}{k_o}$ was the same in each case. This merely emphasises the generality of the solutions based on the point source model which this analogue could provide.

It is also interesting to note that the two parameters $\frac{v}{\alpha}$ and $\frac{q}{k}$ can now be identified as having important significance to the heat flow in welding. Since the ratio $\frac{v}{\alpha}$ arises from the governing equation 3.5, its importance remains fundamental whichever model of welding heat input is selected as a source boundary condition. Moreover, $\frac{v}{\alpha}$ has been shown to act as a scaling factor relating the analogue space variables ϕ, ψ to the "real world" variables x, y. Since, for example, $\phi = \frac{v}{\alpha}.x$ and hence

$$\frac{\partial T}{\partial x} = \frac{\partial T}{\partial \phi} \cdot \frac{\partial \phi}{\partial x} = \frac{v}{\alpha} \cdot \frac{\partial T}{\partial \phi} \quad ,$$

increasing the value of $\frac{v}{\alpha}$ will increase the thermal gradients around the source. Since the ratio $\frac{q}{k}$ arises from considerations of the source boundary condition, it does not seem to have as fundamental importance as the ratio $\frac{v}{\alpha}$. It has already been shown,

however, that the ratio $\frac{q}{k}$ is related to the factor 'a' by equation 3.13. Using this relation and substituting for 'a' in equation 3.9 and re-arranging gives

$$T = (\frac{k_o}{Q}).(\frac{q}{k}).V$$

This implies that increasing the value of $\frac{q}{k}$ will have the effect of increasing the peak temperatures around the source.

It also seems to be important that these are the only independent ratios which can be identified. This implies that, to obtain the same temperature distribution in the welding of materials of the same geometry under different conditions, it is only necessary that the ratios $\frac{v}{\alpha}$ and $\frac{q}{k}$ remain the same.

It should be noted that these findings are in agreement with the expression developed by Wells (2) from Rosenthal's solution for a line source moving with constant velocity in a wide plate of uniform thickness. This relates the maximum width 'd' from the weld centre line ($\mathcal{L}$) of an isotherm T to the welding variables by the expression

$$q = 8kT(\frac{1}{5} + \frac{v}{\alpha}.\frac{d}{4})$$

It can be seen from this that if $\frac{q}{k}$ is kept constant then for a particular isotherm,

$$\frac{v}{\alpha} \propto \frac{1}{d}$$

i.e. increasing $\frac{v}{\alpha}$ will reduce the isotherm width. Since this will be true of all the isotherms, an overall reduction in the isotherm width must imply an increase in the thermal gradient.

It can also be seen that if $\frac{v}{\alpha}$ is kept constant, the effect of

increasing $\frac{q}{k}$ will be to raise the temperature T at any width d. Expressing T in terms of d, the expression becomes

$$T = \left(\frac{q}{k}\right) \cdot \frac{1}{8\left[\frac{1}{5}+\left(\frac{v}{\alpha}\right)\cdot\left(\frac{d}{4}\right)\right]}$$

and it becomes evident that the same T-d relation will occur provided the ratios $\left(\frac{q}{k}\right)$ and $\left(\frac{v}{\alpha}\right)$ are kept constant.

3.3) Application to the Pool Shape Model

In practice, however, the discussion in the preceding section is only true in as much as the assumptions made in developing the original model are true. As has been discussed in the introduction, the Rosenthal - Wells theory can only be applied with any accuracy to points sufficiently distant from the source where the temperature field is no longer dependent upon the exact nature of the source. It has been shown numerically by Pavelic and others (5, 12) that, for points in the HAZ close to the source, the pool shape model proposed by Apps and Milner predicts the temperature field with much greater accuracy. Since this model basically depends on specifying a fixed potential (i.e. the melting temperature) along a curvilinear boundary (i.e. the molten pool boundary), it will be appreciated that such a constant potential boundary condition can readily be imposed on the type of analogue discussed above. Since the specification of this boundary condition does not involve the thermal conductivity k of the conducting medium or the heat input rate q, the equivalent equipotential condition on the analogue must be independent of the analogue conductivity k. This must imply that, on the analogue, any point can be chosen for the origin (i.e. any value of k can be chosen for k_o), and consequently, the equipotential boundary defined by the molten pool boundary can be placed anywhere on the analogue field. For boundary conditions of this type, therefore, the same potential field distribution would result wherever the 'pool' was located on the analogue and no further interpretation of the analogue results would be required (apart, of course, from the potential/temperature relation and the application of the appropriate scale factor $^{V}/_{\alpha}$).

It would, therefore, appear that such an analogue, if constructed, would be useful for the determination of the thermal field during welding using the pool shape model.

In principle, any potential field whose governing equation has the form

$$\text{div } k \text{ grad } T = 0$$

and where "conductivity" k could be varied in the prescribed exponential manner could be used as an analogue field. Electro-conductive analogues, however, would be the most suitable for this application. Not only can electrical conductivity be readily defined and measured but all essential measurements (e.g. potential) can be made easily and with high precision on electric fields. Of the various electric field analogues which have been developed (14, 15), the conductive sheet, electrolytic tank (both for 2-D applications) and impedance network (for 2 and 3-D applications are the three which lend themselves most readily to a variation in conductivity.

Conductive sheet analogues are usually homogeneous in composition but the required variation in conductivity (or in this case, "acceptivity") could be achieved by a similar variation in the thickness of the sheet. If the local thickness of the sheet is t(x), the governing equation for the steady state potential distribution V(x, y) in such a sheet can be written as

$$\frac{\partial^2 V}{\partial x^2} + \frac{\partial^2 V}{\partial y^2} + \frac{1}{t}\frac{\partial t}{\partial x}\frac{\partial V}{\partial x} = 0$$

and if $t = t_o e^x$, this equation reduces to the same form as equation

3.6 (i.e. non-dimensional form of Rosenthal's equation). While this type of analogue would be suitable for 2-D applications, it would be necessary to ensure the variation in thickness of the sheet did not result in a through thickness variation in potential. Subject to this requirement, such an analogue could, for example, be constructed by appropriately machining a slab of graphite and it would have the advantage of providing a continuous analogue field.

The electrolytic tank would in a similar way also provide a continuous analogue, with the depth of the electrolyte varying in the same exponential manner. It would, however, suffer the same restrictions as the conductive sheet.

Impedance networks are less direct analogues than either the conductive sheet or the electrolytic tank as they are based on finite difference approximations to the differential terms in the governing equation. They are, however, by far the most versatile and since the variation in conductivity can be achieved by simply varying the value of the resistive elements, they are the most suitable for this application. The design of such a network analogue for the quasi-static form of Rosenthal's equation is outlined in the following section.

3.4) The Resistance Network Analogue

Consider the non-dimensional form of Rosenthal's quasi-static equation given by equation 3.6

$$\text{i.e.} \quad \frac{\partial^2 T}{\partial \phi^2} + \frac{\partial^2 T}{\partial \psi^2} + \frac{\partial T}{\partial \phi} = 0$$

If the field of interest governed by this equation is covered by a uniformly square finite difference mesh of side h, then at any node i in the mesh, the differential terms in the above equation may be approximated by the central difference expressions

$$\frac{\partial^2 T}{\partial \phi^2} + \frac{\partial^2 T}{\partial \psi^2} \simeq \frac{1}{h^2}(T_1 + T_2 + T_3 + T_4 - 4T_i)$$

and

$$\frac{\partial T}{\partial \psi} \simeq \frac{1}{2h}(T_3 - T_1)$$

where T_i is the temperature at the ith node and T_1, T_2, T_3, T_4 are the temperatures at each of the four surrounding nodes as shown in Fig. 3.1. Substituting for the differential terms in Rosenthal's equation and re-arranging gives the difference equation

$$T_1(1 - h/2) + T_2 + T_3(1 + h/2) + T_4 - 4T_i = 0 \qquad (3.13)$$

Now consider the corresponding element of a resistance network as shown in Fig. 3.2. If the voltage at the ith node is V_i, then applying Kirchhoff's 1st Law at the ith node gives

$$\frac{V_1 - V_i}{R_1} + \frac{V_2 - V_i}{R_2} + \frac{V_3 - V_i}{R_3} + \frac{V_4 - V_i}{R_4} = 0$$

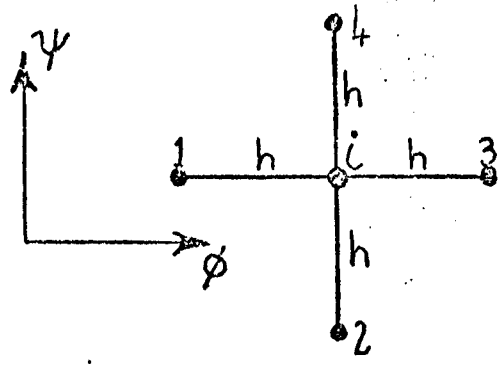

FIG 3·1 FINITE DIFFERENCE ELEMENT

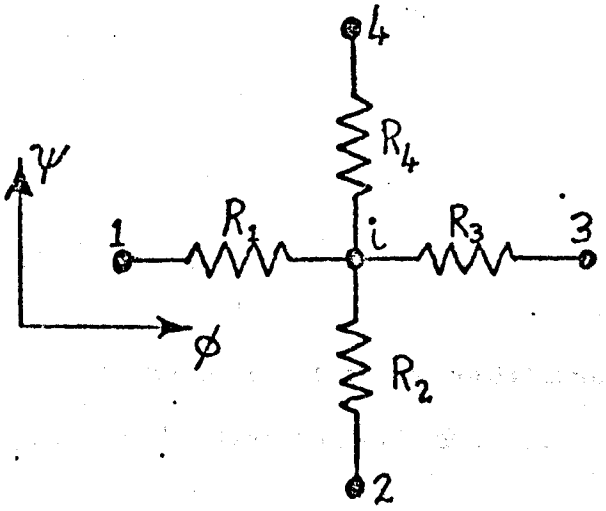

FIG 3·2 RESISTANCE NETWORK ELEMENT

which on re-arranging becomes

$$\frac{V_1}{R_1} + \frac{V_2}{R_2} + \frac{V_3}{R_3} + \frac{V_4}{R_4} - V_i\left(\frac{1}{R_1} + \frac{1}{R_2} + \frac{1}{R_3} + \frac{1}{R_4}\right) = 0 \qquad (3.14)$$

Provided the voltage at any point in the network is simply proportional to the temperature in the corresponding finite difference mesh, then comparison of equations 3.13 and 3.14 shows that the resistance network element can only be a model of the finite difference element if

$$R_2 = R_4 = R_i \quad \text{say}$$

(i.e. no variation of resistance in the γ direction)

and

$$\frac{R_i}{R_1} = (1 - h/2) \qquad (i)$$

$$\frac{R_i}{R_3} = (1 + h/2) \qquad (ii)$$

$$R_i\left(\frac{1}{R_1} + \frac{1}{R_3}\right) = 2 \qquad (iii)$$

It will be noticed that the third of these conditions is satisfied by the other two and that by dividing (i) by (ii),

$$\frac{R_3}{R_1} = \frac{(1 - h/2)}{(1 + h/2)} \qquad (3.15$$

If, as shown in Fig. 3.3, R_1 is the value of each of the resistances at the first node (i.e. $i = 1$) then, following the notation of Fig.

3.3 it can readily be shown that at the ith node

$$R_{i-1/2} = R_1\left(\frac{1 - h/2}{1 + h/2}\right)^{i-2}$$

$$R_i = R_1\left[\frac{(1 - h/2)}{(1 + h/2)}\right]^{i-1} \qquad (3.16)$$

and $$R_{i+1/2} = R_1\left(\frac{1 - h/2}{1 + h/2}\right)^{i-1}$$

where R_1 is arbitary. Equations 3.4 can now be used as the design formulae for a resistance network analogue of Rosenthal's equation 3.6 .

In the development of equations 3.16, no use has been made of the fact that the required variation in resistance (conductivity) is known exactly. The required design formulae can, however, be developed using this knowledge by a technique outlined by Vine (13) and which is particularly applicable for the design of resistance networks where the mesh size is not uniform. This makes this technique applicable for problems with irregularly shaped boundaries (e.g. the curvilinear shape of the weld pool boundary).

As before, consider the field subdivided by a network of lines whose intersections define the field points which are to be represented on the analogue. (Fig. 3.4a). Vine further subdivides the field into small areas called cells (shown by the dotted lines) such that each cell contains one node and the field at that node is taken to be representative of the cell enclosing it.

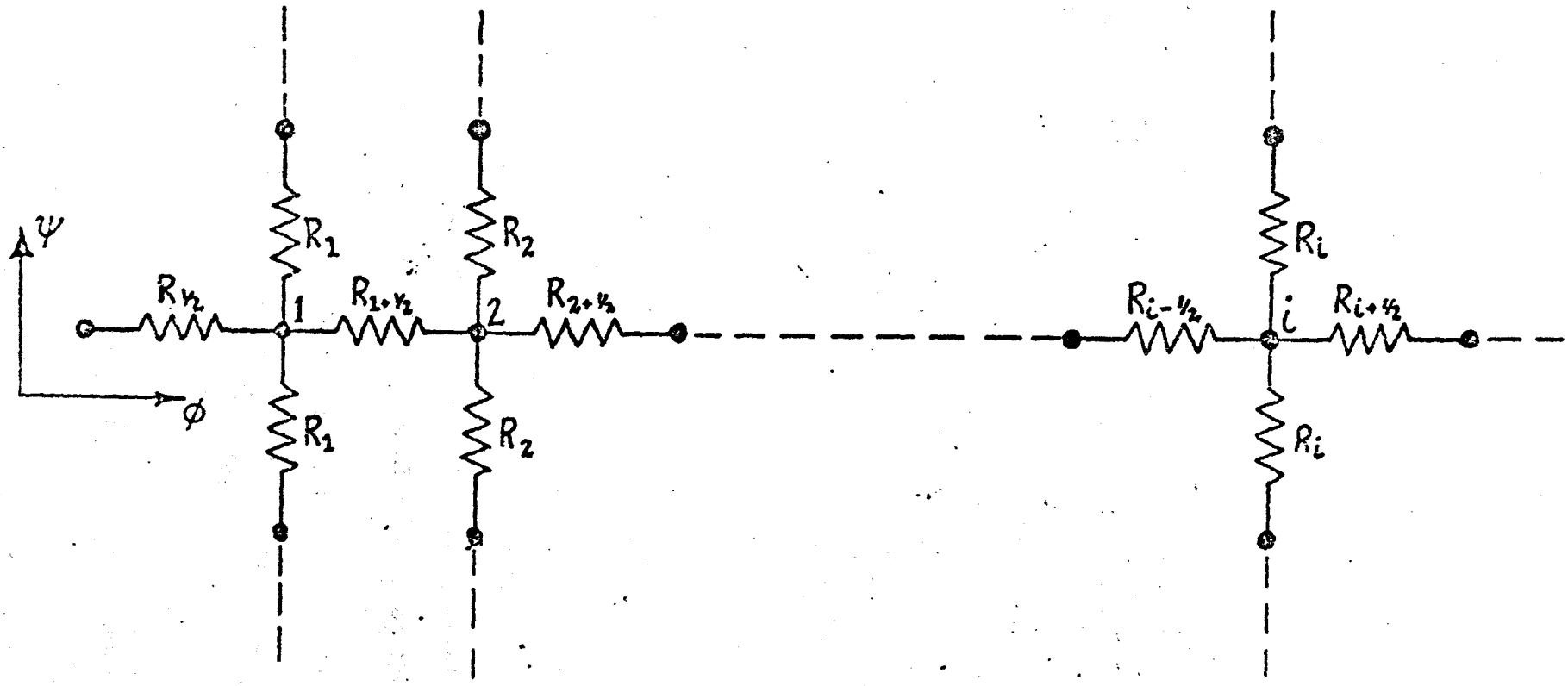

FIG 3·3 RESISTANCE NETWORK ANALOGUE

Now consider one cell C_i whose area is S_i enclosing the ith node. This cell is surrounded by four other cells as shown in Fig.3.4b. As has been shown, Rosenthal's equation 3.6 can be written in the form

$$\text{div } k \text{ grad } T = 0$$

where $$k = k_o e^{\phi}$$

Integrating this equation over the area S_i of the cell C_i gives

$$\iint_{S_i} \text{div } k \text{ grad } T = 0$$

Using the Divergence theorem, this integral may be replaced by the line integral

$$\oint_{P_i} k \frac{\partial T}{\partial n} dP = 0$$

where n is the outward pointing normal from C_i and P_i is the perimeter of the cell. Since the cell structure under consideration is rectangular, the line integral around the perimeter may be written as the sum of the integrals along each of the sides δ_{p_j} $(j = 1,\ldots,4)$

i.e. $$\oint_{P_i} k \frac{\partial T}{\partial n} dP = \sum_{j=1}^{4} \int_{\delta p_j} k \frac{\partial T}{\partial n} dP = 0$$

An approximation for the gradient $\frac{\partial T}{\partial n}$ can now be introduced by writing for side δp_j

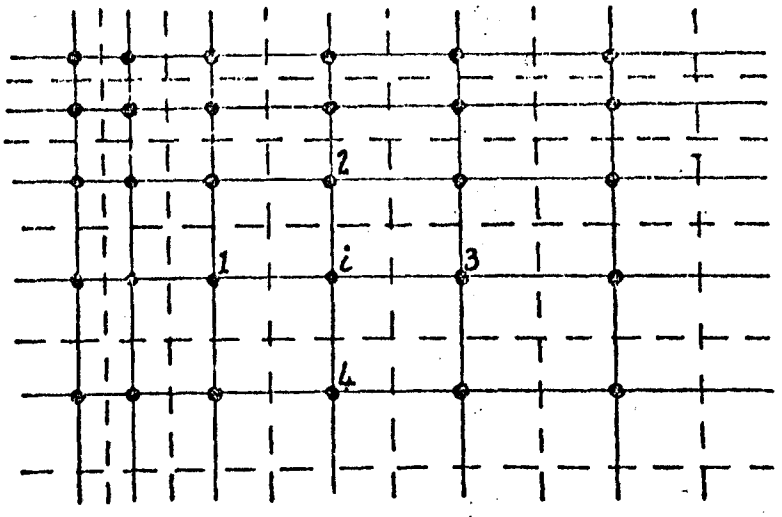

FIG 3·4a DIFFERENCE NETWORK – SHOWN IN FULL LINES AND CELL STRUCTURE – SHOWN IN DOTTED LINES

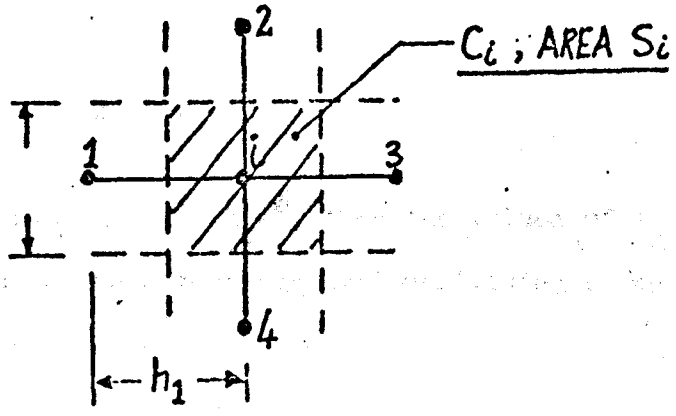

FIG 3·4b THE ith CELL

$$\left(\frac{\partial T}{\partial n}\right)_j = \frac{T_j - T_i}{h_j}$$

where h_j is the separation of the ith and jth nodes.

Substituting for $\left(\frac{\partial T}{\partial n}\right)$ in the above expression and integrating yields

$$\sum_{j=1}^{4} k_j (T_j - T_i)\, \delta p_j = 0 \qquad (3.17)$$

where k_j is the value of the conductivity at the intersection of the cell boundary and the grid line connecting the ith and jth nodes.

N.B This same result could have been obtained by considering the heat flow into the element from each of its neighbours and making the same approximation for the gradient.

Comparison of equation 3.17 with equation 3.14 for the resistance network element shows that the values of the resistances connecting the ith node are given by

$$R_j = \frac{h_j}{k_j\ \delta p_j} \qquad (3.18)$$

Since it is known that $k = k_o e^{\phi}$, then the values of k_j at any node i in the field can be determined and substituted in equation 3.18 to determine the best estimate for R_j.

To illustrate this, consider the case of a uniformly square mesh such that $h_j = h$ for the whole field. The cell structure will then be similarly square and $\delta p_j = h$. Substituting for h_j and δp_j

in the above equation yields

$$R_j = \frac{1}{k_j}$$

If the ith node corresponds to a point (ϕ_i, ψ_i) in the field, then

$$R_i = \left[k(\phi_i)\right]^{-1} = k_o e^{\phi} - 1$$

Following the notation of Fig. 3.3 the following equations may be readily derived

$$\left.\begin{aligned} R_{i-1/2} &= R_1 e^{-h(i-3/2)} \\ R_i &= R_1 e^{-h(i-1)} \\ R_{i+1/2} &= R_1 e^{-h(i-1/2)} \end{aligned}\right\} \quad (3.19)$$

where $x_i = h(i-1)$ and $R_1 = \frac{1}{k_o}$ is arbitrary. These design formulae are comparable with equations 3.16 which were derived without employing the known variation in conductivity. It is useful to compare the ratio $R_{i+1/2} / R_{i-1/2}$ for the two cases.

From equations 3.16,

$$\frac{R_{i+1/2}}{R_{i-1/2}} = \frac{(1-h/2)}{(1+h/2)}$$

and from equations 3.19,

$$\frac{R_{i+1/2}}{R_{i-1/2}} = e^{-h}$$

The latter expression is exactly what is required by the exponential

variation in conductivity and for a grid spacing of h. It is evident, therefore, that there is an error in the resistance values calculated using the central difference approximations. The relative error ε in the ratio $R_{i+1/2}$ calculated by central differences can be expressed as

$$\varepsilon = \frac{(1-h/2)}{(1+h/2)} e^{h} - 1$$

A plot of ε expressed as a percentage, against h is shown in Fig. 3.5 and it should be noted that $\varepsilon \rightarrow 0$ as $h \rightarrow 0$ as indeed it must.

It is obvious therefore from the above that the "cell" approach is to be preferred in deriving the design fromulae for the resistance network analogue of Rosenthal's equation. Indeed, for the design of a resistance network as an analogue of any field whose governing equation can be written in the form

$$\text{div } k \text{ grad } T = 0$$

the cell approach is to be recommended. It can readily be shown that this includes all equations of the type

$$\nabla^2 T + f(x) \frac{\partial T}{\partial x} + g(y) \frac{\partial T}{\partial y} = 0 \qquad (3.20)$$

in which case, the "conductivity" $k(x,y)$ can be expressed as

$$k(x,y) = k_o \exp \left[\int f(x)dx + \int g(y)dy \right]$$

where k_o is an arbitrary constant and $f(x)$ and $g(y)$ are arbitrary functions of x and y respectively. The only restriction on $f(x)$ and $g(y)$ is that they must be integrable at least in the required

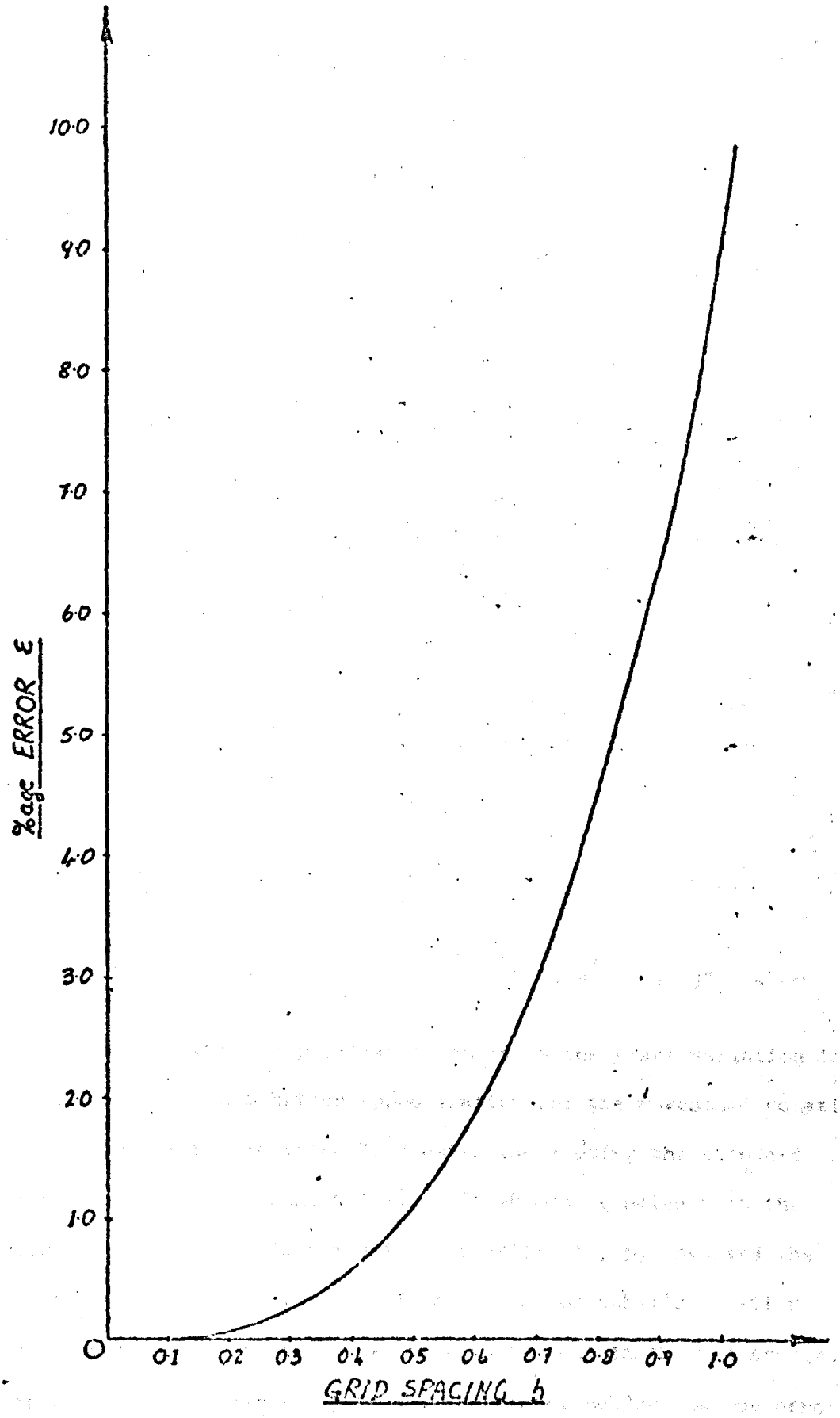

FIG 3·5 EFFECT OF INCREASING GRID SPACING ON RELATIVE ERROR E

range of x and y.

It should also be noted that the "cell" approach provides a useful alternative difference approximation for this class of equations. Consider for example the difference equation 3.17. For a square mesh, this reduces to

$$\sum_{J=1}^{4} k_j(T_j - T_i) = 0$$

If the ith node corresponds to the point (ϕ_i, ψ_i) in the field then

$$k(\phi_i) = k_o e^{+\phi_i}$$

Following the notation of Fig. 3.1 and substituting the apporpriate values for k_j in the above difference equation gives

$$k_o e^{\phi_i}\left[e^{-h/2}(T_1 - T_i) + (T_2 + T_4 - 2T_i) + e^{+h/2}(T_3 - T_i)\right] = 0$$

which on re-arranging becomes

$$e^{-h/2}T_1 + T_2 + e^{+h/2}T_3 + T_4 - (e^{-h/2} + e^{+h/2} + 2)T_i = 0$$

Since this difference approximation embodies the exact variation in conductivity, it is a better approximation for the Rosenthal equation 3.6 than the difference equation 3.13 established using the standard central difference approximations. It should be noted that the numerical analysis of Tanbakuchi and Pavelic (12, 5) involved the direct application of finite differences to Rosenthal's equation (modified to allow for the non-linear variations in thermal properties with temperature) and their analysis is, therefore, subject to the error

discussed above. While the relative importance of this error diminishes with grid size (Fig. 3.5), it is, nevertheless, an error which may be corrected by adopting the above procedure to establish the difference equations. Since this will generally be true of difference approximations for the set of equations characterised by equation 3.20, it is recommended that the cell approach be adopted to establish the difference approximations for such equations.

For the particular application to the design of a resistance network analogue of Rosenthal's equation, it is similarly evident that the design formulae established using the cell approach (equations 3.19) are to be preferred. Due to the specific variation in resistance values which would be required, a practical analogue would be constructed of variable resistors (or potentiometers used as such) whose resistance could be set to the value specified by the design formulae. A network of commercially available standard resistors with preferred values could be designed but of necessity this would involve a variable grid spacing. The overall range of resistance values required would depend upon the range of x in the "real" field and upon the value of $\frac{v}{\alpha}$. To illustrate this, consider the application of such an analogue to study the temperature field around a weld pool 2 cm. long, which is produced by the TIG welding of a thin steel plate at a speed of 0.4 cm/s. The thermal diffusivity α can be taken as 0.075 cm^2/s and the temperature field has to be determined in a region not less than three times the pool length in the direction of welding.

Since $\phi = \frac{v}{\alpha}x$, the required range $\Delta\phi$ on the analogue is given by

$$\begin{aligned}\Delta\phi &= \frac{v}{\alpha}.\Delta x \\ &= \frac{0.4}{0.075} \times 2 \times 3 \\ &= 16\end{aligned}$$

Now the variation in resistance on the analogue is given by

$$R = R_o e^{-\phi}$$

and hence the required range in resistance R is given by

$$R = e^{16} = 8.8861 \times 10^6$$

Thus, if the initial resistance value is chosen as 1Ω, the minimum required value at the other end of the analogue field would be 8.89 MΩ. It can be appreciated that this introduces a serious restriction to the application of such an analogue to welding problems. Assuming a practical limit of 10 MΩ on the range of resistance, the range of ϕ is fixed at 16.1. For certain welding conditions (e.g. high speed welding of low diffusivity materials), this may be insufficient to permit a study of the temperature field surrounding the weld pool. It should also be noted that in a similar way, this rules out completely the possibility of using a variable thickness analogue for the welding problem.

Another disadvantage of the resistance mesh is that, since it is by design a discrete approximation to a continuous system, there are truncation errors which are inherent in the analogue. Furthermore, due to its discrete nature, it would be rather more difficult, although certainly not impossible, to set up the curvilinear shape of the pool boundary on a network analogue.

While these restrictions are not as significant as the required variation in resistance, they do, nevertheless, detract from the appeal of using a resistance network analogue for the welding problem. It was for this reason that such an analogue was not constructed although it certainly could have application to certain welding problems (e.g. where $\frac{v}{\alpha} \leq 1$). It was, however, felt that this study of direct analogues had

i) identified the resistance network analogue as a practical analogue for the study of welding heat flow under certain conditions and

ii) promoted a greater physical understanding of the heat flow problem. The parameters $\frac{v}{\alpha}$ and $\frac{q}{k}$ were identified and given a physical significance.

For these reasons it was decided to pursue the analogue approach and to consider whether there existed a transformed version of Rosenthal's equation for which a practical analogue could be constructed. This is considered in the following chapter.

CHAPTER 4

THE INDIRECT ANALOGUE

It is evident from the preceding chapter that the very large variation in analogue "conductivity" required for the study of welding heat flow is the major drawback to the design of a practical direct analogue. Not even a change of seven orders of magnitude, as can be achieved with the resistance network, is entirely sufficient for such a study. This chapter discusses how a simple transformation of the dependent variable in Rosenthal's equation yields a transformed field equation with the exponential variation effectively removed. Both the design and the construction of practical analogues of this transformed equation are discussed.

4.1) The Rosenthal Transformation and the ϕ Field

Consider again the 2-D quasi-static form of Rosenthal's equation 3.5

$$\text{i.e.} \quad \frac{\partial^2 T}{\partial x^2} + \frac{\partial^2 T}{\partial y^2} + \frac{v}{\alpha} \cdot \frac{\partial T}{\partial x} = 0$$

As a first step in his analysis Rosenthal transformed the dependent variable $T(x,y)$ by writing

$$T(x,y) = e^{-\frac{v}{2\alpha} \cdot x} \phi(x,y) \qquad (4.1)$$

Making this transformation in equation 2.25 gives

$$\frac{\partial^2 \phi}{\partial x^2} + \frac{\partial^2 \phi}{\partial y^2} - \left(\frac{v}{2\alpha}\right)^2 \phi = 0$$

or

$$\nabla^2 \phi - \left(\frac{v}{2\alpha}\right)^2 \phi = 0 \qquad (4.2)$$

The above transformation (equation 4.1) will be termed the "Rosenthal transformation" and the resulting transformed Rosenthal equation 4.2 will be termed the "ϕ equation". The region of space governed by the ϕ equation will be termed the "ϕ field".

Returning to the conductivity analogy, it can be seen that the effect of the Rosenthal transformation on the Rosenthal field is to change its character from the non-homogeneous (exponential variation in conductivity) condition to the homogeneous (constant conductivity) ϕ field. A comparison of the ϕ equation with Laplace's equation indicates that the ϕ field is essentially Laplacian in character but with "leakage" proportional to the ϕ potential at every point in the field.

Therefore, since the ϕ field is essentially homogeneous, an analogue of the ϕ field would not suffer from the same disadvantages as the direct analogues of the Rosenthal field. Such an analogue would, however, have to account for the "leakage" term in the ϕ equation.

4.2) The Equivalent Resistance Network

To discover how an electrical analogue of the ϕ field may be constructed, a simple resistance network analogue of the ϕ equation 4.2 will be developed.

Following the procedure of the previous chapter, consider the region of interest in the ϕ field covered by a uniformly square finite difference mesh of side h. Applying the standard central difference approximation for $\nabla^2\phi$ to equation 4.2 and, following the notation of Fig. 4.1a yields for the ith node of the mesh the difference equation

$$\sum_{j=1}^{4} \phi_j - \phi_i\left[4 + \left(\frac{h.v}{2\alpha}\right)^2\right] = 0 \qquad (4.3)$$

Now consider the corresponding element of a resistance network as shown in Fig. 4.1b. It will be noticed that unlike the resistance element for the direct analogue, the four resistors R radiating from the ith node are all equal in value and that there is a fifth resistor R_i connected between the ith node and earth. It is this resistor which provides the "leakage" discussed above.

If the voltage at the ith node is V_i and at each of the four surrounding nodes V_j $(j = 1, \ldots 4)$ then applying Kirchhoff's 1st law at the ith node gives

$$\frac{V_1-V_i}{R} + \frac{V_2-V_i}{R} + \frac{V_3-V_i}{R} + \frac{V_4-V_i}{R} - \frac{V_i}{R_i} = 0$$

which on re-arranging becomes

$$\sum_{j=1}^{4} V_j - V_i\left[4 + \frac{R}{R_i}\right] = 0 \qquad (4.4)$$

Comparison with equation 4.3 shows that for the resistance network to be an analogue of the ϕ field then it is necessary that

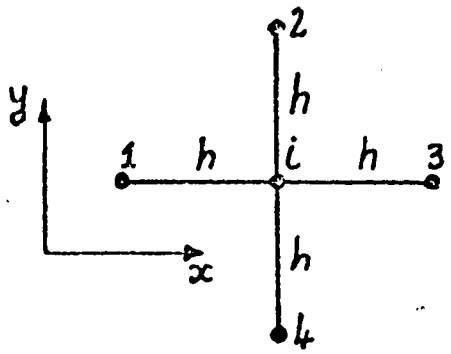

FIG 4.1a FINITE DIFFERENCE ELEMENT

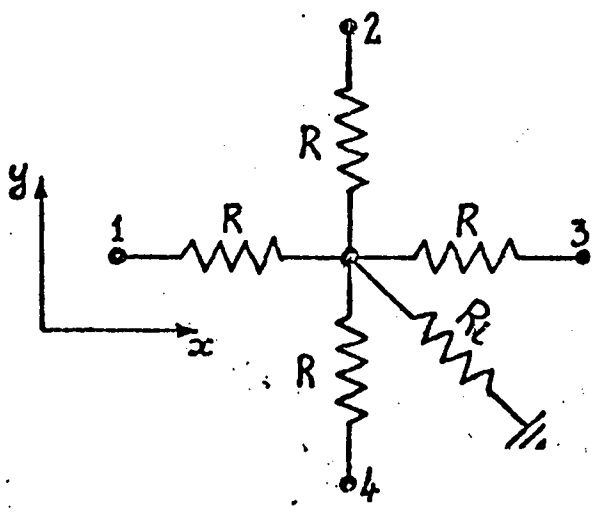

FIG 4.1b RESISTANCE NETWORK ELEMENT

$$\frac{R}{R_i} = \left(\frac{hv}{2\alpha}\right)^2 \qquad (4.5)$$

This is the required design formula for the Ø field analogue. It will be noticed that in this case there is only one design formula (compared with three for the "direct" network analogue) since the Ø field is homogeneous i.e. the value of R is constant throughout the field. The purpose of R_i is, of course, to allow the necessary "leakage" current, characteristic of the Ø field.

If a suitably small and "ideal" value for the grid spacing h is selected, then it can be seen from equation 4.5 that for each different value of $\frac{v}{\alpha}$, there would be a correspondingly different value of $\frac{R}{R_i}$. In practice, however, only one analogue with a fixed value of $\frac{R}{R_i}$ would be used to study various problems with different values of $\frac{v}{\alpha}$. Re-arranging equation 4.5

i.e. $$h = \left(\frac{2\alpha}{v}\right)\sqrt{\frac{R}{R_i}}$$

it can be seen that the distance of real space represented by the grid spacing h will vary with $\frac{v}{\alpha}$. Thus, in a similar way to the direct analogues, the results from a Ø field analogue would require "scaling" for different values of $\frac{v}{\alpha}$. The choice of $\frac{R}{R_i}$ would be a compromise to give reasonable values of the grid spacing h for the range of $\frac{v}{\alpha}$ to be considered.

This establishes the basic design concept for a simple Ø field analogue. Since the exponential term has been effectively "removed" from the Ø field by the Rosenthal transformation, such an analogue would not suffer from the restrictions imposed by the variable conductivity of the direct analogues discussed previously.

4.3) The Conductive Sheet Analogue of the Ø Field

As has been indicated, the Ø field, because of its homogeneous nature, is closely linked to the Laplacian field. A most useful electrical analogue of 2-D Laplacian fields is the plane conducting sheet (e.g. "Teledeltos" paper). It is further shown in the previous section that the leakage characteristic of the Ø field can be modelled by making resistive connections from each node to earth. This suggests that a useful alternative to the resistance network analogue of the Ø field would be a plane conducting sheet of uniform resistivity with a number of resistive connections between the sheet and earth. In this way, the sheet itself would model the Laplacian part of the Ø equation and the resistive connections would provide for the necessary leakage currents to complete the analogue.

To establish the design formula for such an analogue, consider a plane conducting sheet of uniform thickness as shown in Fig. 4.2a. A potential V(x,y) exists in the sheet as a result of boundary conditions imposed at its edges. A distributed leakage current of i A/unit area is extracted from the sheet. For continuity across any infinitesimal element of the sheet, there must exist a current balance such that

$$i_x \delta y + i_y \delta x = (i_x + \frac{\partial i_x}{\partial x}.\delta x)\delta y + (i_y + \frac{\partial i_y}{\partial y}.\delta y)\delta x + i\delta x\delta y$$

where i_x and i_y are the current densities in the x and y directions respectively. (See Fig. 4.2b).

On re-arranging this reduces to

$$\frac{\partial i_x}{\partial x} + \frac{\partial i_y}{\partial y} + i = 0$$

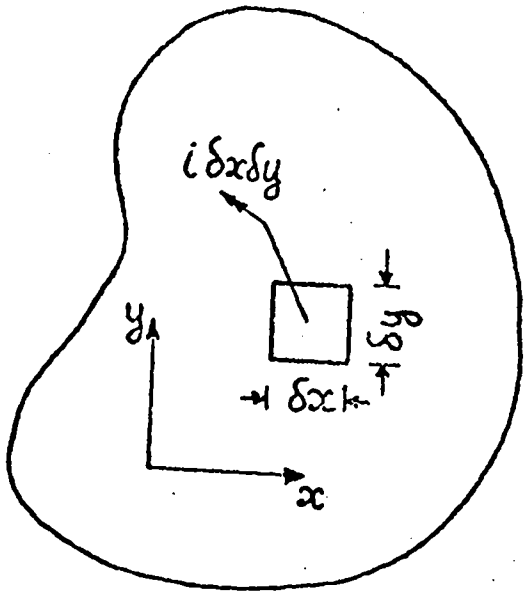

FIG 4.2a PLANE CONDUCTING SHEET WITH LEAKAGE

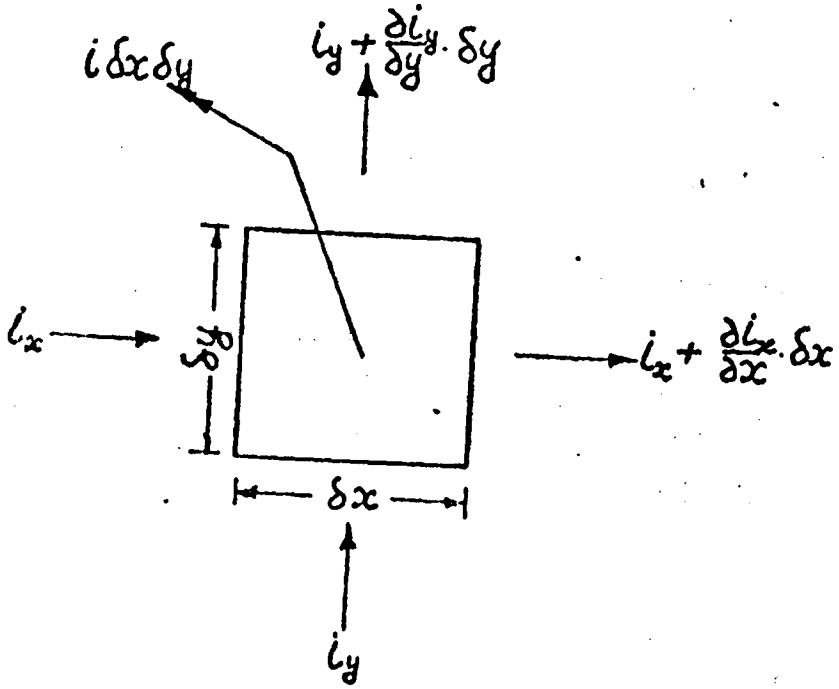

FIG 4.2b ELEMENT OF CONDUCTING SHEET

Now, if $\rho\Omega$ is the resistance per square of the sheet (i.e. the resistance between two opposite edges of any square of the sheet) then

$$i_x = -\frac{1}{\rho}\cdot\frac{\partial V}{\partial x} \qquad \text{and} \qquad i_y = -\frac{1}{\rho}\cdot\frac{\partial V}{\partial y}$$

Substituting for i_x and i_y in the continuity equation yields

$$\frac{\partial}{\partial x}\left(\frac{1}{\rho}\cdot\frac{\partial V}{\partial x}\right) + \frac{\partial}{\partial y}\left(\frac{1}{\rho}\cdot\frac{\partial V}{\partial y}\right) - i = 0$$

Providing the resistance per square of the sheet is uniform (i.e. the sheet is homogeneous) this reduces to

$$\frac{\partial^2 V}{\partial x^2} + \frac{\partial^2 V}{\partial y^2} - \rho i = 0 \qquad (4.6)$$

If $V(x,y)$ is measured with respect to some arbitrary 'earth' potential and the distributed leakage current density $i(x,y)$ is approximated by making a resistive connection from each element of the sheet to earth then

$$i = \frac{V}{R\,\delta x\,\delta y}$$

where $R\Omega$ is the value of the resistance between each sheet element and earth as shown in Fig. 4.3.

Substituting for i in the above equation 4.6 gives

$$\frac{\partial^2 V}{\partial x^2} + \frac{\partial^2 V}{\partial y^2} - \frac{V}{R\delta x\delta y} = 0$$

Now, if the resistors are arranged in a square mesh of side h with respect to the sheet, then the equation may be written as

$$\frac{\partial^2 V}{\partial x^2} + \frac{\partial^2 V}{\partial y^2} - \frac{\rho V}{Rh^2} = 0 \qquad (4.7)$$

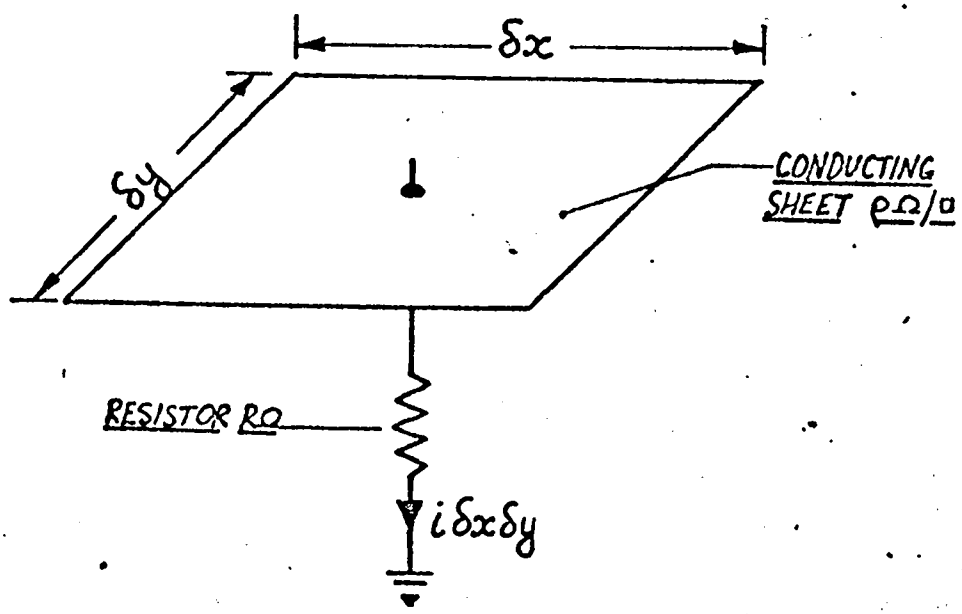

FIG 1.3 RESISTIVE CONNECTION FROM SHEET ELEMENT TO EARTH

Comparison of this equation with the ϕ equation 4.2, shows that, for the conductive sheet with resistive connections to be an analogue of the ϕ field,

$$\frac{\rho}{R} = \left(\frac{hv}{2\alpha}\right)^2 \qquad (4.8)$$

This is the required design formula for the conductive sheet analogue and is comparable with equation 4.5 for the resistance network analogue. The discussion on the application of equation 4.5 applies in a similar way to equation 4.8.

It can be appreciated that the conductive sheet analogue should at least be as good an approximation to the ϕ field as the resistance network. Although the accuracy of the sheet analogue is still dependent upon the resistor spacing h, the Laplacian component should, at least in theory, be modelled exactly.

There is, however, a more obvious advantage to the conductive sheet analogue. The study of the welding problem involves setting the pool shape as a boundary condition on the analogue. Such a curvilinear boundary can more readily be imposed on the continuous surface of the conductive sheet than on the discrete nodal construction of the resistance network.

Thus, an analogue of the ϕ field is not only free from the restrictions of the direct analogue, but the advantages of a continuous field analogue can also be employed. The required transformation from the Rosenthal field to the ϕ field obtained from equation 4.1 as

$$\phi(x,y) = e^{+\frac{v}{2\alpha}.x} \; T(x,y) \qquad (4.9)$$

can readily be applied to the isothermal pool shape boundary and its transform applied to the conductive sheet analogue. Although the transform will, of course, no longer be an equipotential, a variable potential boundary can be easily handled on an electrical analogue. Having obtained the required $\emptyset$ field distribution, the transform required to relate $\emptyset(x,y)$ to the temperature field $T(x,y)$ is given directly by equation 4.1. This inevitably involves some computation, but this can be handled manually with the use of tables of the exponential function (15) and/or a small calculator.

For these reasons, the conductive sheet analogue of the $\emptyset$ field is an attractive concept for the analysis of welding heat flow. The construction of such an analogue, employing equation 4.8 as the design criterion, is reported in the following section.

4.4) Analogue Construction

As discussed in the previous section, the concept of a $\emptyset$ field analogue is based on a homogeneous conducting sheet with resistive connections. Various conducting sheet analogues have been developed (13,14) and used to provide solutions of Laplacian field problems. For the following reasons, the most commonly used is graphitised paper or "Teledeltos";

i) its resistance per square is compatible with accurate measurements of potential using standard instruments.

ii) it is essentially homogeneous and isotropic although, like all paper and most rolled materials, it is slightly anisotropic

the resistance per square in the direction of the roll being somewhat greater than in the across roll direction (see Table 4.2)

iii) it is easily shaped (i.e. cut with scissors)

iv) connections and boundaries can easily be made on the paper using conducting paint (usually a suspension of silver in a volatile solvent).

Since it is also reasily available commercially, it is the obvious choice of conductive sheet for this application.

It has also been appreciated for some time that it is possible to adapt conducting sheet analogues to solve non-Laplacian field problems. In particular, Simmons (17) describes how Poissonian type field problems in heat conduction may be analysed if current is passed through an array of resistors to a Teledeltos sheet. In this way, uniform generation of heat within a conducting medium may be simulated. While Simmons apparently did not consider the possibility of extracting current from the sheet to simulate heat loss from the surface of a conducting medium (which, as is shown in Appendix 2a, may be simply a ϕ field) there is little difference in principle and he did establish the method by which simple and reliable connections between an array of resistors and a Teledeltos sheet may be made.

To test whether the principle of extracting current from a Teledeltos sheet would be suitable for the ϕ field application, a trial model was constructed. The design of the Mk I analogue allowed for a rectangular field of dimensions 175 x 250 mm. A typical section through the analogue is shown in Fig. 4.4 The resistors, with wires trimmed to suit were located in a square pattern in holes drilled into the Tufnol block. The resistor spacing was 12.5 $\pm$ 0.5 mm and they were held securely by the clamping plate screwed to the bottom surface of the block. The lower ends of the resistors were soldered to copper wires interconnected to form

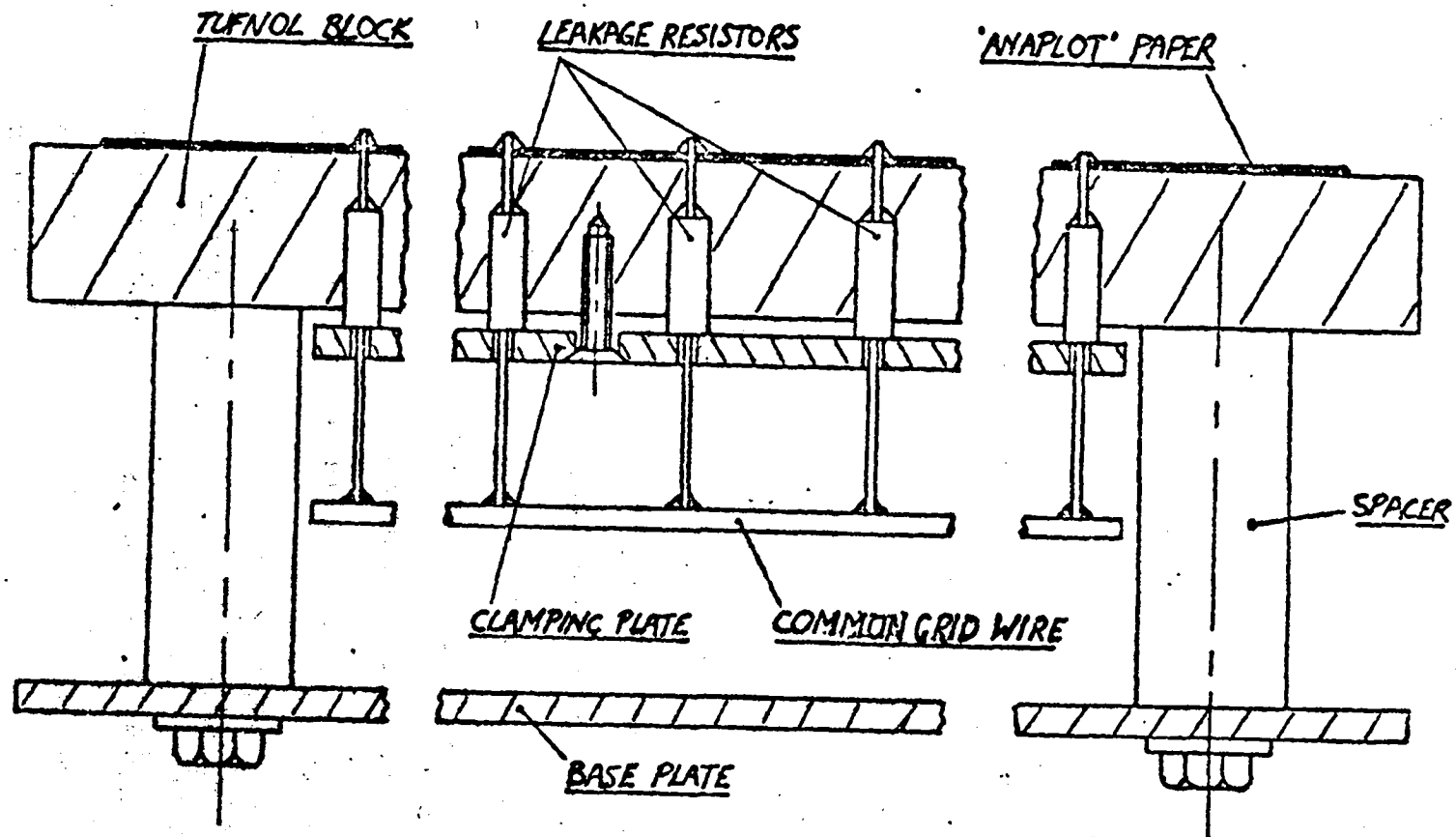

SCALE 2:1 APPROX.

FIG 4·4 SECTION THROUGH MkI ANALOGUE

a common grid connection to all the resistors. This is shown in Plate 4.1. The upper ends of the resistors, projecting 2mm above the top surface of the block were connected to the paper by small spots of silver conducting paint as shown in Plate 4.2. These connections were made by passing a small loop of fine wire, holding a drop of silver paint, over the top of the projecting resistor wire and depositing the drop on the paper. (This technique, similar to that used by Simmons, has proved to be quite successful in practice). The details of the electrical components are given in Table 4.1. The resistor value of 2.2 kΩ was selected as it is compatible with the resistance/square of Anaplot paper. This was estimated by measuring the lengthwise resistance of 250 x 25mm strips of the paper cut in the "in roll" and "across roll" directions. The measured value was then divided by 10 to get the resistance/square. An Avo Universal Bridge (type B 150 manufactured by Avo Ltd.) was used to measure the resistance. The results are given in Table 4.2. Each quoted value is the average of four tests. The results show a considerable range between rolls although it was found that the quoted values were quite consistent within each roll.

4.5) Mk I Analogue Evaluation

To test the accuracy of the Mk I analogue, it was used to predict the solution to a simple 1-D problem. This was then compared with the analytical solution for the same problem.

From equation 4.7, the 1-D analogue equation is given by

$$\frac{\delta^2 V}{\delta x^2} - \frac{\varrho}{Rh^2} \cdot V = 0 \qquad (4.10)$$

COMPONENT	DESCRIPTION	MANUFACTURER/SUPPLIER
RESISTORS	2.2 ± 2% kΩ, 0.5W, THICK FILM	R.S. COMPONENTS LIMITED
GRID WIRE	18 GAUGE TINNED COPPER WIRE	R.S. COMPONENTS LIMITED
CONDUCTING PAPER	"ANAPLOT" PAPER (TELEDELTOS TYPE SPECIFICALLY FOR ANALOGUE WORK)	SENSITISED COATINGS LIMITED
SILVER PAINT	ELECTRICALLY CONDUCTING	SENSITISED COATINGS LIMITED

TABLE 4.1 MAIN ELECTRICAL COMPONENTS

ROLL NO.	RESISTANCE/SQUARE kΩ	
	"IN ROLL"	"ACROSS ROLL"
1	1.138	1.018
2	2.365	2.615
3	2.365	2.740

TABLE 4.2 RESISTANCE/SQUARE OF ANAPLOT PAPER

PLATE 4.1 MKI ANALOGUE GRID CONNECTION /
PLATE 4.2 DETAIL OF MKI ANALOGUE FIELD

PLATE 4.1 MKI ANALOGUE GRID CONNECTION /
PLATE 4.2 DETAIL OF MKI ANALOGUE FIELD

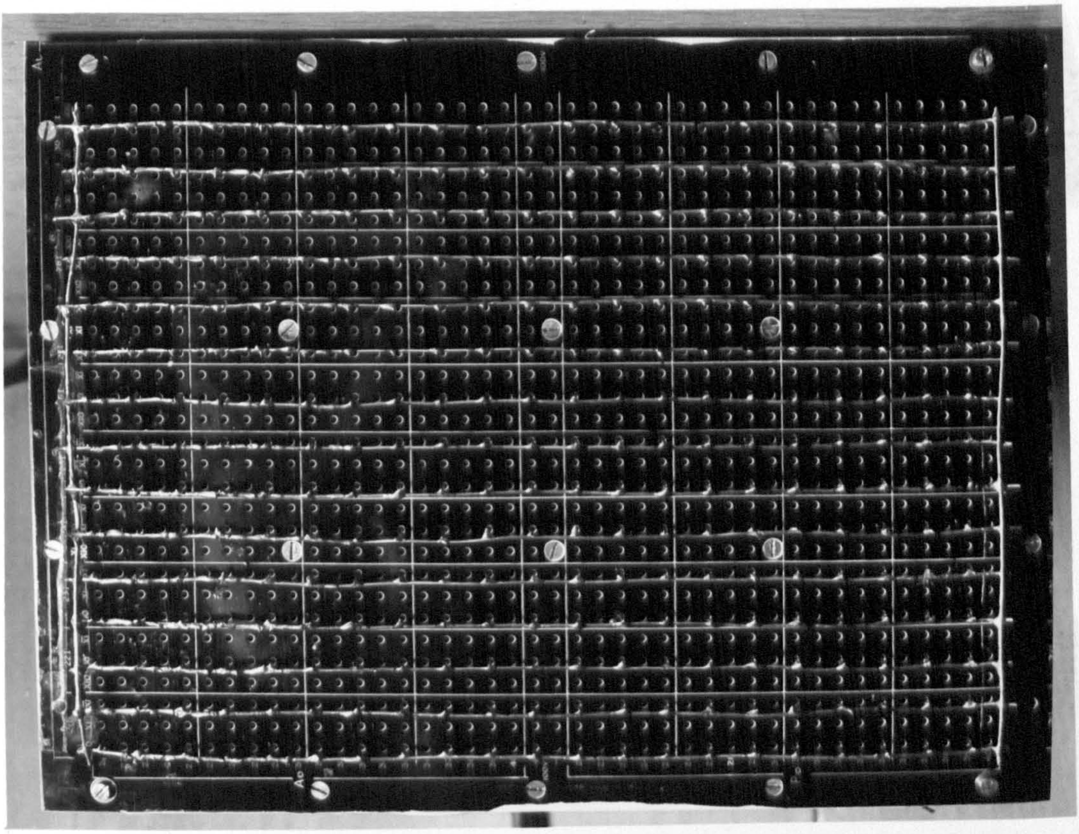

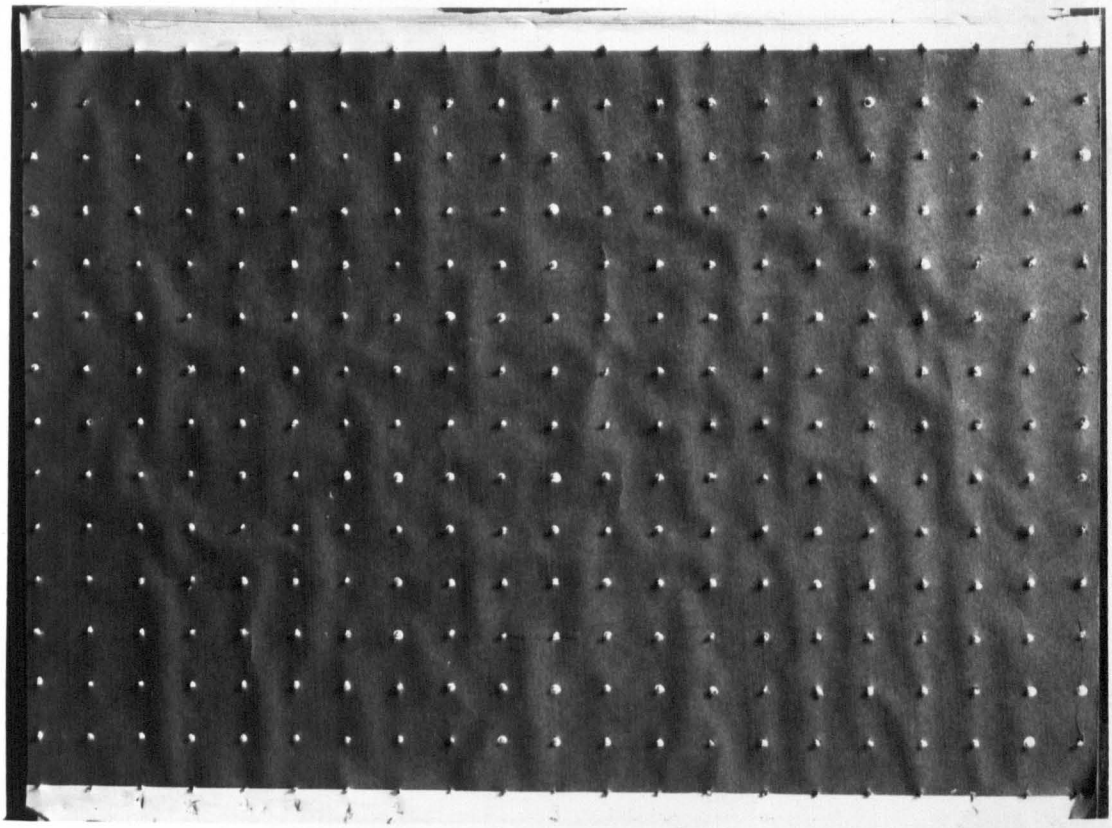

and the boundary conditions selected were

$$\text{at} \quad x = 0, \qquad V = V_o$$
$$x = \ell \qquad V = 0$$

To set up this problem on the analogue, two parallel strips of silver paint were applied to the Anaplot paper. To provide a suitable range of x, the full width of the field was used. Since there were fifteen resistors across the width of the field,

$$\ell = 14h$$

where h is the analogue spacing.

To ensure that the field between the strips was 1-D, the strips were applied along the full length of the analogue. The experimental arrangement is shown in Fig. 4.5.

The two strips were connected (with wires stapled to the paper and coated with silver paint) across the terminals of a regulated DC supply (Multireg 731, manufactured by Weir Electronics Ltd.). The common grid connected to the analogue resistors was also connected to the -ve terminal of the power supply to provide the necessary leakage currents from the paper. The power supply was set to give an output of 10.00V DC (i.e. $V_o = 10.00$). A digital voltmeter (type TM 1450, manufactured by Solartron Ltd.) was used to make potential measurements between a probe held in contact with the analogue field and zero. Measurements were made at each resistor point lying in a perpendicular between the two boundaries i.e. at 15 points, the 1st and 15th being at the boundary potentials. This was repeated at each of five different sections along the length of the field as indicated in Fig. 4.5. A general view of the

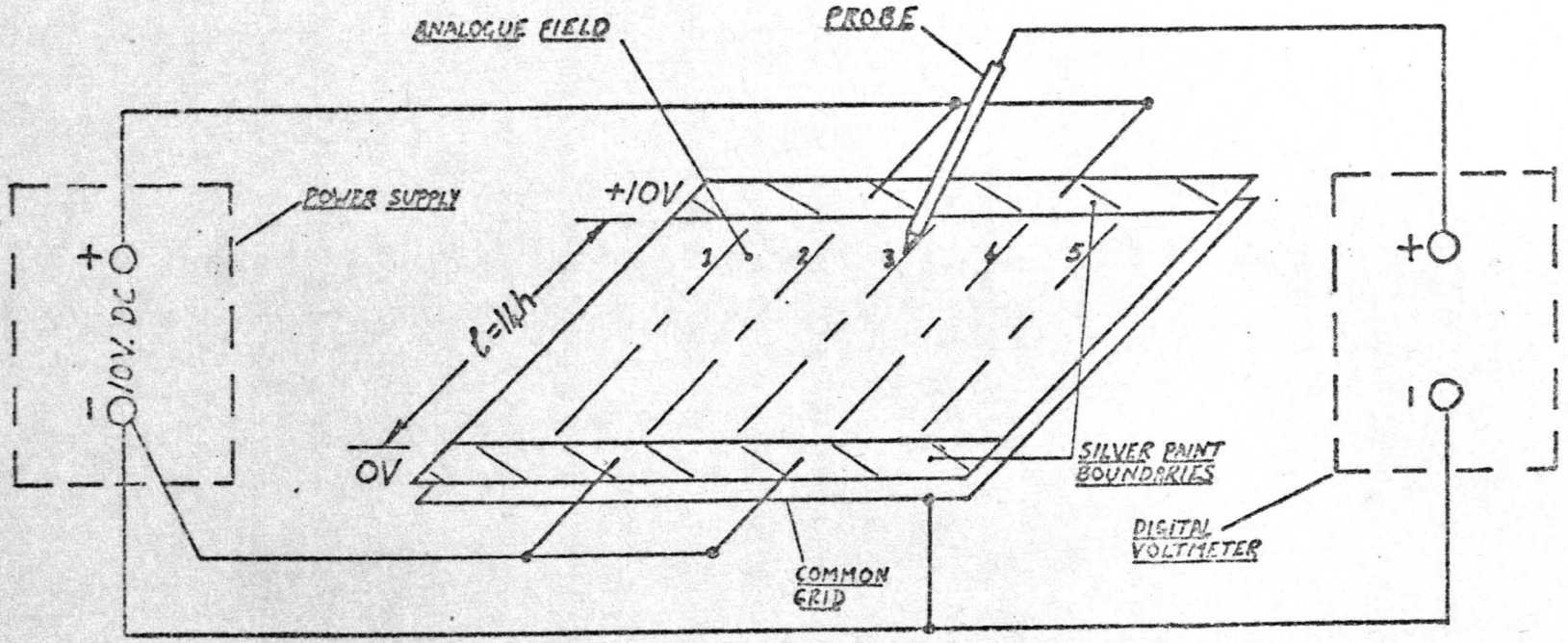

FIG 4.5 SCHEMATIC DIAGRAM OF ELECTRICAL CIRCUIT FOR EVALUATION TESTS

experimental arrangement is shown in Plate 4.3.

For this test, paper from roll 1 was used with the "in roll" direction corresponding to the x direction. Thus from Table 4.2.

$$\frac{\rho}{R} = \frac{1.138}{2.2} = 0.517$$

It can readily be shown that the analytic solution of equation 4.10 with the above boundary conditions is given by

$$V = 10. \frac{\sinh\left[\sqrt{\frac{\rho}{R}}(14-x)\right]}{\sinh\left[\sqrt{\frac{\rho}{R}}.14\right]} \qquad (4.11)$$

For the value of $\frac{\rho}{R}$ quoted above, this theoretical distribution is shown in Fig. 4.6 compared with the experimentally derived curve. The experimental value used at each 'x' is the average value of the measurements made at each of the five sections along the length of field. While the two curves show a good agreement in form, there is, in fact, a consistent divergence with increasing x. Due to the small values of potential involved at $x > 7$, this is not clearly shown in Fig. 4.6 but is evident if the same curves are plotted logarithmically as shown in Fig. 4.7. It is evident from this divergence and from the general similarity in nature of the two curves that the value of $\frac{\rho}{R}$ used in the theoretical calculation is too large. In using the quoted value of ρ, it is assumed that the connection of the resistors to the paper has no effect on the resistance per square of the paper. This is somewhat unrealistic as the finite area of each spot of silver paint, although small, has the effect of reducing the resistance of the paper between each

PLATE 4.3 MKI ANALOGUE: EXPERIMENTAL ARRANGEMENT

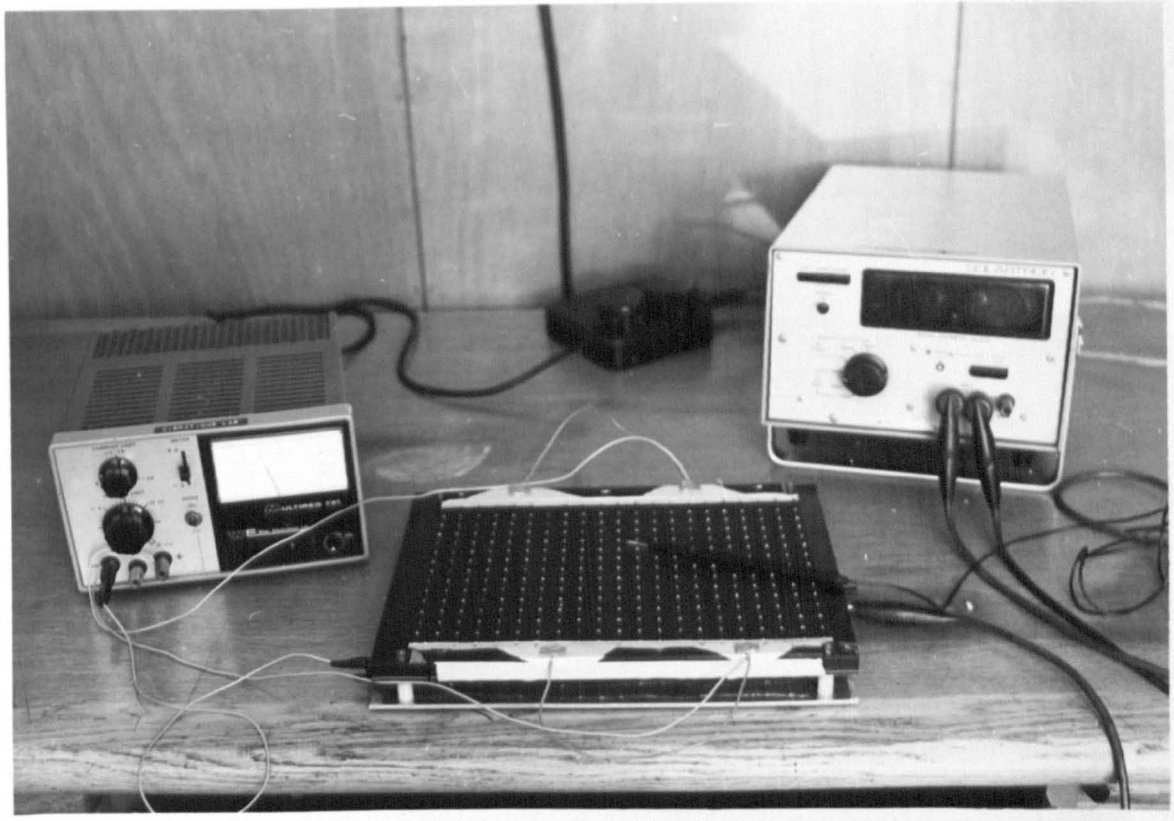

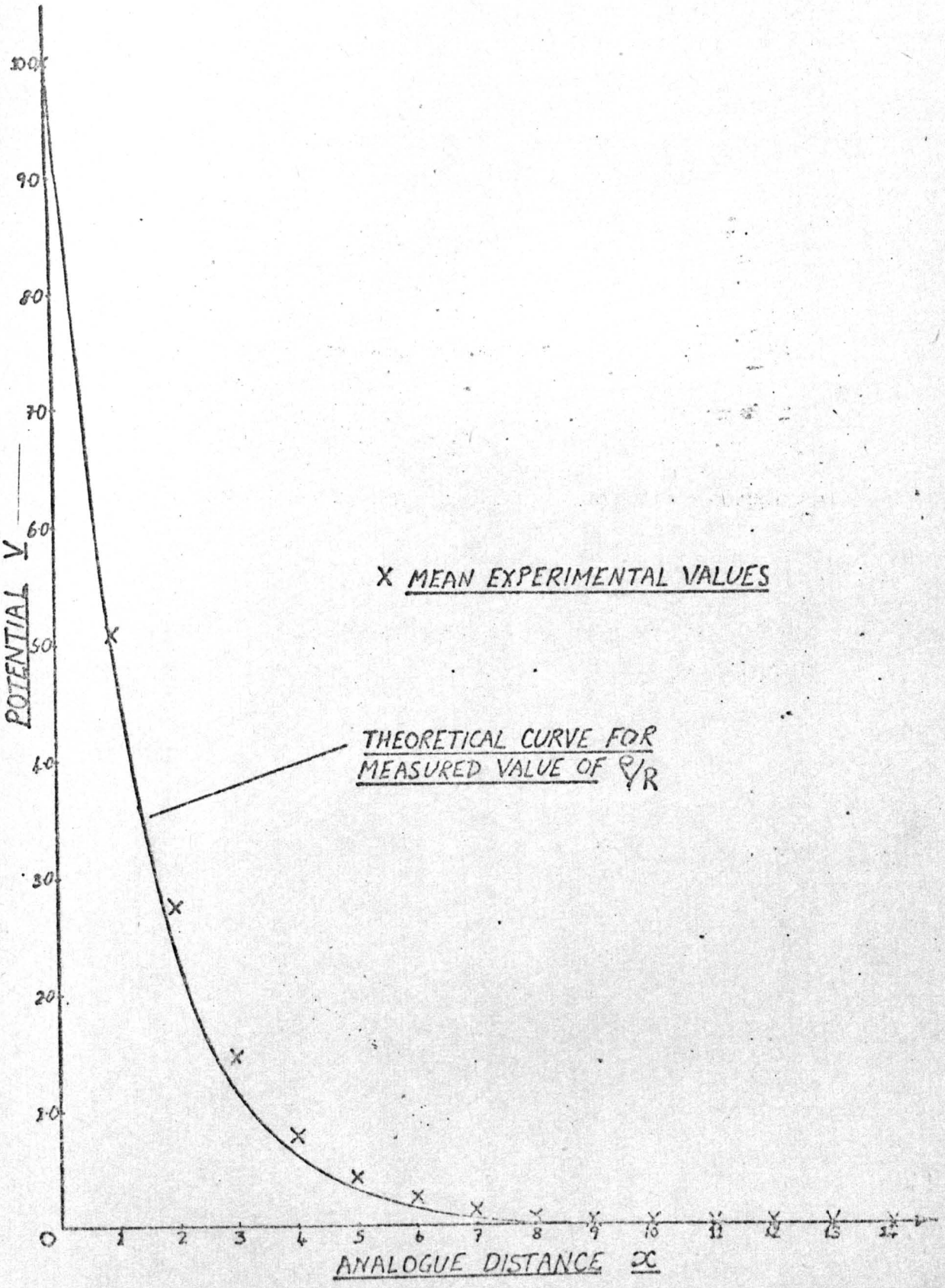

FIG 4·6 MkI ANALOGUE EVALUATION

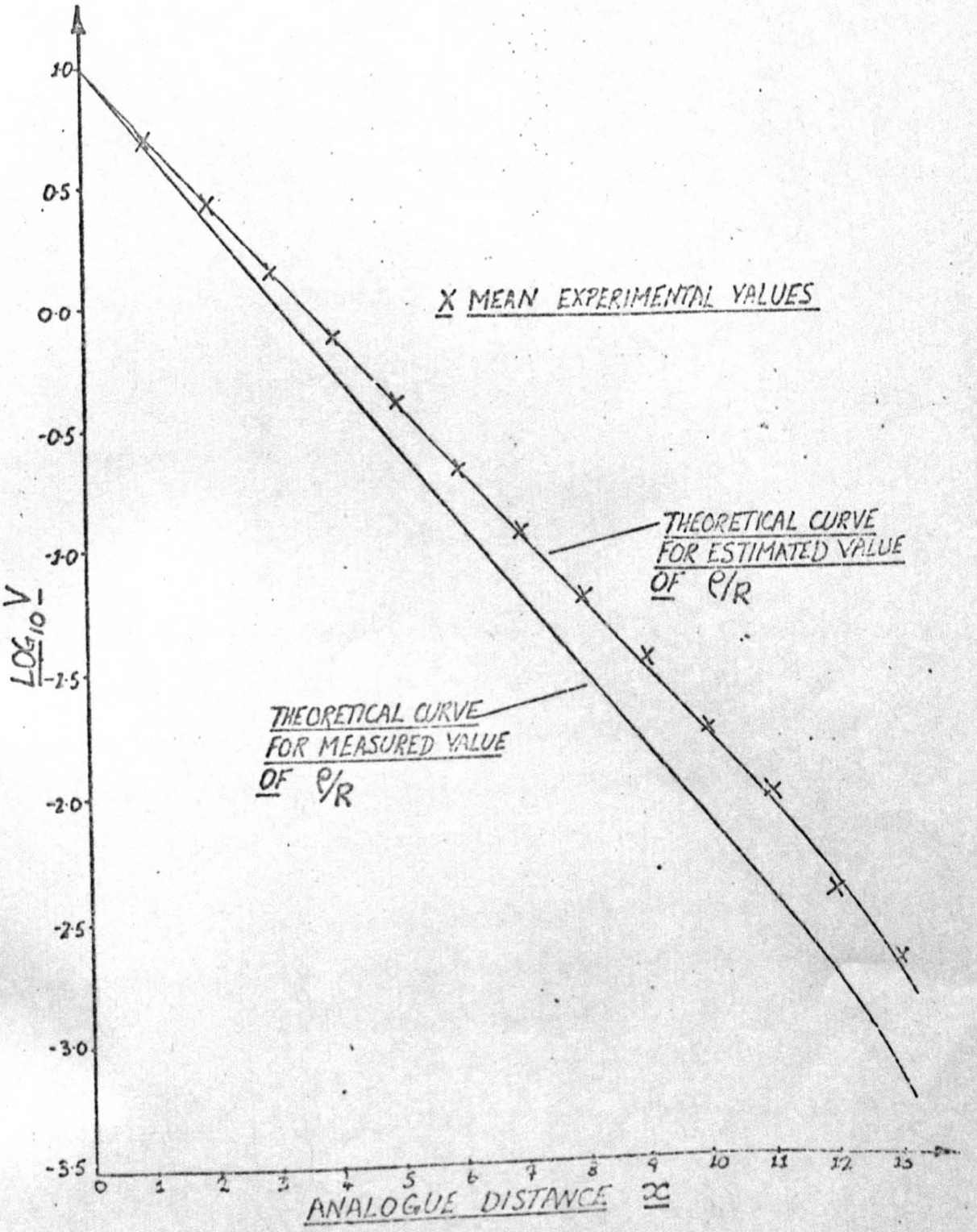

FIG 4·7 Mk I ANALOGUE EVALUATION

connection and hence of reducing the effective resistance per square. To obtain an estimate of the effective value of $\frac{\rho}{R}$, the following procedure was adopted.

Consider the central difference approximation for $\frac{\partial^2 V}{\partial x^2}$ applied to equation 4.10. If the node spacing is also h and V_1 and V_2 are the potentials at the nodes "above" and "below" the ith node respectively, then equation 4.10 becomes

$$\frac{1}{h^2}(V_1 + V_2 - 2V_i) - \frac{\rho}{Rh^2}.V_i = 0$$

On re-arranging this gives

$$\frac{\rho}{R} = \frac{V_1 + V_2}{V_i} - 2 \qquad (4.12)$$

By substituting the experimental values for V_1 and V_2 at each node i in equation 4.12, values for $\frac{\rho}{R}$ throughout the field were obtained. The distribution of these values about the arithmetic mean value of 0.4033 is shown in Fig. 4.8. The theoretical curve using this value of $\frac{\rho}{R}$ is also shown in Fig. 4.7.

The results showed an excellent agreement between the experimental points and the theoretical curve plotted for the estimated value of $\frac{\rho}{R}$. For most of the results plotted the deviation of the experimental values was less than 5%, only one value deviating by more than 10% from the theoretical value. This indicated that the above technique for estimating the analogue factor $\frac{\rho}{R}$ is extremely useful despite its approximate nature. It also showed that the analogue field was a good model of equation 4.10 (i.e. a ϕ equation). Comparison of the results for each section showed that the analogue

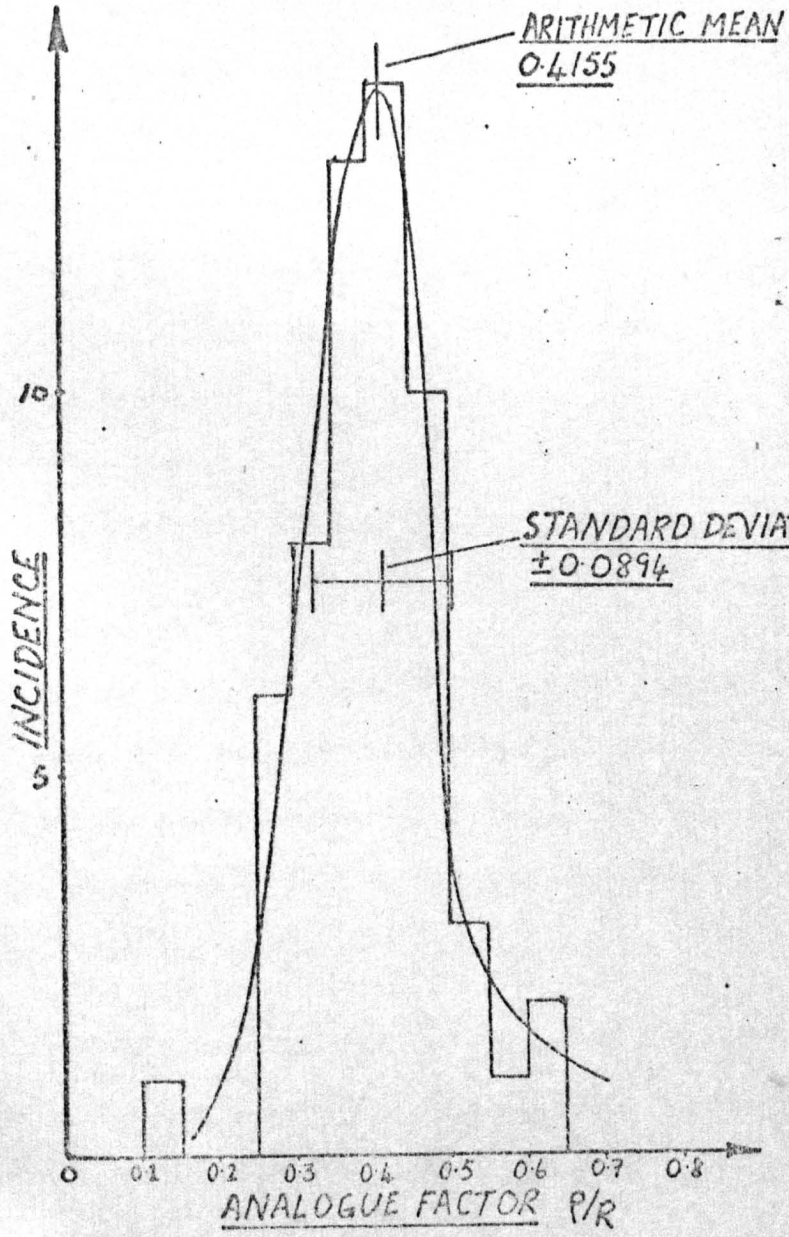

FIG 4·8 DISTRIBUTION OF ESTIMATED VALUES OF ANALOGUE FACTOR P/R

was substantially 1-D, the largest deviation from the mean value at any value of x being less than 12%. The largest deviations were invariably found at either sections 1 and 5 (see Fig. 4.5), these being subject to edge effects. This is shown in the equipotential plot in Fig. 4.9. The equipotential lines were plotted using an Alpha PR Field Plotter manufactured by Sensitised Coatings Ltd. This device detected the null-point when the probe potential balanced a pre-set potential and caused a spark to pass between the probe tip and the paper leaving a small mark on the paper. By varying the pre-set potential, equipotential lines were plotted on the paper. The analogue field connected to the plotter is shown in Plate 4.4.

It was not, however, possible to use the plotter for actual measurements as it had insufficient resolution at potentials less than 1% of the maximum potential. While this is normally sufficient for most applications, in the case just described, approximately half the field lay within this range.

This highlighted one disadvantage of the Mk I analogue. While very good agreement with theory was obtained for readings down to 0.1% of the maximum potential and reasonable agreement (i.e. within 12%) down to 0.05%, it was felt that this was exceeding the resolution which could be reasonably expected of the analogue design.

Before considering the application of the analogue to the welding problem, it was, therefore, decided to construct a second analogue on a similar principle but with a reduced value of $\frac{\rho}{R}$ in an attempt to overcome this difficulty.

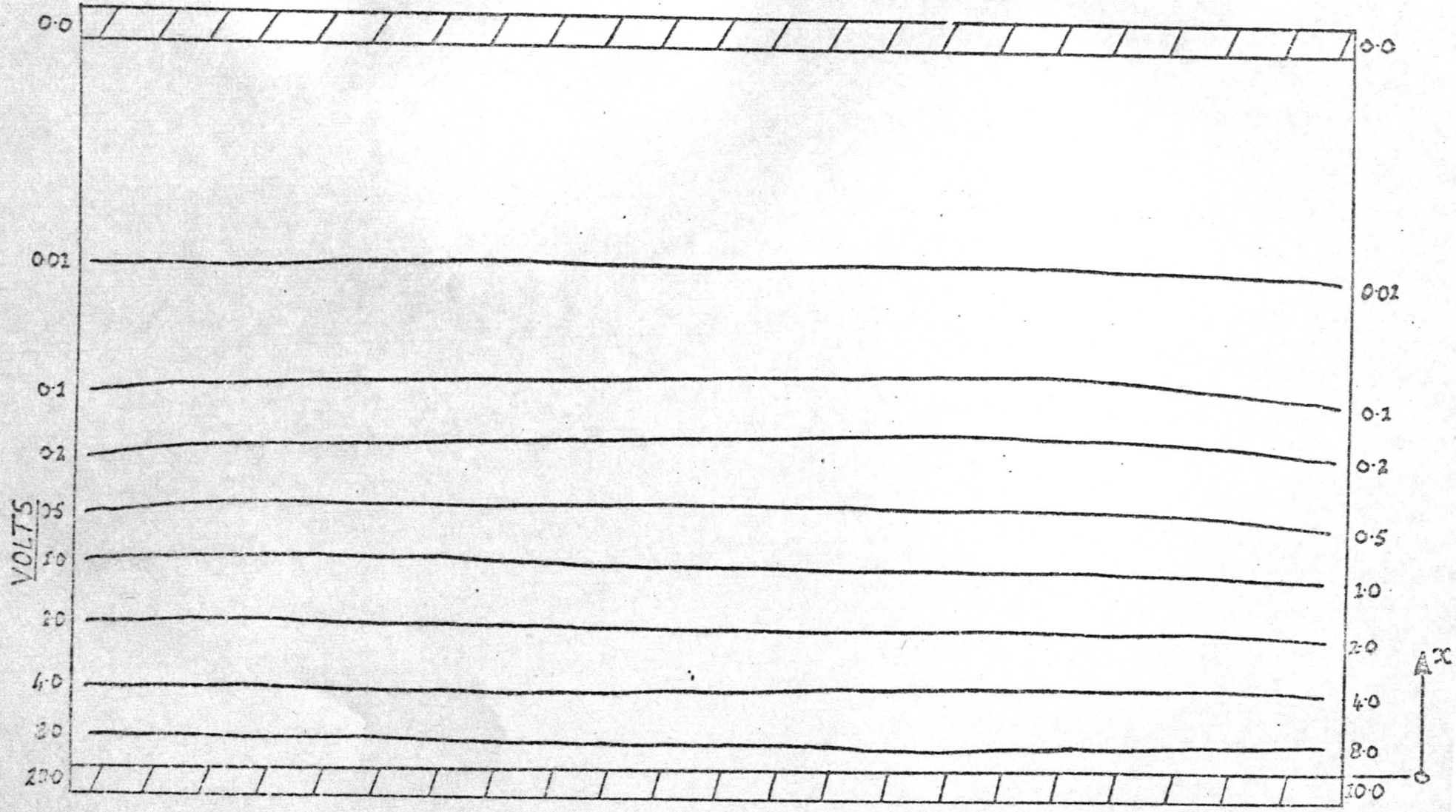

FIG 4·9 MkI ANALOGUE EVALUATION : EQUIPOTENTIAL PLOT

PLATE 4.4 MK1 ANALOGUE CONNECTED TO ALPHA PR PLOTTER

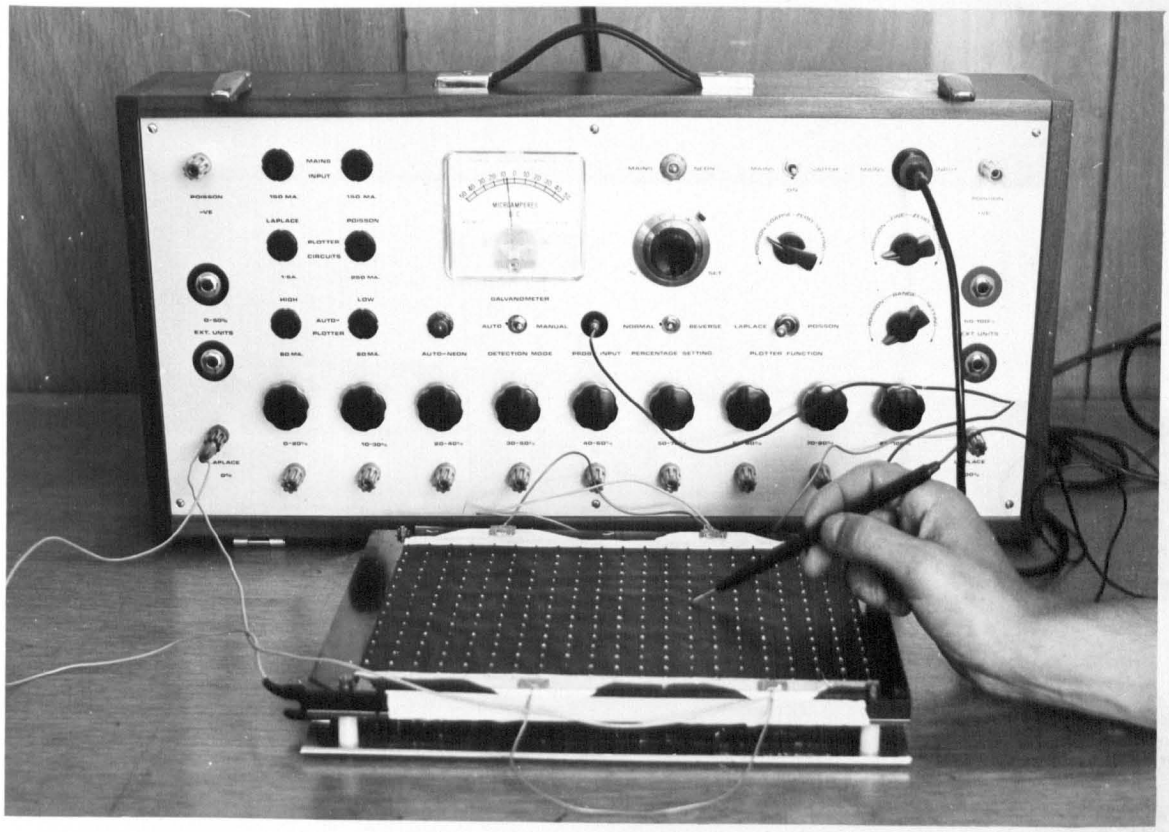
MAINS INPUT
150 MA.
150 MA.
LAPLACE
POISSON
PLOTTER CIRCUITS
1·5A.
250 MA.
HIGH
LOW
AUTO-PLOTTER
50 MA.
50 MA.
MICROAMPERES
GALVANOMETER
AUTO-NEON
AUTO
MANUAL
DETECTION MODE
NORMAL
REVERSE
LAPLACE
POISSON
PLOTTER FUNCTION
0-50%
EXT. UNITS
0-20%
10-30%
20-40%
30-50%
40-60%
70-90%

4.6) Mk II Analogue : Design, Construction and Evaluation

Design

The application of the conductive sheet, ϕ field analogue to the welding problem was discussed in general terms in section 4.3. There are, however, certain specifications which are required in the design of a ϕ field analogue for this application.

For the welding problem, the shape of the weld pool boundary would be painted onto the analogue with silver paint. Account would have to be taken of the required variation in potential along the length of the "pool" on the analogue (see section 4.3). Measurements of analogue potential would then be made in the immediate vicinity of the "pool" to correspond with the HAZ of the actual weld.

It is, therefore, necessary that the analogue spacing h as determined by the design formula (equation 4.8) should be such that the weld pools can be suitably accommodated on the analogue field. That is, for a fixed value of $\frac{\rho}{R}$, the distance of real space represented by the resistor spacing will vary with $\frac{V}{\alpha}$. Thus, the value of $\frac{\rho}{R}$ must be selected to correspond with the welding parameters to be considered.

In order to make meaningful predictions of the thermal field in the HAZ, it is also necessary that the required potential measurements in the corresponding analogue region should be as accurate as possible. Since this would be a region of large potential gradient (being in the vicinity of the high potential "pool" boundary), the limiting factor on this accuracy is not the accuracy of the

measuring instrument, but the resolution of the analogue field itself. From the discussion on the resolution of the Mk I analogue in the previous section, this would indicate that the selected value of $\frac{\rho}{R}$ should be as small as possible.

As discussed in the next chapter, it was decided to restrict the study to the single pass, full penetration welding of thin mild steel plate using the Tungsten Inert Gas (TIG) process. For this purpose, a special welding rig was constructed to provide the necessary data for analogue analysis. For the purposes of this discussion, however, the relevant data is the range of available welding speeds v. The rig design allowed for $0.04 < v < 0.4$ cm/s. However, for the welding of $\frac{1}{8}$" (3.2 mm) thick, mild steel plate used in the tests, speeds of less than 0.1 cm/s were not encountered. Using the value of $\alpha = 0.075$ cm^2/s for mild steel quoted by previous investigators (4,9) and substituting in the design formula (equation 4.8) gave the range of analogue spacing h in terms of $\frac{\rho}{R}$.

i.e. $$0.375\sqrt{\frac{\rho}{R}} < h < 1.5\sqrt{\frac{\rho}{R}} \text{ cm} \qquad (4.13)$$

It should be noted that the smallest value of h occurs at the highest welding speed and conversely.

To keep the value of $\frac{\rho}{R}$ as low as possible, it was decided to use paper from Roll 1 (see Table 4.2) which had the lowest value of resistance/square and to select the resistance value of R = 7.5 kΩ on the same resistor spacing of 12.5 mm as the Mk I analogue. Although, as shown in the previous section, the actual value of ρ is dependent upon the silver paint connections between the paper and

the resistors, the resulting range of the analogue spacing h can be estimated by assuming ρ = 1.0 kΩ per square. Substituting for these values of ρ and R in 4.13 gives

$$0.14 < h < 0.55 \text{ cm}$$

This range of h was found to be compatible with the pool sizes obtained from experiment (see Chapter 6).

Construction

This provided the necessary data for the construction of the Mk II analogue. The same overall field size of 175 x 250 mm was used but, to increase the analogue resolution in the region surrounding the pool boundary, it was decided to reduce the resistor spacing over this region by a factor of 2 i.e. from 12.5 mm to 6.25mm. The location of resistors over the analogue field is shown by crosses in Fig. 4.10. Since the pool shapes encountered in the tests proved to be essentially symmetric about the weld $\mathcal{C}$, the heat flow was also assumed to be symmetric about the $\mathcal{C}$. For this reason, only half of the actual field was modelled by the analogue and the resistor layout shown in Fig. 4.10 was designed for AB to correspond with the weld $\mathcal{C}$.

For continuity over the analogue field, it can be seen from equation 4.7 that

$$\frac{1}{h^2} \cdot \frac{\rho}{R} = \text{constant}$$

where, in this case, h is the resistor spacing.

Assuming that for the same sheet of paper ρ = constant then

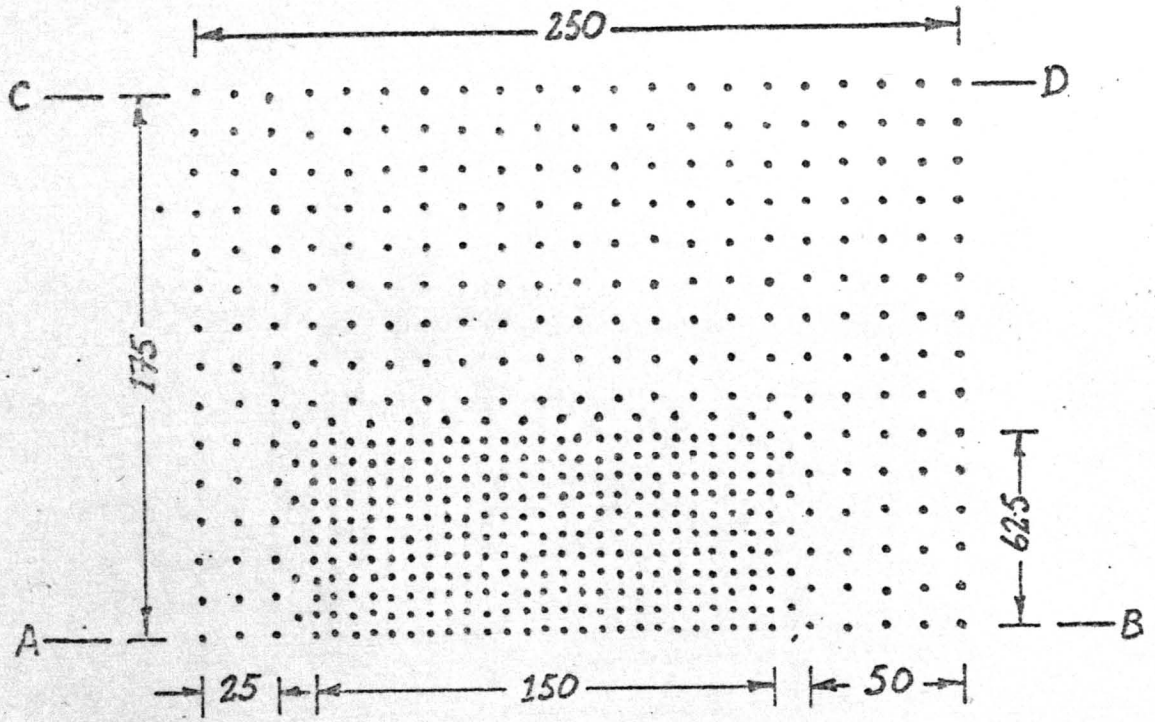

ALL DIMENSIONS IN mm.

FIG 4·10 PLAN VIEW OF MkII ANALOGUE RESISTOR LAYOUT

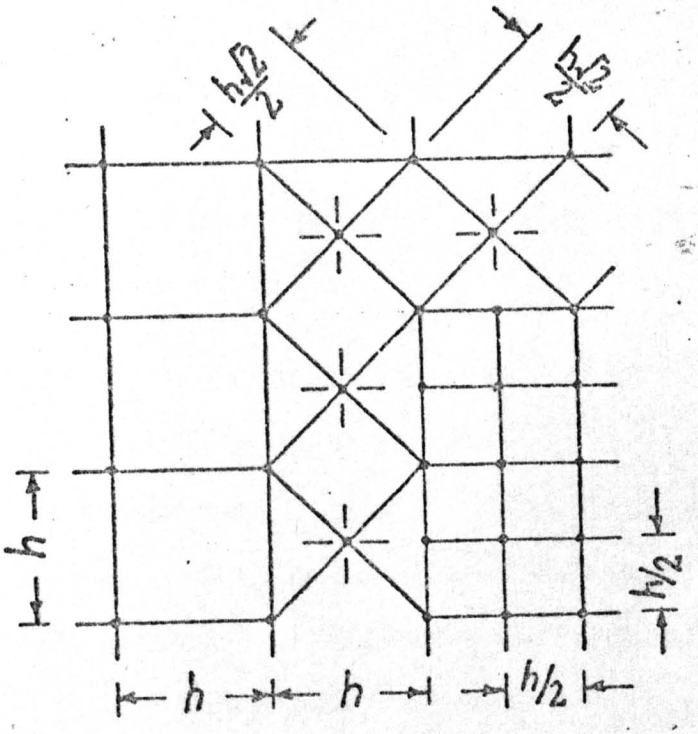

h = 12·5 mm.

FIG 4·11 RESISTOR SPACING SHOWING TRANSITION REGION

it can be seen from Fig. 4.11 that

$$\frac{R_\ell}{R_s} = \left(\frac{h}{2} \cdot \frac{1}{h}\right)^2 = \frac{1}{4}$$

where R_ℓ is the resistance value over the coarse spacing and R_s is the resistance value over the fine spacing. For R_ℓ = 7.5 kΩ, the required value of R_s is therefore, 30 kΩ. A similar argument gives the resistance value of 15 kΩ in the transition zone between the coarse and fine regions.

Using these resistance values and following the layout and spacings given in Figs. 4.10 and 4.11, the Mk II analogue was constructed in a similar way to the Mk I. Due to availability of the required values, ± 2%, 0.5W metal oxide resistors (supplied by RS Components Ltd.) were used. These were slightly larger than the thick film type used previously but they were located in the 1 cm thick Tufnol block in a similar way as shown in Fig. 4.12. Instead of securing the resistors with a clamping plate, however, they were simply glued to the block using "Araldite" epoxy resin. The bottom ends of the resistors were soldered to the common grid as before. The Tufnol block was mounted on a wooden frame which served not only to protect the analogue but also to provide a suitable backing board to whic the paper could be secured. The electrical connections to the boundaries were made by pinning wires to the painted boundaries using drawing pins pressed firmly into the board. A general view of the Mk II analogue field with an imposed pool boundary is shown in Plate 4.5.

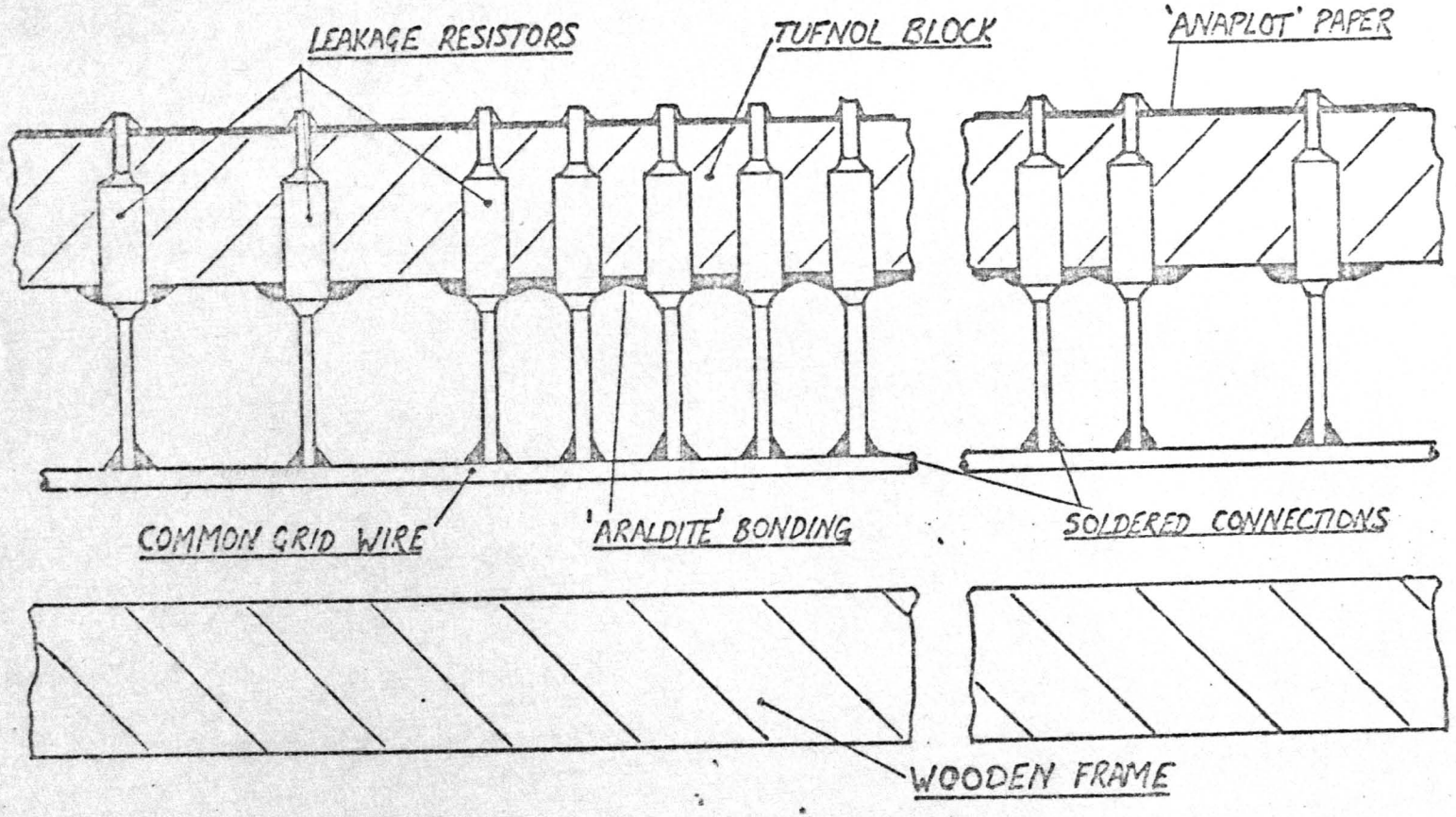

FIG 4.12 SECTION THROUGH Mk II ANALOGUE SHOWING DETAIL OF CONSTRUCTION

PLATE 4.5 MKII ANALOGUE FIELD

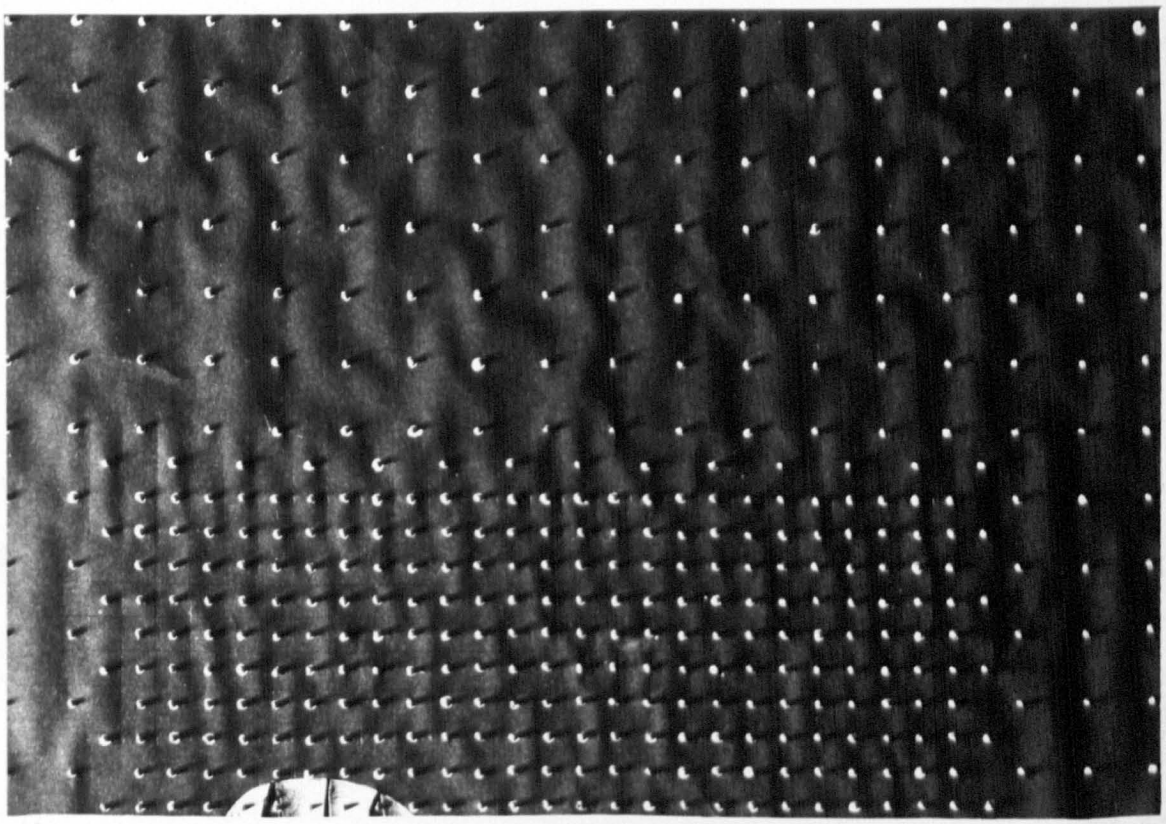

Evaluation

The solution to the 1-D problem discussed in section 4.5 was again used to evaluate the Mk II analogue and to estimate the value of $\frac{\varrho}{R}$.

With reference to Fig. 4.10, a boundary was painted along edge AB and set at + 10V with respect to the boundary painted along CD. The electrical apparatus was identical with that used previously and shown schematically in Fig. 4.5. Measurements of potential were made at each of 15 equally spaced resistors lying on a perpendicular between each boundary. This was repeated along each of six sections along the length of the field.

The value of the field parameter was estimated in the same way as before and found to be 0.1327. Using this value, the theoretical curve (equation 4.11) was plotted as shown in Fig. 4.13. The experimental points shown for comparison are the average of the readings from the six sections at each value of x. For each point considered the % age deviation from the mean value for each of the sections considered was less than 10%. Invariably, the maximum deviation from the mean occurred at either of the extreme sections which were subject to edge effects. With the exception of the two lowest values (i.e. x = 12,13) the deviation of the mean experimental values from the theoretical curve was less than 6%. This is shown more clearly in the logarithmic plot, Fig. 4.14, and demonstrates the good agreement between the experimental points and the theoretical curve.

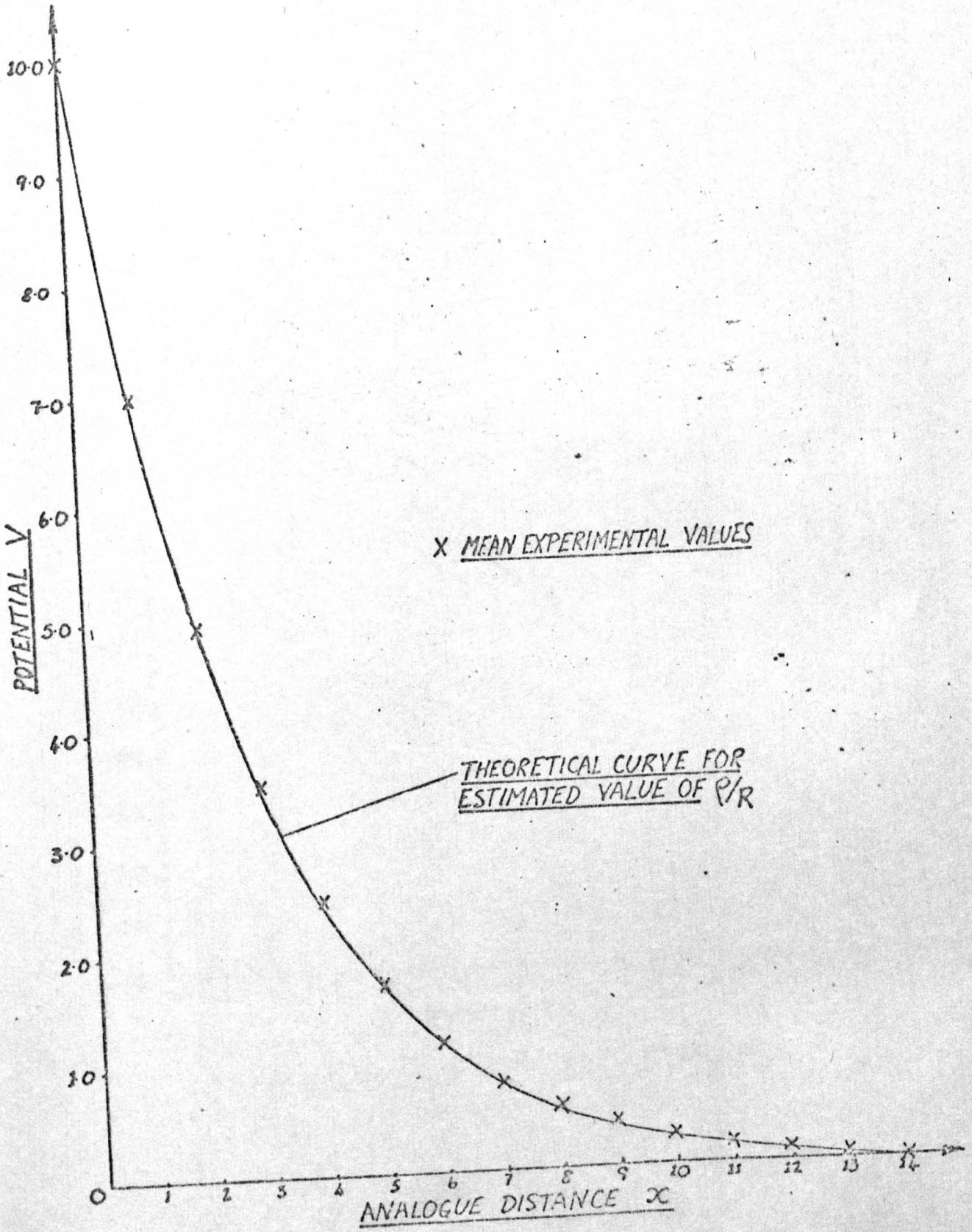

FIG 4:13 Mk II ANALOGUE EVALUATION

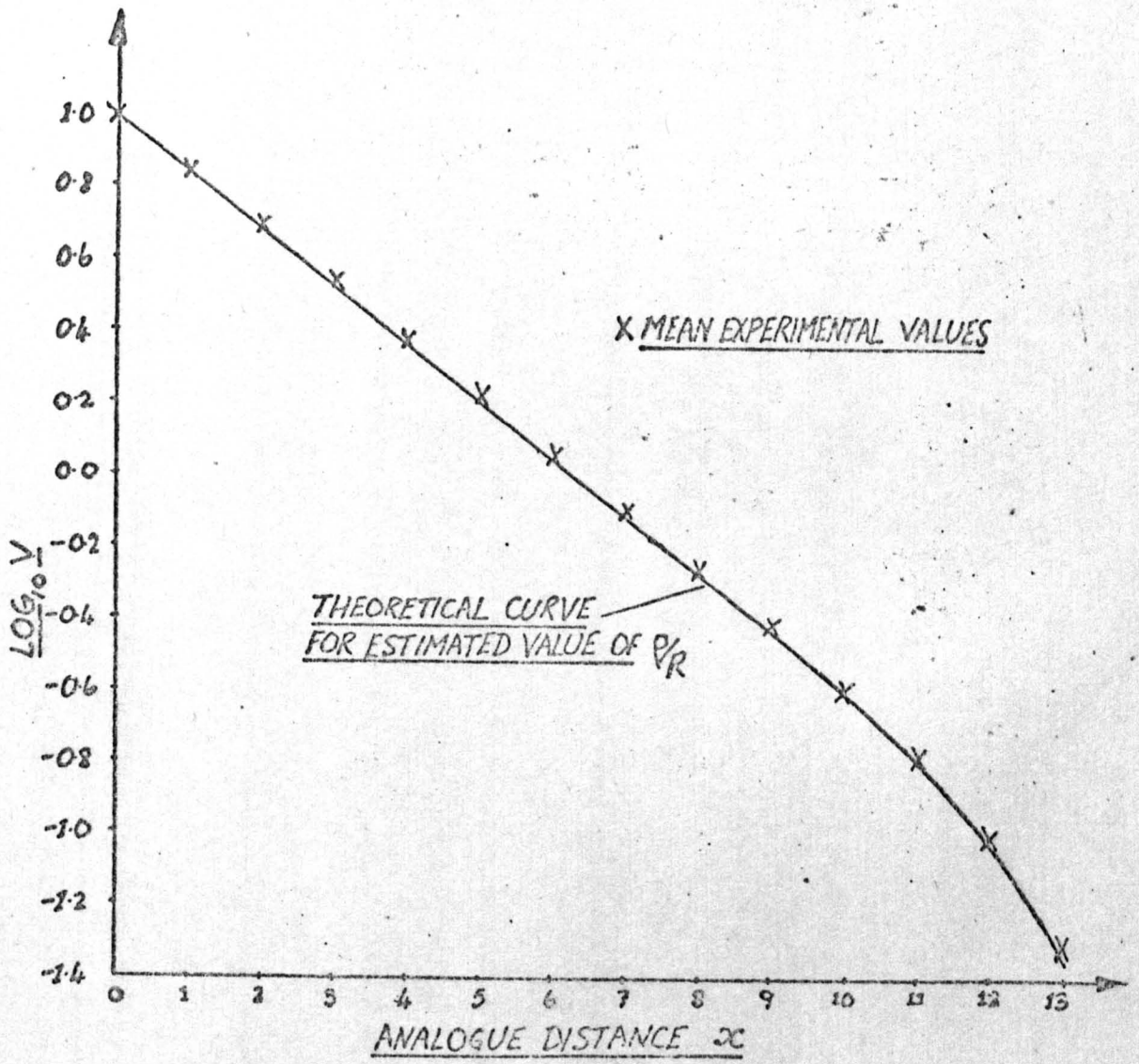

FIG 4·14 Mk II ANALOGUE EVALUATION

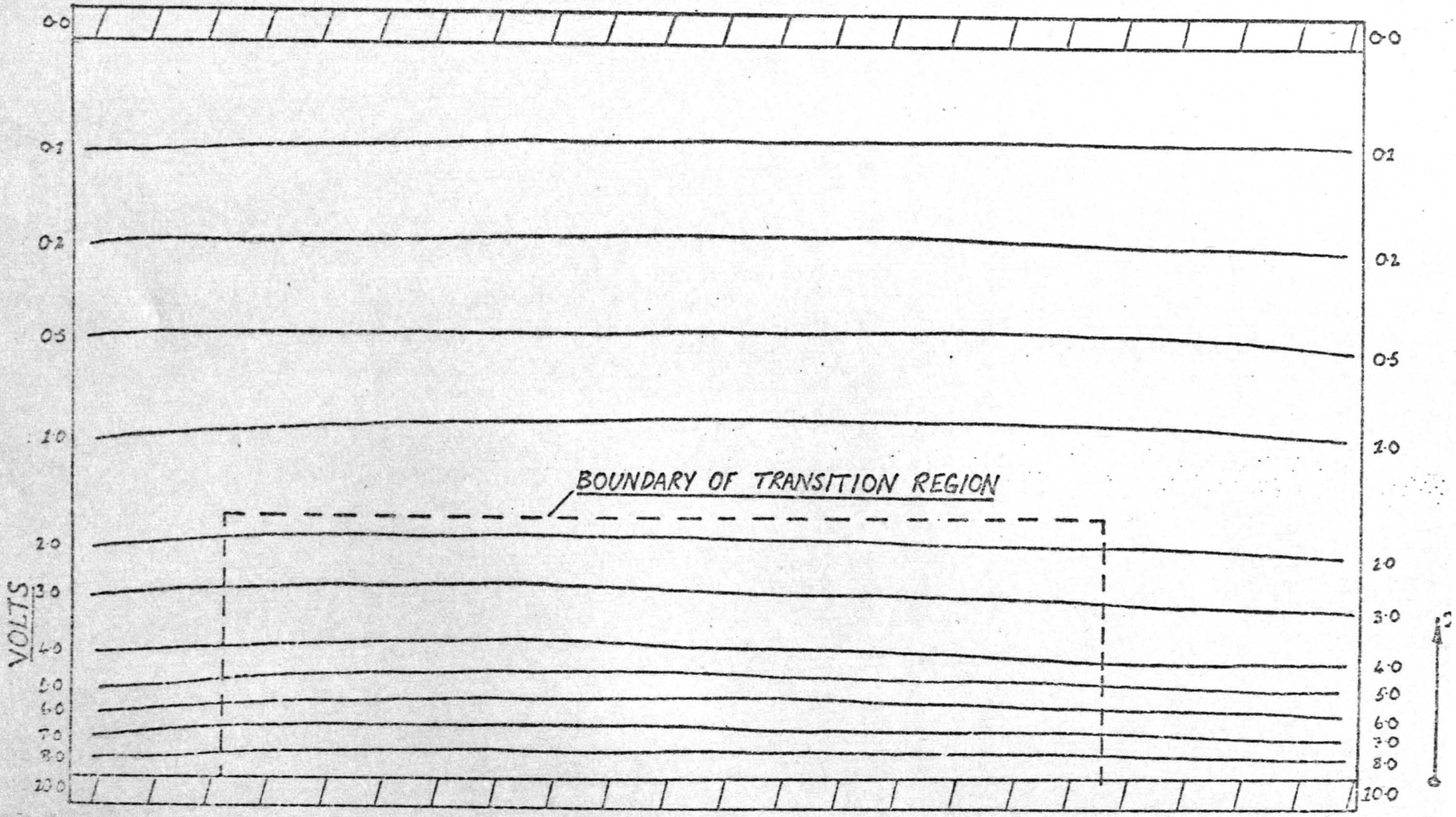

FIG 4·15 MkII ANALOGUE EVALUATION : EQUIPOTENTIAL PLOT

The results also indicated that there was no measurable effect introduced by the transition region separating the coarse and fine resistor spacing. The transition region occurs at $5 \leqslant x \leqslant 6$ on Fig. 4.13 and 4.14 and the smooth behaviour of the experimental points on either side of this region is evidence of the negligible effect introduced by the transition region. This is also demonstrated by the linearity of the equipotentials shown in Fig. 4.15. This plot was again made using the Alpha P.R. Plotter.

These results demonstrated the accuracy of the Mk II analogue in solving a simple 1-D ϕ field problem. It remained to test its value in predicting the thermal field during welding. This is discussed in Chapter 6.

CHAPTER 5

THE WELDING TEST RIG : DESIGN AND CONSTRUCTION

5.1) Introduction

Having constructed and successfully tested a ϕ field analogue, it remained to test its application to predicting the thermal field in the HAZ during welding. To perform this test, a comparative series of experiments was proposed as outlined in the block diagram shown in Fig. 5.1

The shape of the weld pool from each test would be used, with the appropriate transformation, as the boundary condition on the Mk II analogue. The resulting ϕ field would be plotted and, using the inverse transformation, the corresponding thermal field in the HAZ predicted. This result would then be compared with the temperature measurements in the HAZ made directly during the welding test. The welding tests were, therefore, required to provide data on

i) weld pool shape and associated welding conditions

and

ii) temperatures in the HAZ during welding.

For such tests to be realistic, it was evident that the welding process should, as far as possible, also comply with the constraints and assumptions made in the design and construction of the Mk II analogue. It was, however, felt that such constraints should not involve a welding procedure that was too far removed from normal welding practice. To meet these somewhat conflicting ideals, it was necessary that

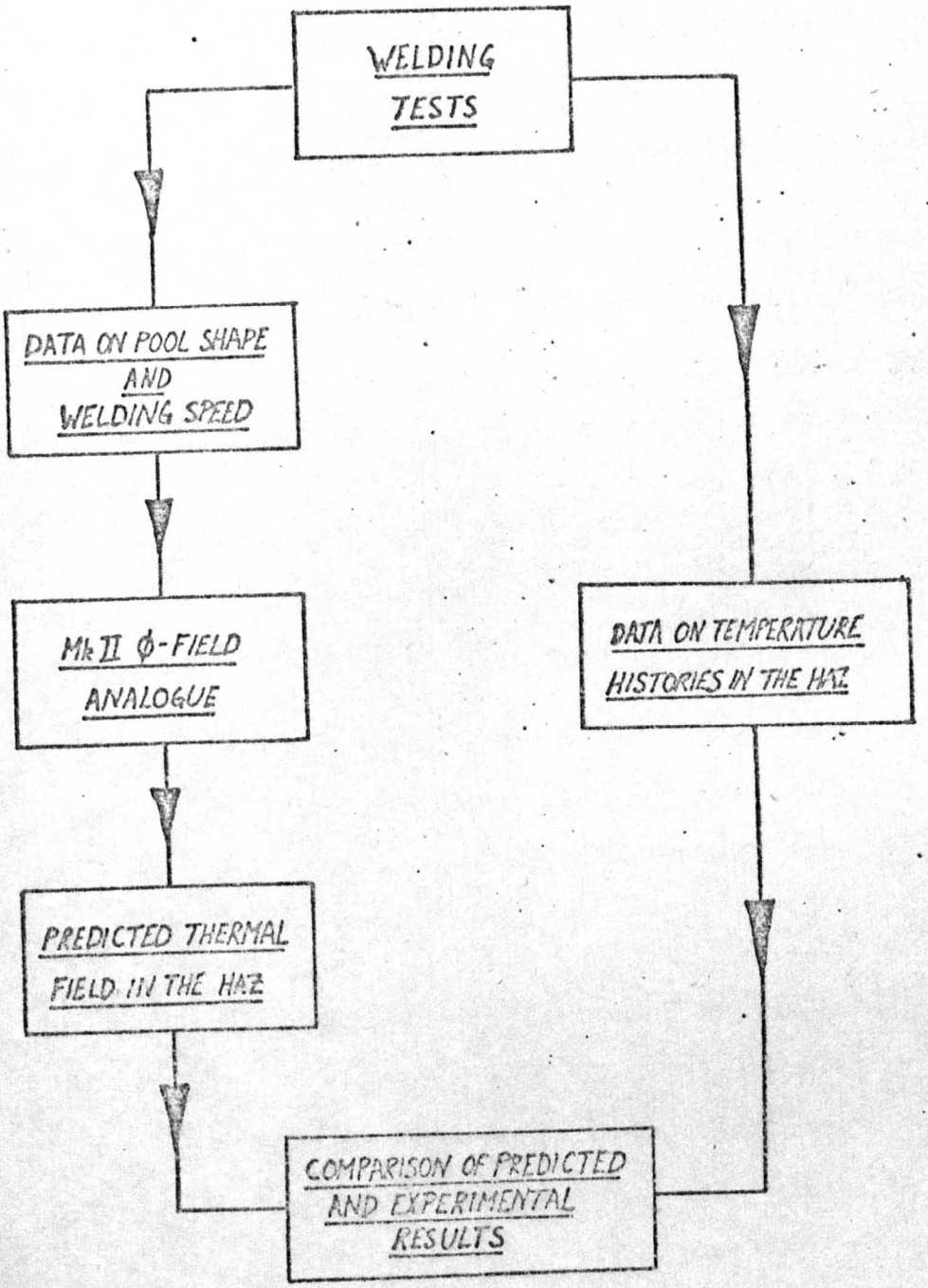

FIG 5·1 COMPARATIVE TEST PROCEDURE

i) the test welds be made at a constant speed along a straight line so that Rosenthal's equation (equation 1.2) would govern the quasi-static temperature distribution around the weld pool. (It was, of course, not possible to enforce the further condition that the thermal properties of the parent metal be independent of temperature)

ii) the weld pool (and hence the welding parameters) be maintained constant during the weld. Any fluctuations in the pool shape would introduce short term thermal transients in the parent metal and would, therefore, invalidate the quasi-static assumption.

iii) single pass, full penetration welding of thin flat plate be used to ensure that, as far as possible, the weld pool and, hence, the surrounding thermal field was 2-D.

To fulfill condition i), it was decided that a semi-automatic welding process should be used with the welding head mounted on a motorised carriage designed to travel in a straight line at a controlled speed.

To meet the controllability requirement of condition ii), a continuous electric arc process was felt to be most suitable. In fact, the non-consummable Tungsten Inert Gas (TIG) process was selected, using argon as the shielding gas. Since feed control equipment was not readily available, it was further decided that filler wire would not be used. This did not present a serious limitation since condition iii) restricted the tests to thin plate. Mild steel was chosen for the parent metal as being cheap and readily available and a plate thickness of 1/8" (3.2 mm) selected as this would provide a reasonable size of weld pool while maintaining the

2-D requirement. Following the suggestion of Roberts and Wells (18), the complete width of the plate was specified to be not less than 20d, where d is the maximum width of the molten pool. The length of the test plate was fixed by the traverse length of the welding rig (see section 5.4).

The detailed design of the welding rig, based on this specification, is described in the following sections.

5.2) General Description

The welding rig consisted basically of an argon-arc torch mounted on a controlled speed linear traverse assembly. The welding power was supplied to the torch from a standard commercially available power source. The traverse assembly was powered by a motor and gear box assembly and was mounted on a base plate supported on a "Dexion" frame trolley. A plan view showing the arrangement on the base plate is shown in Drawing 5.1*

The test plate was clamped onto a set of raised studs screwed into the base plate as shown in Drawing 5.2, View on A-A. The clamps and studs were arranged symmetrically about the weld axis. The distance between opposing clamps was 10cm, so that any chilling effect which they had on the test plate did not significantly affect the thermal field in the HAZ.

*Engineering Drawings 5.1, 5.2 and 5.3 are enclosed at the end of the thesis.

To record the temperature history of points in the HAZ during welding, thermocouples were located in the test plate. The thermocouple wires were passed, from the bottom surface of the test plate, between the supporting studs and connected to a terminal block mounted on the front panel of the trolley. The voltage output of the thermocouples was recorded on a y-t chart recorder.

The welding arc was struck between the electrode of the torch (cathode) and the test plate (anode). The torch was then passed along the length of the plate at constant speed. The progress of the weld could be viewed through a window (made from high density, ultra violet filter glass) mounted on a screen hinged to the front of the trolley.

A high velocity jet of argon from a nozzle mounted behind the torch was used to eject the molten metal from the weld pool at a predetermined point during a test weld. The shape of the resultant 'hole' specified the molten pool boundary.

A panel on the front of the trolley housed all the equipment necessary to control the progress of a weld. With a little practice, the operator could maintain a visual inspection of a test weld through the window, allowing him to make adjustments to the controls as necessary.

A general view of the power supply, argon supply and control valves, chart recorder and welding trolley (with the screen in position) is shown in Plate 5.1. The same general view with the screen removed to show the arrangement of the welding equipment on the trolley is given in Plate 5.2.

PLATE 5.1 WELDING TEST RIG WITH SCREEN IN POSITION/
PLATE 5.2 WELDING TEST RIG WITH SCREEN REMOVED

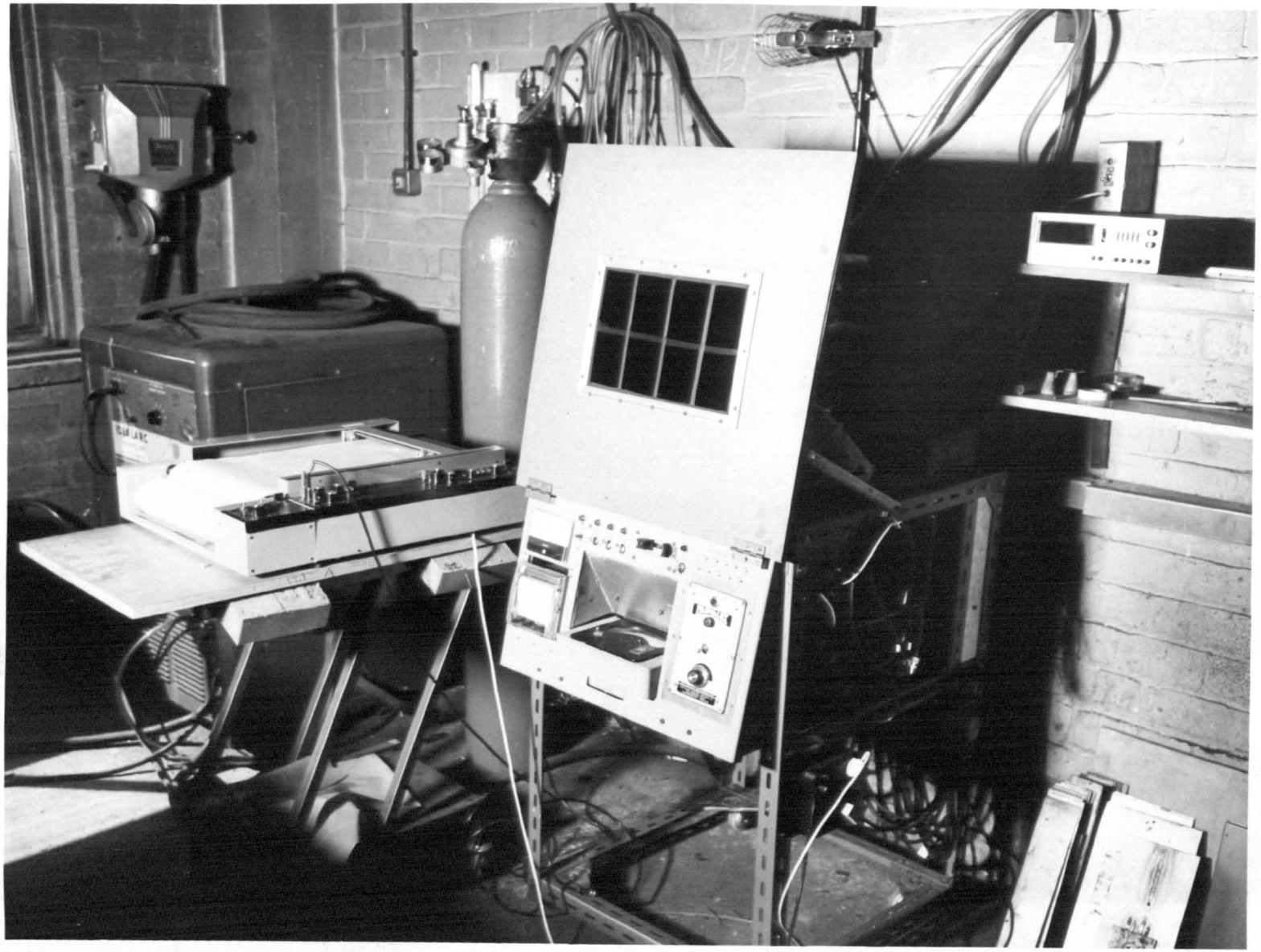

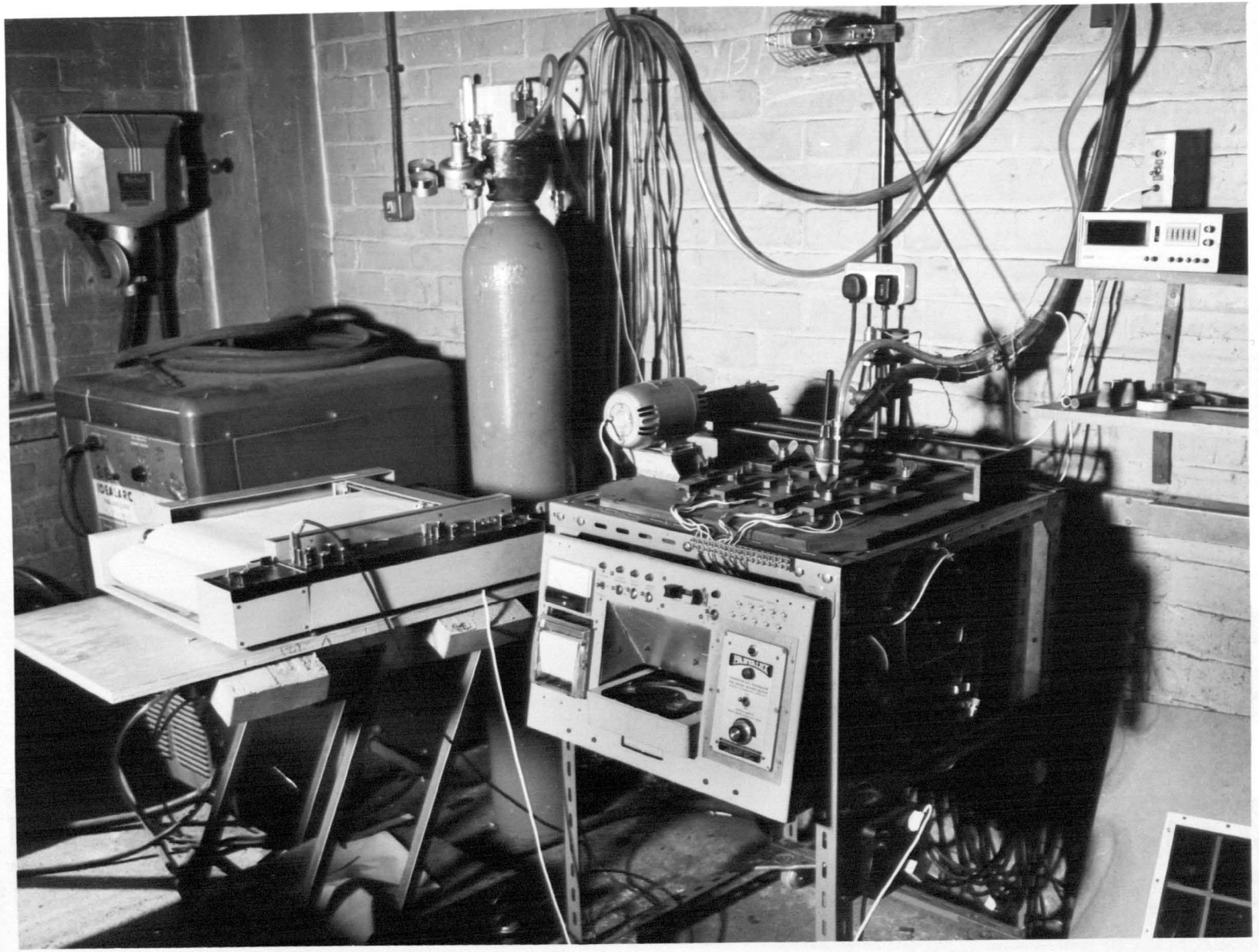

5.3 The Torch Carriage Assembly

A detail of this assembly is shown in Drawing 5.2, View on B-B. As shown, the handle of the welding torch was secured to the carriage assembly by a round clamp. This was designed to allow the torch to be rotated in a vertical plane about the clamp and, thus, to be swung clear of the test plate.

Adjustment of arc height was achieved by the vertical movement of a crosshead to which the torch clamp was attached. The crosshead, restrained by two parellel guide rods, was raised or lowered between two fixed crossheads by a lead screw of 2 mm pitch which was rotated manually by a calibrated knob at the top of the assembly. The circumference of the knob was marked off into forty divisions, each division corresponding to a vertical movement of the crosshead of 0.05 mm.

To set the arc height, the torch was clamped to the crosshead, as described above, such that the axis of the electrode was perpendicular to the surface of the test plate. By rotating the calibrated knob, the torch was lowered until the tip of the electrode was seen to just touch the surface of the test plate. Making a small allowance for backlash, the torch was then raised to the required arc height by turning the knob through the appropriate number of divisions. The crosshead was then locked in position by tightening a locknut on the lead screw. An arc height of 3.5mm was used throughout the tests.

As an additional facility to measure arc height, a linear displacement transducer was mounted on the assembly as shown. However, for the purpose of the welding tests, the arrangement described above was found to be adequate.

5.4 The Powered Traverse

The torch carriage assembly was mounted with linear ball bushings onto two guide rods lying parallel to the axis of welding. The carriage was propelled along these guide rods by a power screw attached to the lower fixed crosshead of the carriage. The power screw passed through the gear box which comprised a worm and worm wheel gear assembly. The centre of the worm wheel was threaded to accommodate the power screw so that as the worm wheel turned, the power screw was drawn, without rotating, through the centre of the worm wheel. The worm was connected, via a flexible coupling, to a 1/4 H.P., D.C., shunt motor. The worm and worm wheel gear had an overall reduction ratio of 50:1. The motor and gear box assembly is shown in Drawing 5.2, View on C-C.

Power to the motor was supplied, via a reversing switch (which reversed the direction of the motor and hence of the torch carriage assembly) from a mains operated control unit mounted on the front panel of the trolley. This unit served as both a rectifier and a speed control for the motor. Both the motor and the control unit were manufactured by Parvalux Electric Motors Ltd. With this arrangement, the carriage speed could be varied from 0.04 to 0.4 cm/s over a traverse length of 40 cm.

In order to make measurements of the carriage speed independent of the control unit, a separate timing system was devised. This consisted of a timer (manufactured by Racal Instruments Ltd.) activated on a "once on-once off" basis by a roller type micro-switch located on the lower fixed crosshead of the carriage assembly. The micro-

switch was activated by the roller passing over four pins set in two slides fixed to the base plate as shown in Drawings 5.1 and 5.2, View on B-B. The two pins on each slide were set at 5 cm apart so that, as the micro-switch passed over them, the time for the carriage to traverse 5 cm was recorded on the timer. The actual welding speed (i.e. the carriage speed) could then be easily calculated.

5.5 Welding Equipment

Power to the arc was supplied from an "Ideal Arc TIG 300/300 (manufactured by the Lincoln Electric Co.), power source. Operating in its medium range, this source was capable of delivering 165A, D.C. which was quite adequate for the welding of the thin mild steel plate used in the tests. The welding torch (Type W450, manufactured by BOC Ltd.) was connected directly to the power source which also supplied cooling water and argon to the torch. Thoriated tungsten electrodes, 3/32 ins. in dia., ground to a 45° point were used throughout the tests. The "earth" connection was made from a brass stud screwed into the base plate, via a heavy duty cable to the power source.

Having switched the power source on and selected the desired current range and polarity (for all tests, D.C., electrode -ve was used), the welding operation was controlled by a small unit mounted on the front panel of the trolley. This consisted of a spring loaded slide connected to the rack of a rack and pinion gear. The initial movement of the slide activated a micro-switch which in turn tripped the main contactor in the power source and triggered the high frequency arc starter unit. Once the arc was established, the high frequency

unit was automatically cut out. Further movement of the slide caused the rotation of the pinion gear which was attached to the spindle of a potentiometer. This was connected to the control unit in the power supply and by varying the potentiometer, the arc current could be varied up to the pre-set maximum. The positioning of the slide, therefore, also controlled the arc current.

In order to measure the arc current, a 250A current shunt was installed in the "live" line (i.e. the line connected to the electrode) inside the power supply. This was connected through an isolating switch to a calibrated meter movement mounted on the front panel of the trolley.

A suitably calibrated voltmeter was connected through an isolating switch across the "live" and "earth" lines to measure arc voltage. To prevent damage to the meters from the high frequency starter, readings of arc current and voltage were only made once the arc was fully established.

5.6 The Blow-Out Valve Assembly.

To determine the shape of a weld pool, the molten metal was ejected from the test plate at a pre-determined instant by directing a high velocity jet of argon onto the molten pool from a nozzle mounted on the welding torch. The ejected metal passed through the groove cut for this purpose in the base plate and was collected in a splash tray suspended below the base plate.

The argon flow was controlled by the valve assembly shown in Drawing 5.3 and Plate 5.3. This arrangement also served to supply the normal flow of argon to the welding torch. The argon supply (from a bottle at 2500 psi and reduced with a standard pressure regulating valve to 100 psi) was connected to the inlet of a solenoid operated poppet valve (manufactured by Schrader Ltd.). In the normal position, this valve connected the supply to the flow control valve set to deliver 8 $ft.^3/hr.$ to the welding torch (via the power supply).

The solenoid valve was activated by a switch mounted on the front panel of the trolley. This shut the normally open outlet port and opened the normally closed outlet port to the supply line. Argon at 100 psi was, thus, delivered directly to the blow out nozzle mounted on the torch. Non-return valves prevented "blow back" through the normally open line. Part of the high pressure flow was, however, allowed to pass through the power supply to the torch so that the electrode was protected from sudden exposure to oxygen during the blow out. Due, however, to the pressure losses through the non-return valve, power supply and torch assembly, practically all of the high pressure flow passed through the blow out nozzle.

This nozzle was made from a length of 1/8 ins. dia. bore, copper tube slightly flattened at its end. The nozzle was mounted on a bracket fixed to the welding torch and directed such that the jet impinged onto the test plate below the electrode i.e. during welding onto the molten pool. A close-up of this arrangement, showing a pool boundary after a blow out is shown in Plate 5.4 and Drawing 5.2, Part View on X.

PLATE 5.3 ARGON VALVE ASSEMBLY/
PLATE 5.4 WELDING TORCH AND BLOW-OUT NOZZLE/
FIGURE 5.2 THERMOCOUPLE JUNCTION IN POSITION
& PLATE 5.5 MACRO-SECTION THROUGH THERMOCOUPLE JUNCTION (X10)

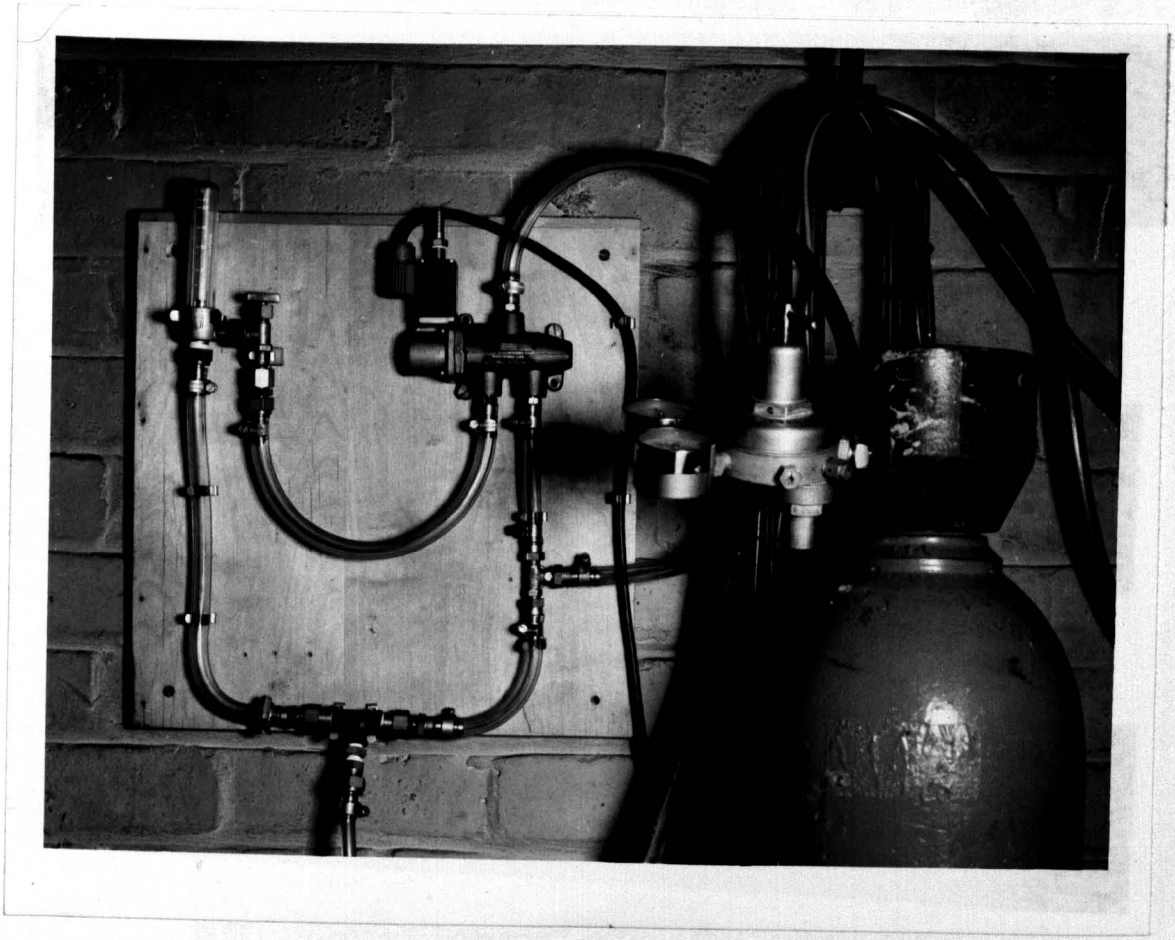

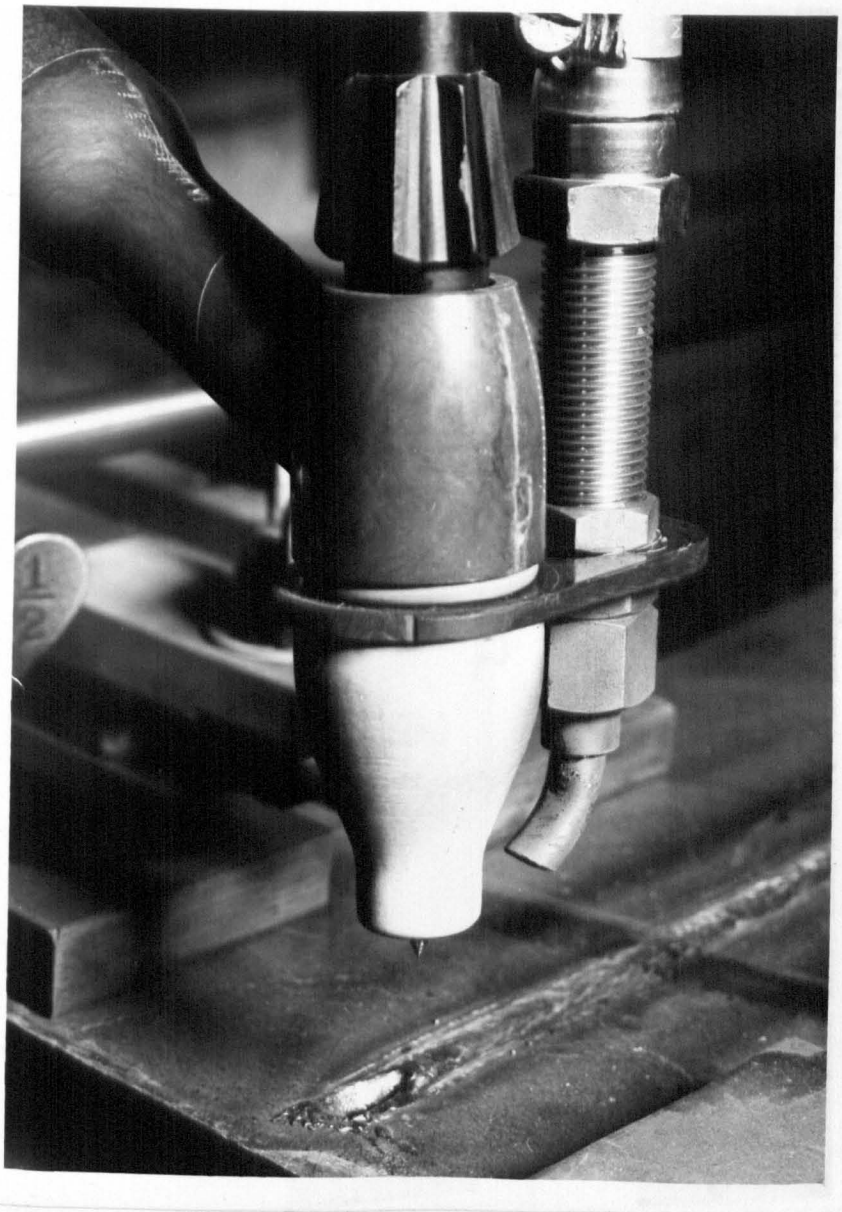

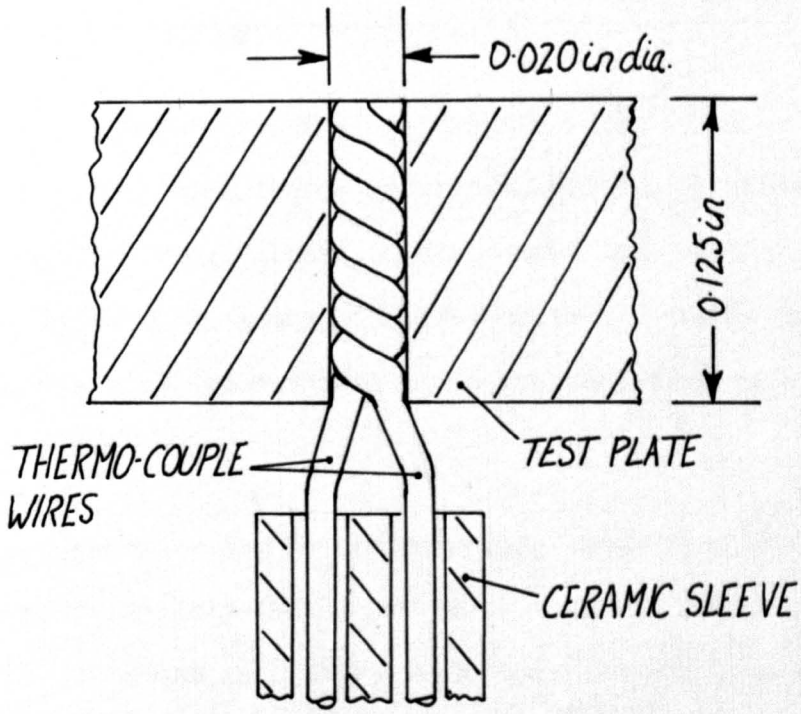
0·020 in dia.
0·125 in
THERMO-COUPLE WIRES
TEST PLATE
CERAMIC SLEEVE

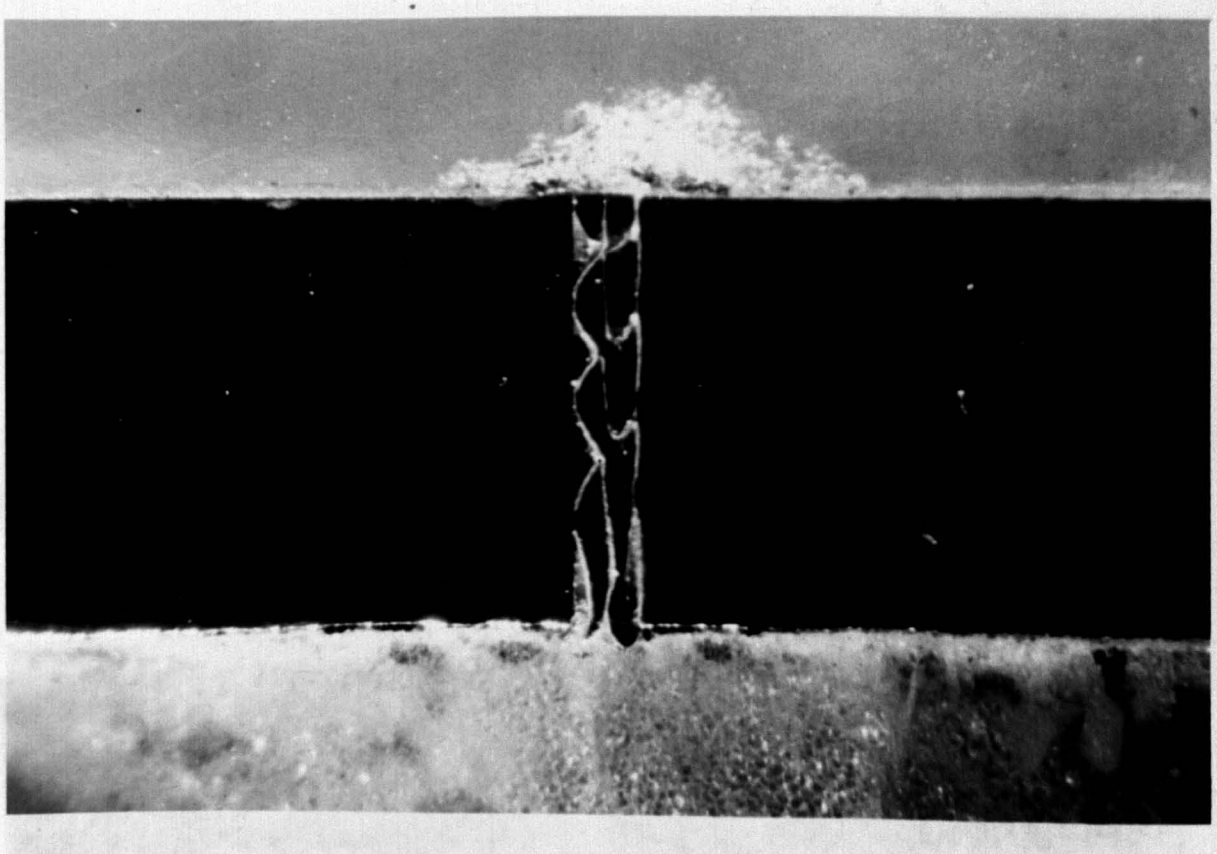

5.7 Temperature Measurement.

As previously indicated, the comparative tests required the measurement and continuous recording of temperatures in the HAZ during welding. For this purpose, nickel-chromium/nickel-aluminium thermocouples (type T_1/T_2 manufactured by British Driver - Harris) were located in the HAZ of the test plate and connected to a chart recorder.

These thermocouples had a substantially linear response (0.04157 mV/°C) up to approximately 1200°C and while this was somewhat below the melting point of the mild steel test plate (1420°C), it was felt that this provided a coverage of the HAZ temperature range sufficient for the purpose of the tests. To give a fast response while still maintaining reasonable mechanical strength, a wire diameter of 0.010 ins. (0.25 mm) was selected.

A junction was formed by tightly twisting the ends of the two wires together to give a twisted length of about 1 cm. The junction was then located in a 0.020 ins.(0.50 mm) dia. hole in the test plate by passing the twisted section through the hole from the bottom surface of the plate. The wires were then drawn through from the top surface of the plate until the end of the twisted section was tightly fixed inside the hole at the bottom surface of the plate. The portion of the twisted length protruding above the top surface of the plate was trimmed off until the junction was flush with the surface. A section through such a junction is shown schematically in Fig. 5.2 and a microsection through an actual junction shown in Plate 5.5. The contact between wires and wire and plate achieved by this technique

is evident in this micrograph. New junctions were made for each test.

From the junction, the wires were passed through a twin bore ceramic sleeve approximately 10 cm long and then individually through high temperature flexible sleeving. Thus insulated, the wires were passed from the junction underneath the test plate, between the studs supporting the plate to a terminal block mounted on the front panel of the trolley. By taking the wires underneath the test plate, they were protected from any damage from the arc. In this way up to four thermocouples were mounted on any one test plate.

From the terminal block, co-axial cable was used to carry the signal from the thermocouples to a twin gang wafer switch and hence to the chart recorder. Since this was a single channel recorder, it was necessary to switch from one thermocouple to another as the test proceeded. A wiring diagram of this arrangement is shown in Fig. 5.3.

The chart recorder used was of the single pen, y-t type (26000 series, manufactured by Bryans Southern Instruments Ltd.). On the y-axis of the recorder, the sensitivity was set at 2 mV/cm over the 28 cm width of the paper and a paper speed of 5 s/cm selected. These settings were maintained throughout the tests.

In a typical test, the thermocouples would be equally spaced along the length of the weld and at a known distance from the weld axis. The recorder would then be switched from one thermocouple to another as the front of the weld pool crossed a mark previously scribed on the test plate at a fixed distance (usually 6.25 mm) in front of each thermocouple. Since, for the duration of each test, the welding speed was maintained constant, each thermocouple was

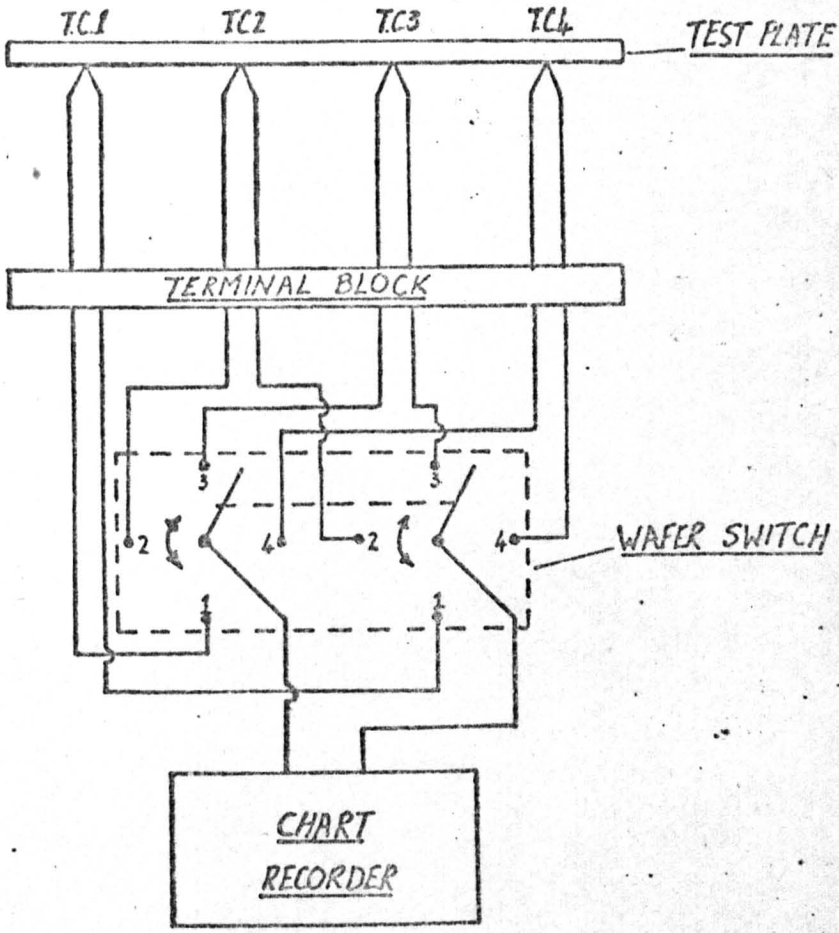

FIG 5·3 THERMO-COUPLE SWITCH ARRANGEMENT

monitored on the recorder for the same length of time.

This arrangement proved to be a satisfactory alternative to simultaneous multi-channel recording as the results reported in the next chapter indicate. Due to the available width of paper on the recorder used, the full calibrated range of 1200°C could be easily accommodated on the paper at a sensitivity of better than 50°C/cm. For this reason, estimates of temperature could be made to within 10°C over the entire 1200°C range.

5.8) Weld Test Procedure

As stated earlier, the weld tests were required to provide data on pool shapes and associated temperature histories for linear, full penetration welding of thin, mild steel plates. It was decided that these conditions would be satisfactorily met, if instead of butt welding two plates, the test welds were made by simply running a weld along the centre of a single plate. This procedure made it somewhat easier to maintain stable arc conditions and, to some extent, also reduced the need to use filler wire which would normally have been required for TIG butt welding of 1/8 in. thick plate.

Preliminary tests indicated that full penetration welds could be achieved in this way for welding currents in the range 90 - 140 A. The corresponding welding speeds ranged from 0.12 - 0.26 cm/s. While it was not possible to achieve complete two dimensionality over the entire weld pool for these conditions (the penetration angle at the front of the weld pool on the weld axis being as great as 40° at the highest speeds), it was felt that complete penetration from the maximum width to the tail end of the weld pool was a satisfactory criterion. In this way, only the initial rapid rise in temperature of points in the HAZ could be possibly affected by the penetration front of the weld pool. Peak temperatures and cooling rates would be subject to 2-D heat flow conditions.

To ensure that the thermal field on the HAZ was independent of the size of the test plate, a minimum plate width of 15 cm was used for all the tests. This met with the specification suggested by Roberts and Wells(18) for test plate dimensions, since the maximum pool width encountered for the above range of conditions was 0.7 cm.

For the location of thermocouples etc., a test length of 35 cm was found to be adequate (see Fig. 5.4).

All the test plates were cut to these dimensions from 1/8 in. sheet mild steel from stock and, prior to welding, were cleaned and degreased. Thermocouples were located in the plate as described in section 5.7. A typical thermocouple arrangement is shown in Fig. 5.4.

For each test, the plate was clamped to the test rig with its ℄ aligned with the welding axis of the rig and the test completed by running a weld, at a controlled arc current and speed, along the length of the plate. The chart recorder was switched from one thermocouple to another as the front of the weld pool crossed the scribe marks. (see Fig. 5.4 and section 5.8) Measurements of arc current and voltage were made during the test (see section 5.5) and readings of traverse times noted (see section 5.4). In each test, the weld pool was blown out (see section 5.6) 3 cm before the weld pool reached the end of the plate.

Three typical welds (taken from test welds) are shown in Plates 5.6a and 5.6b. These indicate the uniformity in width of weld along the length of each specimen as well as the complete penetration achieved. Three examples of blown out pools are shown in Plate 5.7. The very clean edges of the weld pool boundaries should be particularly noted. Plate 5.8 shows a micro-section of one edge of such a blow out. The section has been etched to show the grain structure and it is evident that only traces of molten metal (to a thickness of 0.5mm) have been left adhering to the parent plate after the blow out.

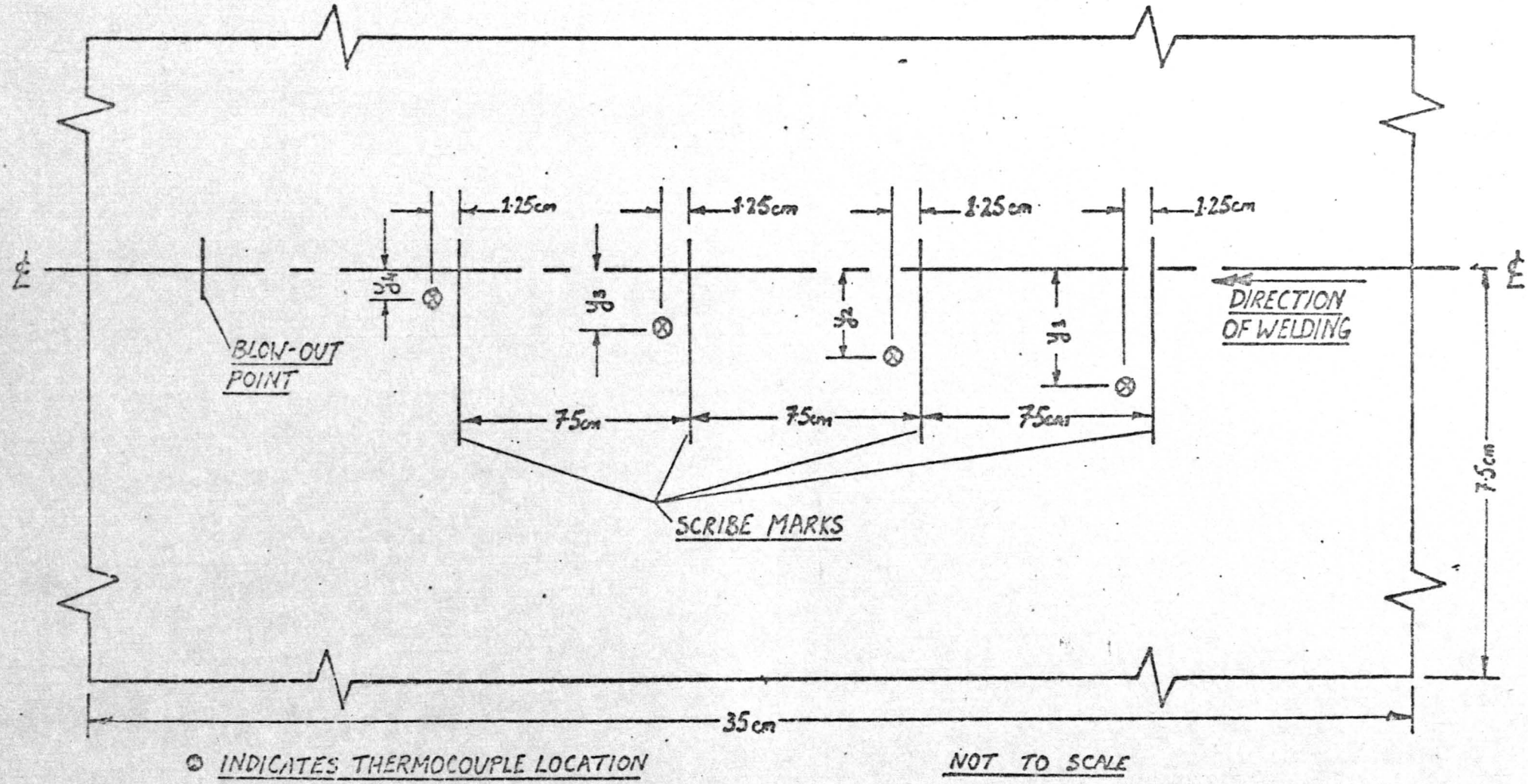

FIG 5·4 PLAN VIEW OF TEST PLATE SHOWING THERMO-COUPLE ARRANGEMENT

PLATE 5.6 THREE TYPICAL TEST WELDS

(a) TOP SIDE
(b) REAR SIDE

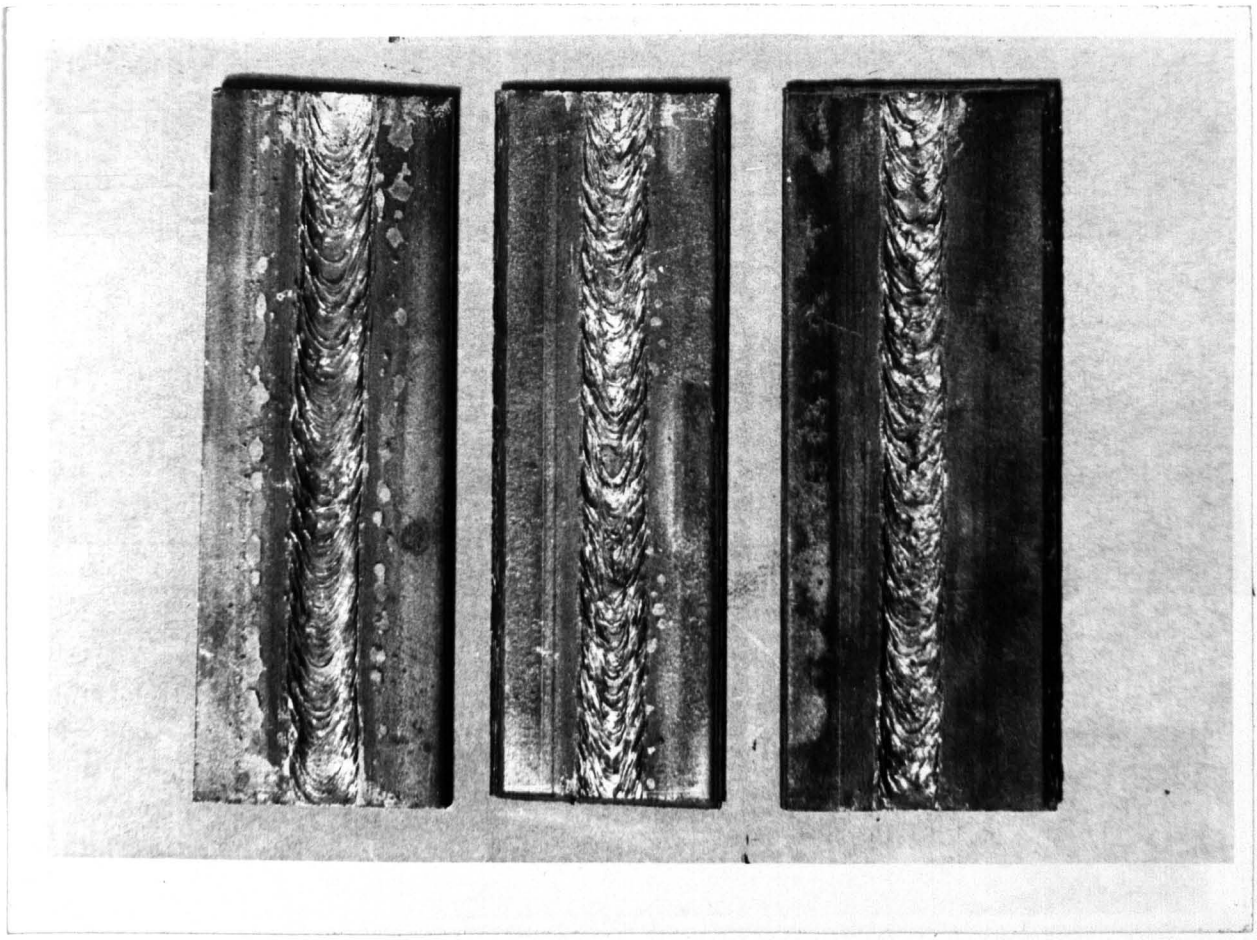

(a)

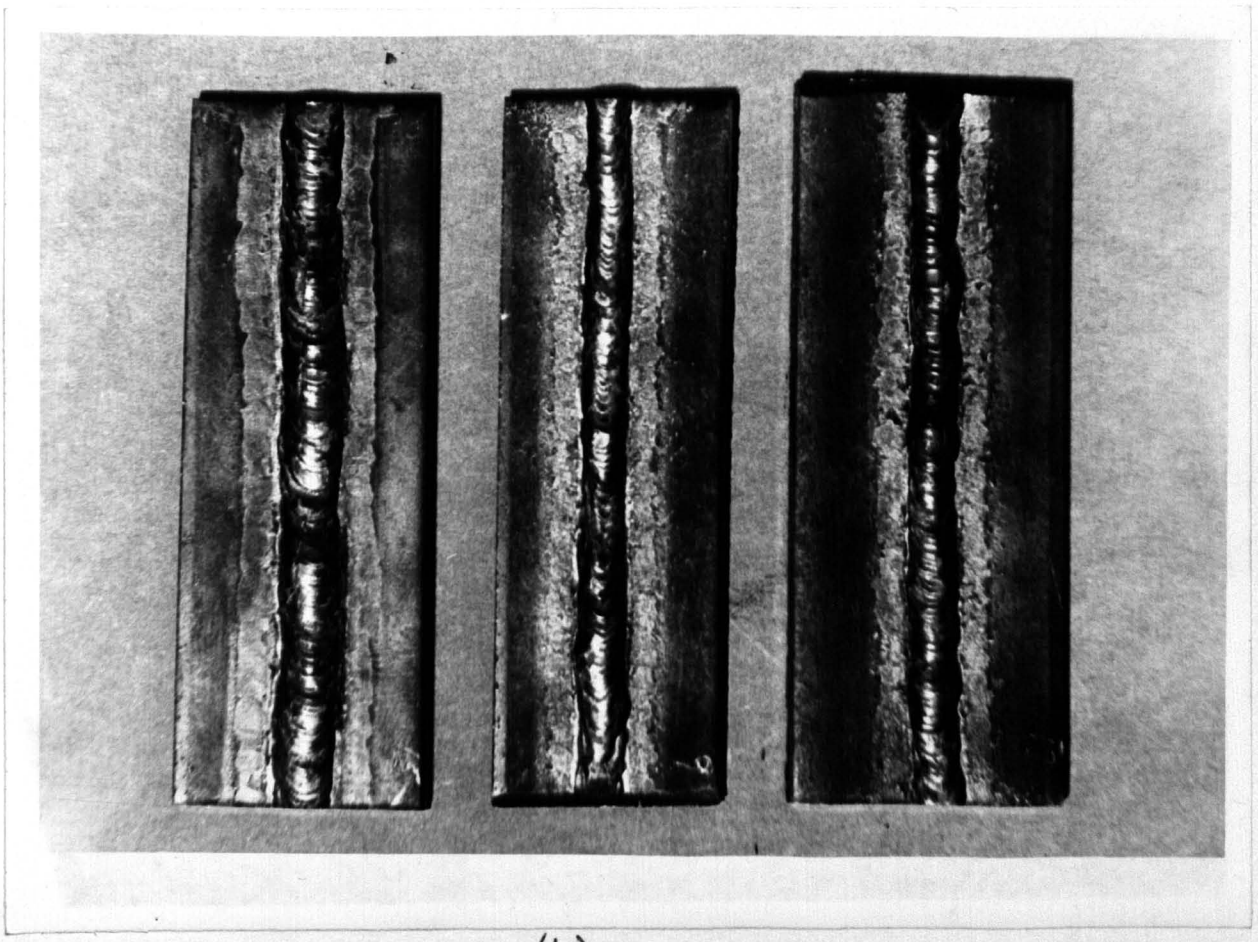

(b)

PLATE 5.7 THREE TYPICAL "BLOWN-OUT" WELDS
& PLATE 5.8 MICRO SECTION SHOWING ONE EDGE OF A "BLOWN-OUT" WELD (X34)

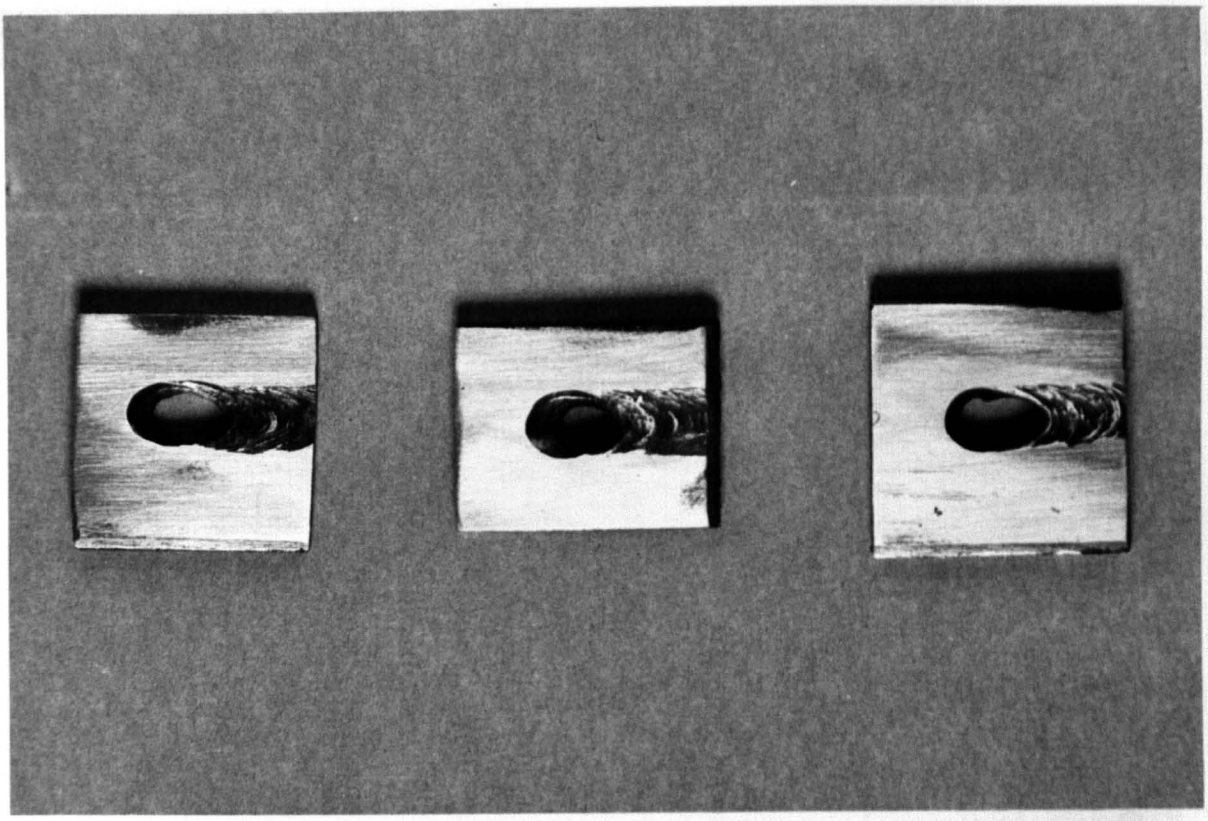

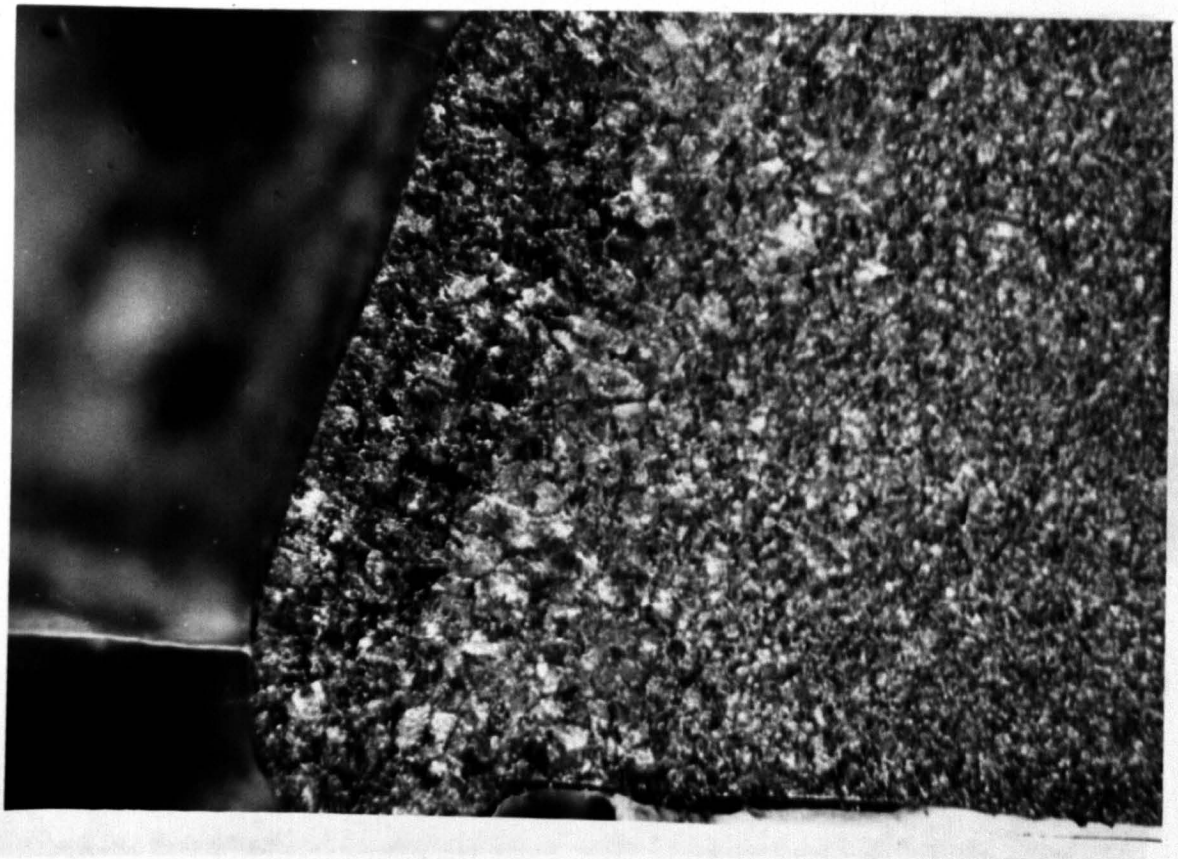

A typical themocouple recording is shown in Fig. 5.5. The thermocouple was located 0.200 ins (0.51 cm) from the $\mathcal{L}$ of a 138A, 0.25 cm/s weld. From subsequent measurement of the weld pool width, this corresponded to a distance of 0.055 ins (1.4 mm) from the edge of the weld pool. The temperature axis gives the recorded temperatures above ambient (20° C approx). The zero in the time scale corresponds to the instant when the front of the weld pool was in line with the thermocouple location. The extremely rapid rise in temperature (250° C/s approx) up to the peak temperature of 1040° C and the somewhat slower initial cooling rate (45° C/s approx) should be noted. The cooling rate gradually decreases with time until, 40 secs. after reaching peak temperature, it is reduced to 6.5° C/s.

The value of the $\mathcal{L}$ field analogue in predicting temperature histories of this nature is discussed in the following chapter.

N.B. It is also interesting to note the "hump" in the cooling curve (highlighted by the dotted, smooth continuation of the cooling curve) corresponding to the exothermic eutectoid transition. From the graph, it can be seen that the start of the transition (690° C) has been suppressed below the equilibrium transition point of 723° C.

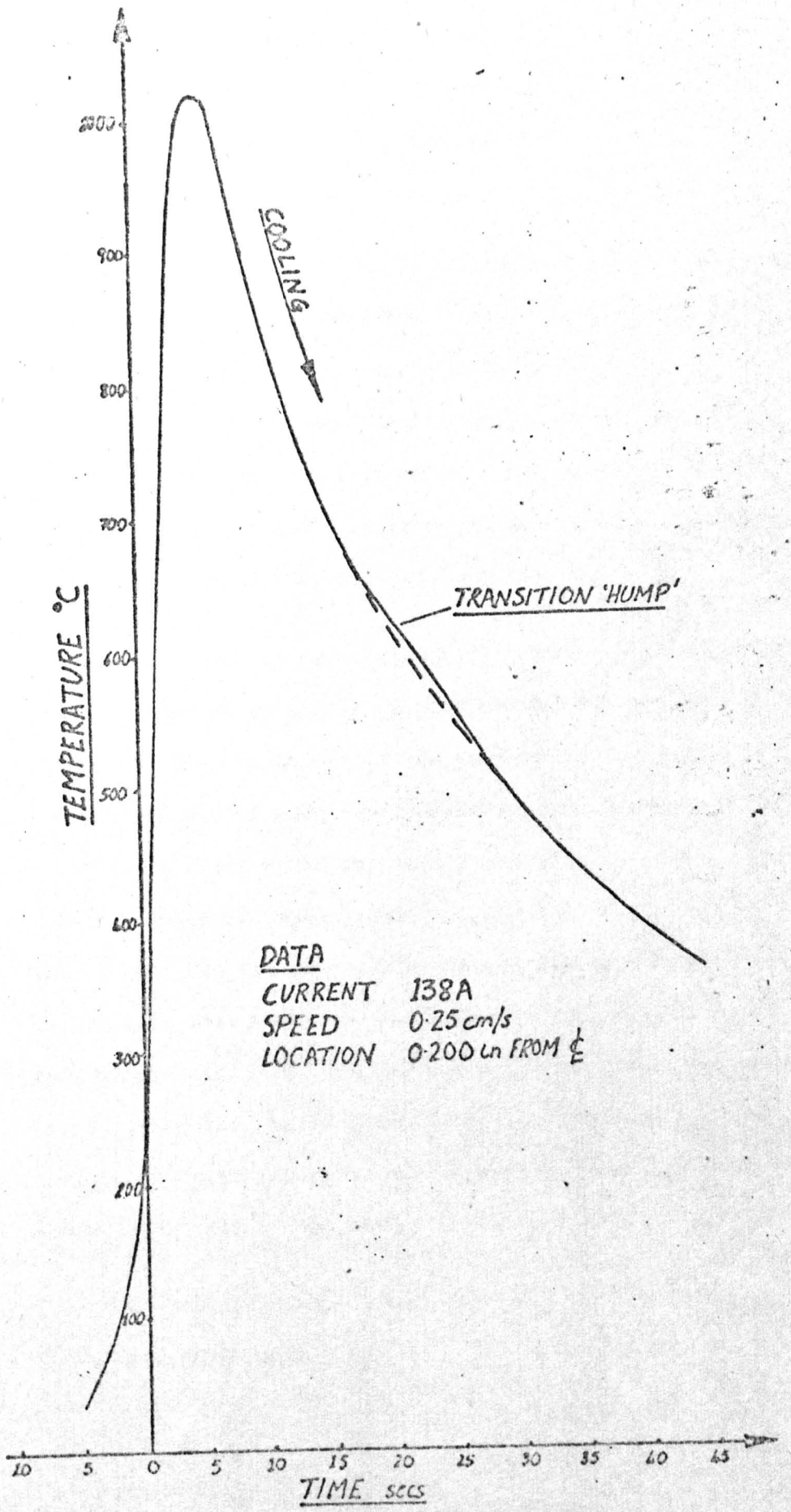

FIG 5·5 EXPERIMENTAL TEMPERATURE HISTORY

CHAPTER 6

TEST RESULTS

As discussed in Chapter 5, the main purpose of this study was to determine to what extent the thermal field in the HAZ during welding could be predicted using analogue techniques. To evaluate the $\emptyset$ field analogue for this purpose, it was decided to perform a series of tests in which experimentally determined temperature histories would be compared with analogue predicted histories for points in the HAZ (see Fig. 5.1).

However, before commencement of these comparative tests, it was essential to determine to what extent the thermal field with respect to the electrode (or the weld pool) remained constant for nominally constant welding conditions. Any serious fluctuation in the thermal field would invalidate the quasi-static assumption and make any analogue predictions meaningless. If the thermal field with respect to the pool shape did not remain constant along the length of a test weld, it would also be meaningless to associate temperature histories measured at different points along the weld (i.e. using the single channel recorder with switching between thermocouples as described in sections 5.7 and 5.8) with the pool shape determined by the blow-out at the end of the weld.

For these reasons, it was decided to undertake the initial tests discussed below.

6.1) Consistency Tests

If the thermal field with respect to the electrode for the welding test procedure described in section 5.8 were quasi-static, then it is evident that all points lying on a line parallel to the welding axis would experience the same temperature history (appropriately stepped in time). To test for consistency of the thermal field, it was, therefore, sufficient to test the repeatability of the temperature history of points lying at the same distance from the welding axis during a particular test weld. The repeatability of such temperature histories and hence consistency of the thermal field was investigated by the following procedure.

Three thermocouples were located 5.0 ± 0.005 in. (12.70 ± 0.01 cm) apart on a line a fixed distance from the ℄ of the test plate as shown in Fig. 6.1. A test weld was then passed along the ℄ of the plate with the arc current and speed being kept as constant as possible. By switching from one thermocouple to another (see sections 5.7, 5.8), the output from each thermocouple was recorded in turn for the same length of time (i.e. the time taken for the weld to traverse 5.0 in.). These recordings were then compared for repeatability.

A typical result from such a test with the three recordings superimposed is shown in Fig. 6.2. Again the temperatures shown are above ambient and zero on the time axis corresponds to the instant when each thermocouple was in line with the front of the weld pool.

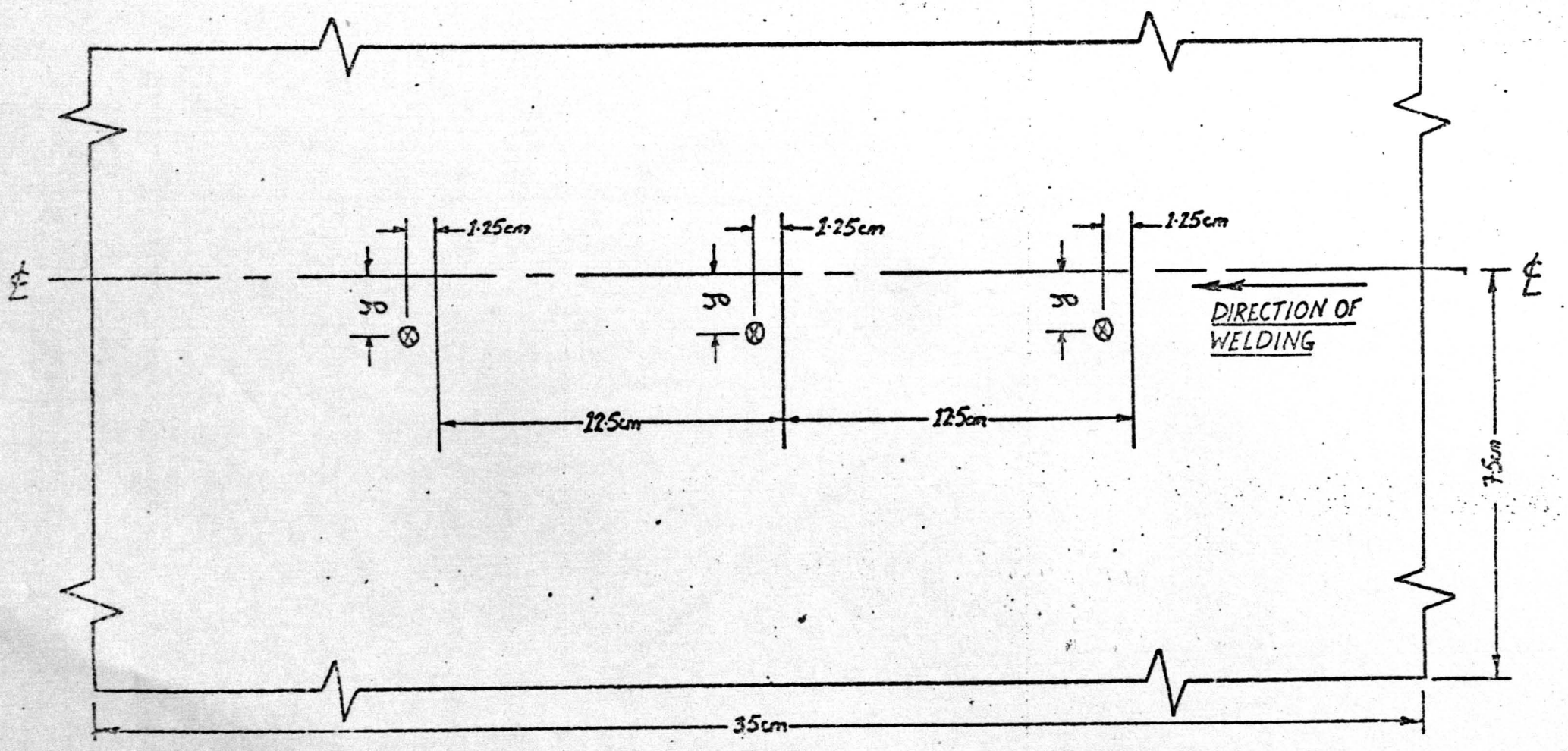

FIG 6·1 THERMO-COUPLE ARRANGEMENT FOR CONSISTENCY TESTS

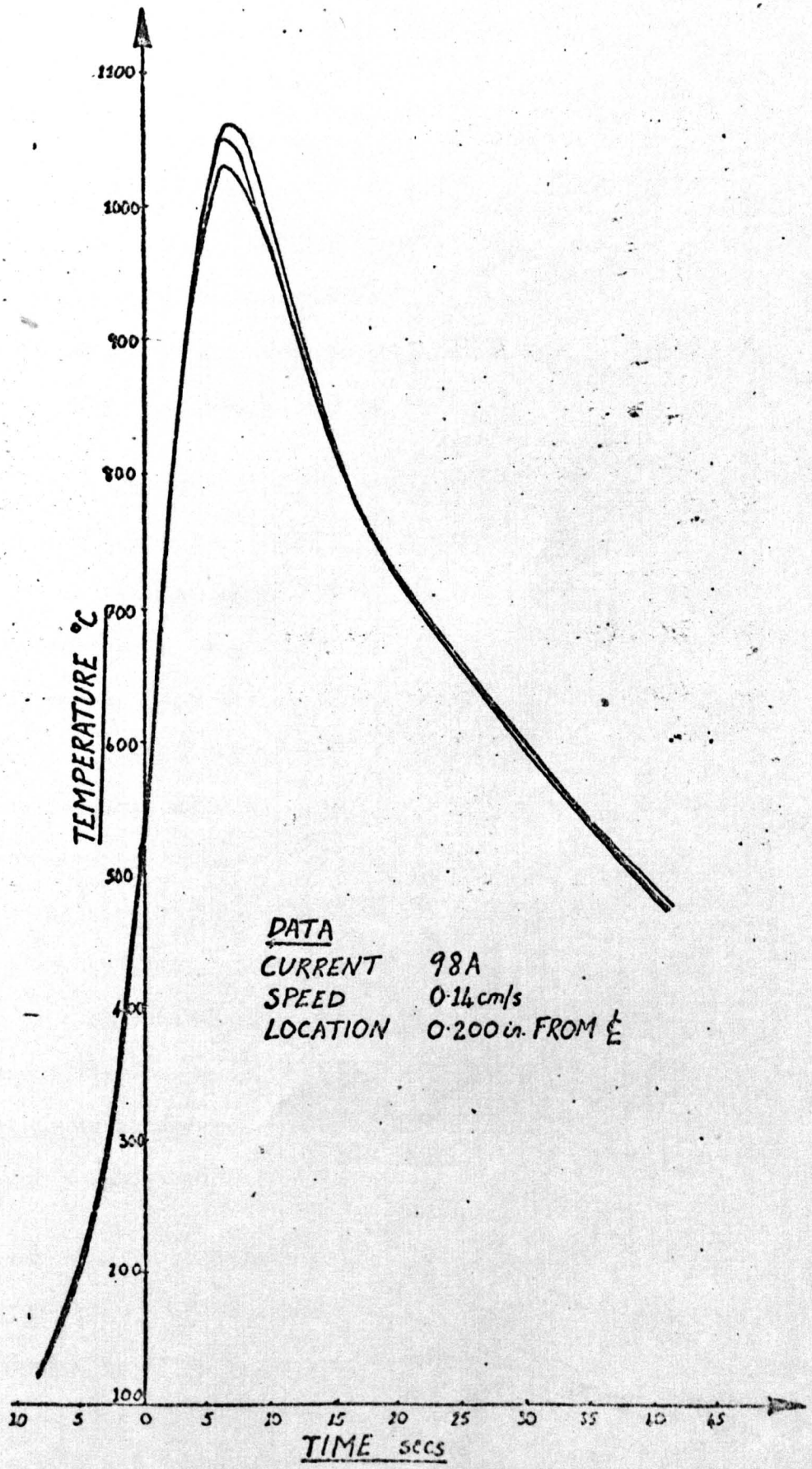

FIG 6·2 CONSISTENCY TEST RESULT

The tests were repeated for two different sets of welding conditions (nominally 100A at 0.15 cm/s and 138A at 0.25 cm/s). For each set of conditions, three separate tests were made with the thermocouple line located 0.175, 0.200 and 0.250 in. from the weld ℄ respectively. The results from these tests are given in Table 6.1. The four temperatures in each group refer, in descending order, to the peak temperature and the temperatures 5s, 15s and 30s after peak respectively.

All the tests showed excellent repeatability in the heating curve up to the peak temperature. Indeed, as typified by Fig. 6.2, the three superimposed heating curves were almost indistinguishable in each test. From Table 6.1, the maximum % age difference (referred to the minimum) in peak temperatures was less than 5% in all cases tested. Considering the large thermal gradients involved and the accuracy of the thermocouple recording and interpretation, this difference is comparable with the experimental errors (e.g. an error of $\pm$ 0.005 in. in the location of a thermocouple from the nominal distance from the weld ℄ could, itself, give rise to an error of $\pm$ 30°C in the peak temperature). A maximum difference of less than 5% was also found for the cooling curves as indicated by the temperatures at 5, 15 and 30s after peak temperature.

These results indicated the validity of the quasi-static assumption for the welding procedure and conditions described above. They also indicated that the test technique of switching between thermocouples was adequate for the purpose of the tests.

THERMOCOUPLE DISTANCE FROM ℄ (in)	WELDING CURRENT (A) AND SPEED (cm/s)	RECORDED TEMPERATURE AT PEAK, 5, 15 & 30 s AFTER PEAK (°C ABOVE AMBIENT)		
		TC1	TC2	TC3
0.175	102 0.17	1102 952 682 479	1097 923 667 469	1068 923 682 469
	138 0.25	1209 957 686 479	1197 962 682 483	1150 962 672 456
0.200	98 0.14	1097 957 720 527	1083 957 725 546	1054 948 720 541
	138 0.25	1059 885 638 450	1039 856 641 450	1035 880 631 430
0.250	98 0.15	933 817 648 488	894 798 633 483	923 821 657 469
	139 0.26	841 789 630 440	880 822 599 440	880 783 624 430

TABLE 6.1 CONSISTENCY TEST RESULTS

6.2) Comparative Test Procedure

Having gained the required confidence in the test procedure from the consistency tests, it finally remained to complete the comparative tests between analogue predicted and experimentally measured temperature histories. The test procedure followed is outlined below.

The Mk II analogue was prepared by connecting a fresh sheet of Anaplot paper (from Roll 1) to the field resistors with silver paint as described previously (section 4.6). Prior to fitting the paper on the analogue, a pattern of 0.5 mm dia. holes, corresponding to the resistor layout on the analogue (see Fig. 4.10), was punched through the paper so that it could be fitted accurately and without tearing onto the field resistors.

The analogue parameter $\sqrt{\frac{\rho}{R}}$ was then estimated by the procedure detailed in section 4.6. Adopting the same 1-D test procedure, the accuracy of the analogue was also evaluated.

From a test weld, the pool shape and welding speed v were determined as described in section 5.8. A Baty 600 Reflex Projector with a magnification of x 10 was used to give an accurate profile of the pool shape.

Before painting the pool shape onto the analogue field, the appropriate "scaling factor" had to be determined. The scaling factor was defined as the distance on the analogue field which represented unit distance on the test plate. This was determined by first calculating the distance of real space which was represented by the analogue resistor spacing h. Re-arranging the analogue

design formula (equation 4.8) gives

$$h = \frac{2\alpha}{v} \cdot \sqrt{\frac{\rho}{R}} \qquad (6.1)$$

Substituting for the welding speed v and the estimated value of $\sqrt{\frac{\rho}{R}}$, (α always being taken as 0.075 cm^2/s), in the above equation gave the required value of h. The corresponding scale factor was then calculated by dividing the actual resistor separation on the analogue by h.

The contour of the pool shape, appropriately scaled, was then painted onto the surface of the analogue using silver paint. Only one symmetrical half of the pool shape was considered and it was located on the analogue so that the entire pool lay in the finely divided region with its major axis (i.e. the welding axis) coincident with edge AB shown in Fig. 4.10. A typical pool shape on the analogue is shown in Plate 6.1. The straight cut edge along the remainder of the axis of symmetry (i.e. edge AB) simulated the adiabatic heat flow conditions across the real welding axis.

From the Rosenthal transformation (equation 4.1), it is evident that the isothermal molten/solid interface defining the pool boundary is not an equipotential on the ϕ field. From equation 4.9,

$$\phi(x,y) = e^{+\frac{v}{2\alpha} \cdot x} \cdot T(x,y)$$

and substituting for $T(x,y) = T_m$ where T_m is the melting point of the parent material gives

$$\phi_m(x) = T_m \cdot e^{+\frac{v}{2\alpha} \cdot x} \qquad (6.2)$$

PLATE 6.1 WELD POOL SIMULATION ON THE MKII ANALOGUE

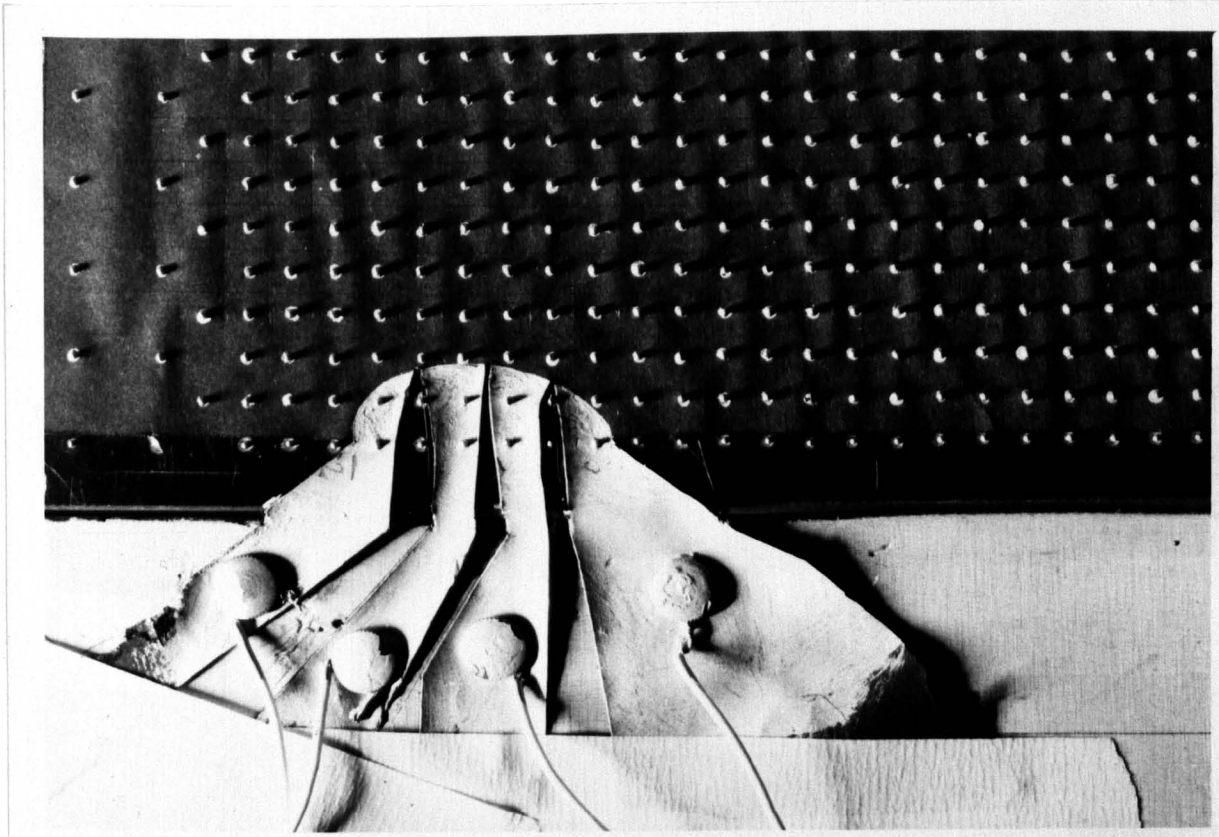

for the required variation in $\emptyset$ potential along the length of the pool.

Using the value of T_m = 1500°C above ambient for mild steel (4,18), the variation in $\emptyset$ potential was calculated by assuming that the origin of x was directly beneath the electrode of the welding torch (i.e. the Rosenthal co-ordinates shown in Fig. 1.1). The continuous nature of this variation was approximated by dividing the length of the pool into four regions and assuming the potential within each region to be constant. The potential assigned to each region was the value calculated from equation 6.2 for the mid-point of the region. As shown in Plate 6.1, each region was effectively separated from the others by removing a segment of the pool shape along the dividing line between adjacent regions. In this way, the only electrical contact between different regions of the pool was through the analogue field itself.

The required potential was applied to each region using the circuit shown schematically in Fig. 6.3. The power source (Multireg 731, manufactured by Weir Electronics Ltd.) was connected across a cascade of 4 x 5 kΩ potentiometers connected in parallel. Each region was connected to a single potentiometer which was adjusted until the required potential for that region was obtained.

The common grid was connected to the -ve (i.e. zero) terminal of the power source as before. As shown in Fig. 6.3, connection to the -ve terminal was also generally made to the edge opposite the axis of symmetry on the analogue although tests showed that its removal had no measurable effect on the $\emptyset$ field in the vicinity of the pool shape.

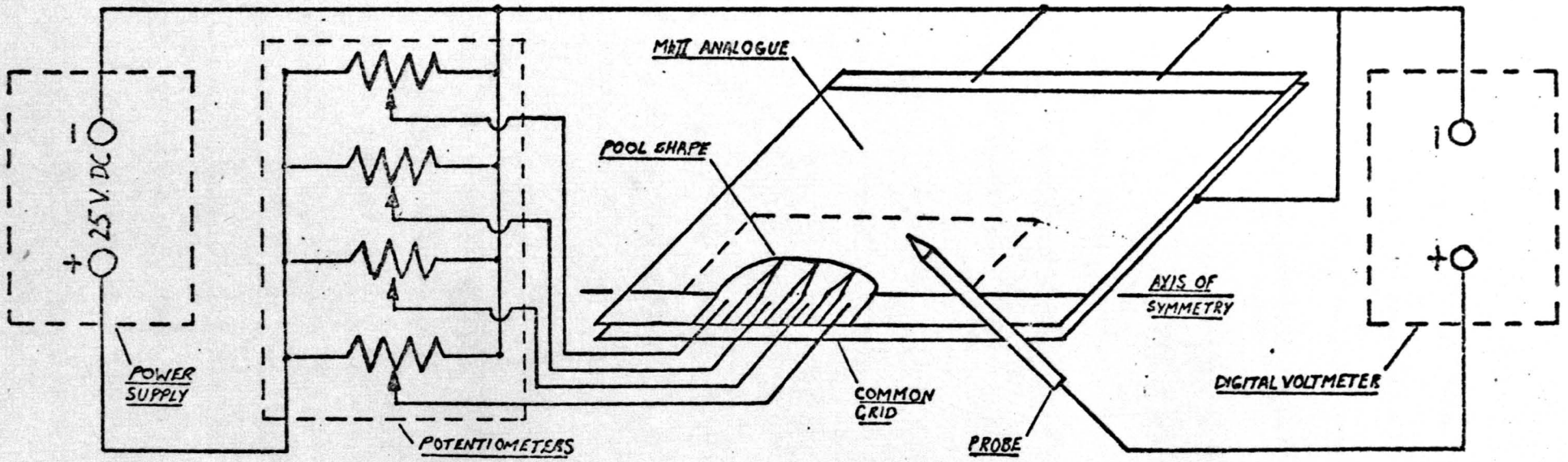

FIG 6·3 ELECTRICAL ARRANGEMENT FOR Ø-FIELD STUDIES

Measurements of $\emptyset$ potential were made using a probe connected to a digital voltmeter (Type LM 1450, manufactured by Solartron Ltd.) as for the evaluation tests (section 4.6) and as shown in Fig. 6.3. A general view of this arrangement is shown in Plate 6.2.

Measurements of $\emptyset$ potential were made at known distances (i.e. fixed values of x) along lines drawn parallel to the axis of symmetry. The separation of these lines from the axis was made to correspond to the distances at which thermocouples were located from the welding axis on the test plate.

These readings of potential were then converted to temperatures by the Rosenthal transformation

$$\text{i.e.} \qquad T(x,y) = e^{-\frac{v}{2\alpha}.x} \cdot \emptyset(x,y) \quad ,$$

(care being taken that the analogue distances were first reduced to "real" distances i.e. values of x by dividing by the scale factor).

This enabled plots of temperature T(x) for various values of y to be drawn. To facilitate comparison with the temperature-time plots obtained from the thermocouple recordings, the x values of the analogue were converted to t (time) values by dividing by the welding speed v. The origin for the temperature-time plots was arbitrarily taken as the leading edge of the weld pool. i.e. the origin on the analogue was shifted to the front of the pool and distances referred to that origin were converted to times by dividing by the welding speed. Direct comparison of the analogue predicted and experimentally measured temperature histories could then be made.

PLATE 6.2 MKII ANALOGUE: EXPERIMENTAL ARRANGEMENT FOR COMPARATIVE TESTS

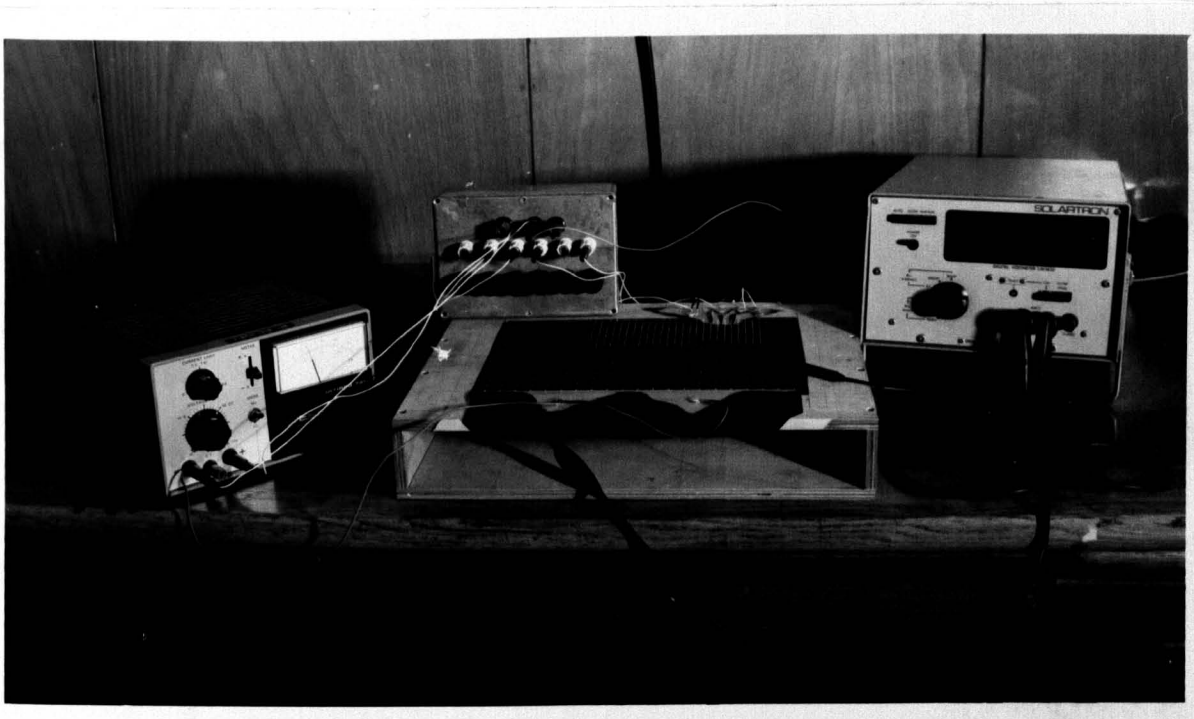
SOLARTRON

For completeness, the $\emptyset$ field surrounding each pool shape studied was plotted using the Alpha PR Plotter in a similar way to the equipotential plots made during the evaluation tests (section 4.6). Allowance was, of course, made for the variation in potential along the pool boundary.

6.3) Results

Three experimental temperature histories, determined from one such test (Test A) are shown in Fig. 6.4. The thermocouples were located 0.250, 0.225 and 0.200 in. from the axis of a 106A, 0.14 cm/s weld. The resultant pool shape is shown marked A in Plate 6.3.

For the above welding speed and for the particular sheet of Anaplot paper used ($\sqrt{\frac{\rho}{R}} = 0.365$), the scaling factor was 3.224. Using this value, the half profile marked A in Fig. 6.5 (drawn using the Baty Reflex Projector as described in the previous section) was transcribed onto the analogue field. From equation 6.2, the required potentials at each of the four regions of the pool shape were, starting from the front, 17.24, 13.06. 9.93 and 7.76V. These were applied to the analogue using the electrical circuit shown in Fig. 6.3.

The perpendicular distances from the axis of symmetry on the analogue to the lines corresponding to the thermocouple locations on the test plate were calculated by multiplying the distance of each thermocouple from the weld axis by the scaling factor e.g. for the thermocouple located at 0.250 in. from the welding axis, the corresponding line on the analogue was located at a distance of

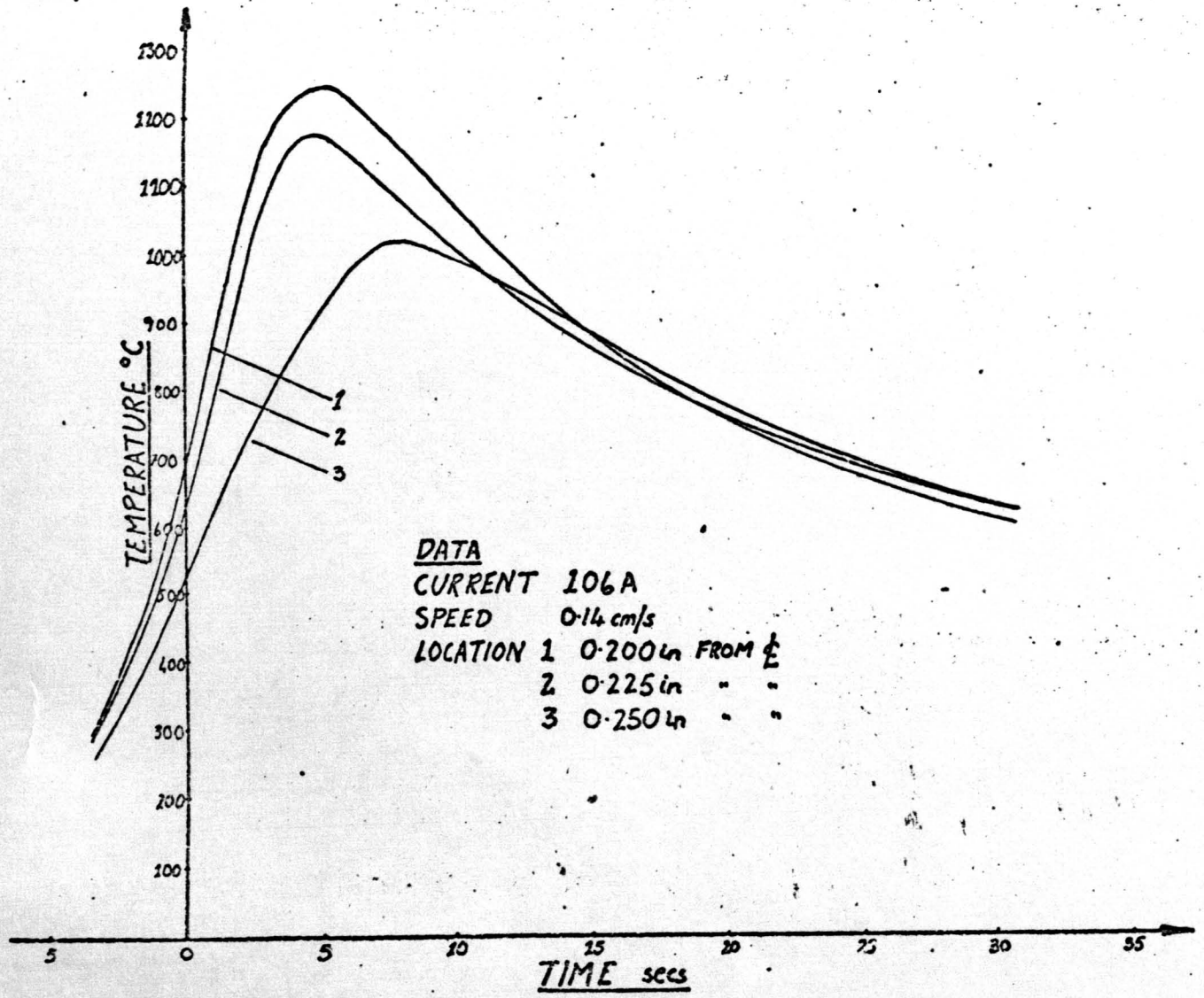

FIG 6·4 TEST A EXPERIMENTAL RESULTS

PLATE 6.3 "BLOWN-OUT" WELDS FOR TESTS A & B

B A

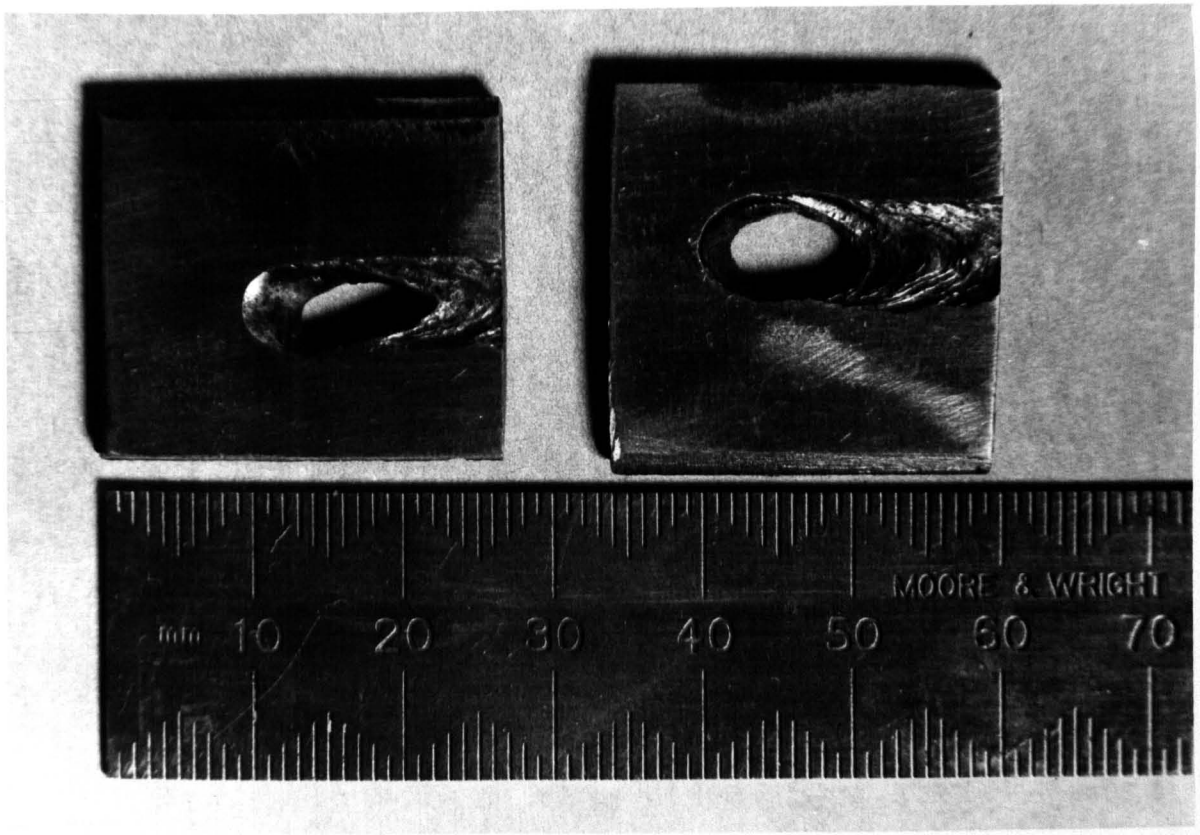

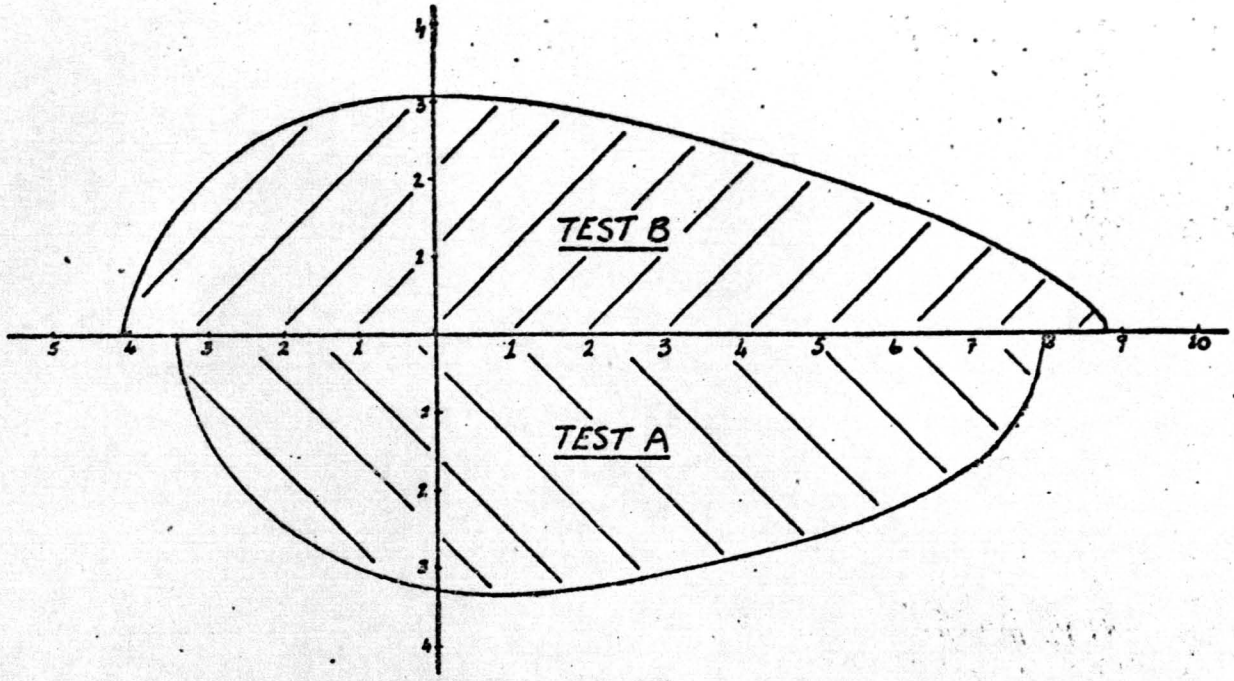

DIMENSIONS IN mm MAGNIFICATION X10

FIG 6·5 WELD POOL PROFILES

0.250 x 3.224 in. from the axis of symmetry. The potential distribution along each of these lines was measured using the digital voltmeter.

These ϕ potential distributions (i.e. $\phi(x)$) were then transformed to temperature histories (i.e. $T(t)$) as described in the previous section. These analogue predicted temperature histories are shown compared with the corresponding experimental histories in Figs. 6.6, 6.7 and 6.8. The ϕ field distribution about the pool shape is shown by the equipotential plot in Fig. 6.9. This was copied directly from the analogue field on a 1:1 scale. Fig. 6.9 also shows the lines, corresponding to the thermocouple locations, along which the ϕ potential distributions were measured.

For comparison Figs. 6.10 - 6.14 show a similar set of results (Test B) relating to a 138A, 0.25 cm/s weld. The change in time scale in Figs. 6.10 - 6.13 should be noted. For this test, the thermocouples were located 0.175, 0.200 and 0.250 in. from the welding axis. The pool shape for this test is shown marked B in Plate 6.3 and the corresponding profile marked B in Fig. 6.5. The required potentials at the four regions of the pool shape were 24.30, 15.00, 8.45 and 4.57V respectively. The scaling factor for the above welding speed was calculated as 6.017 (the estimated value of $\sqrt{\frac{\rho}{R}}$ being 0.358 in this case).

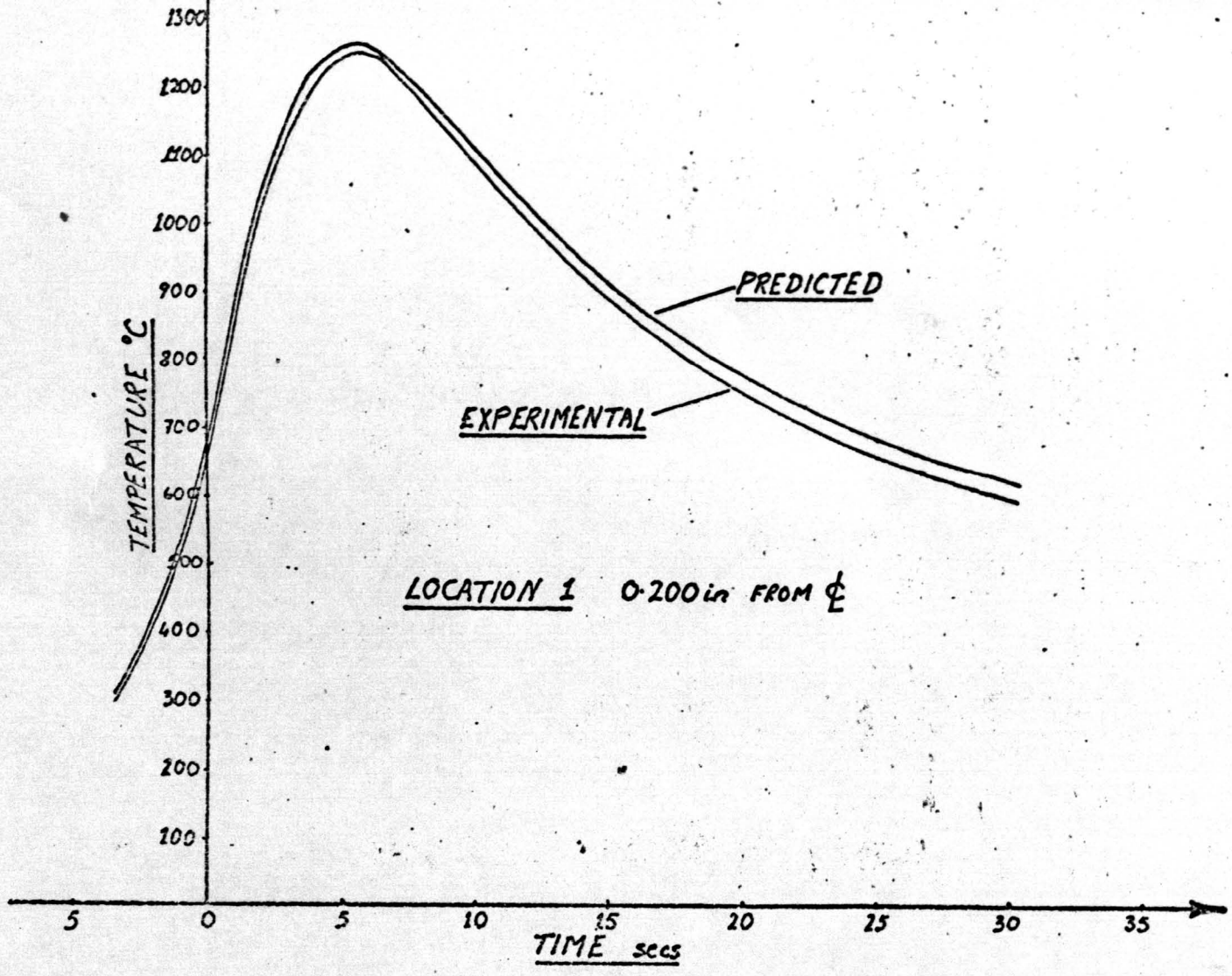

FIG 6·6 TEST A COMPARISON 1

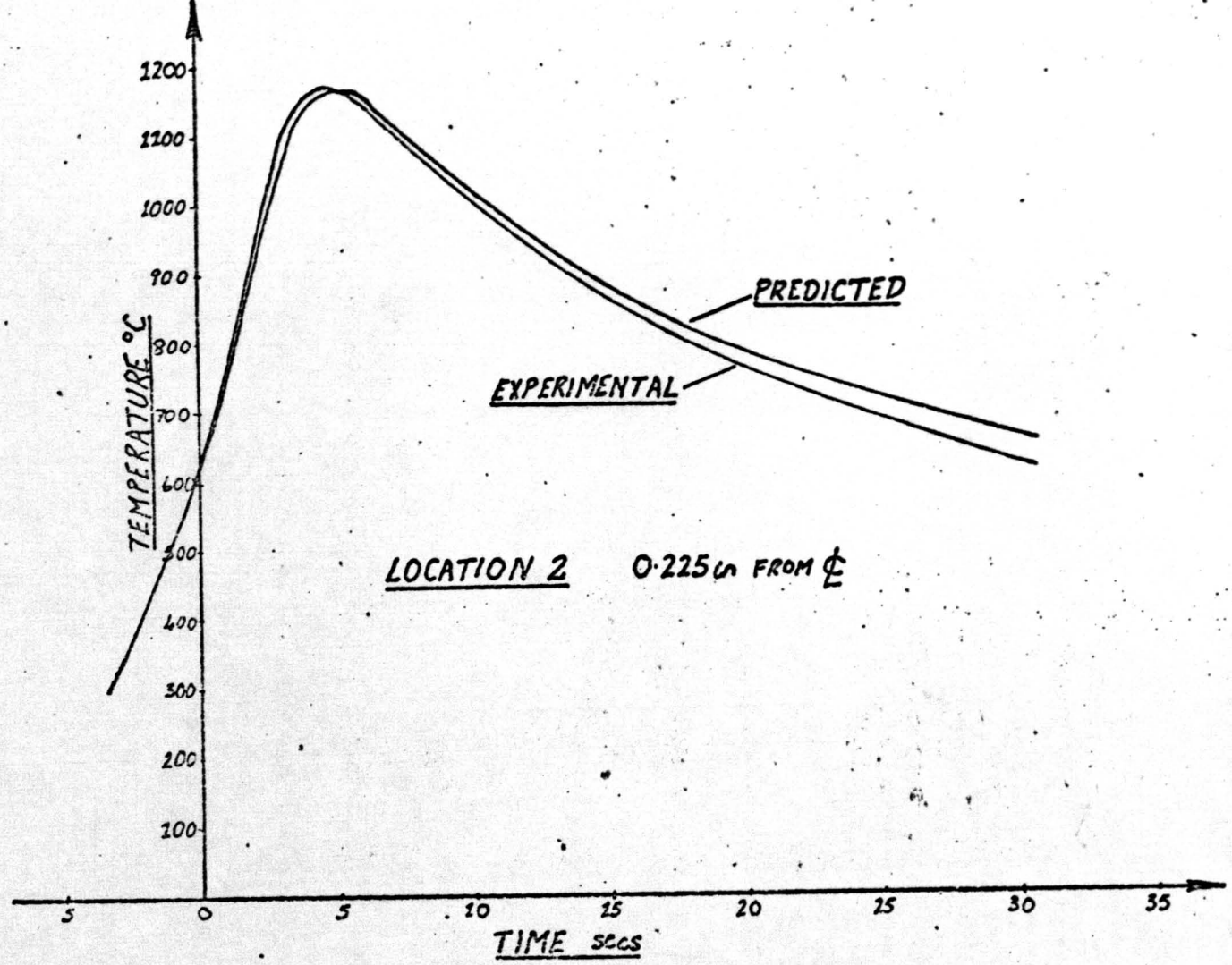

FIG 6·7 TEST A COMPARISON 2

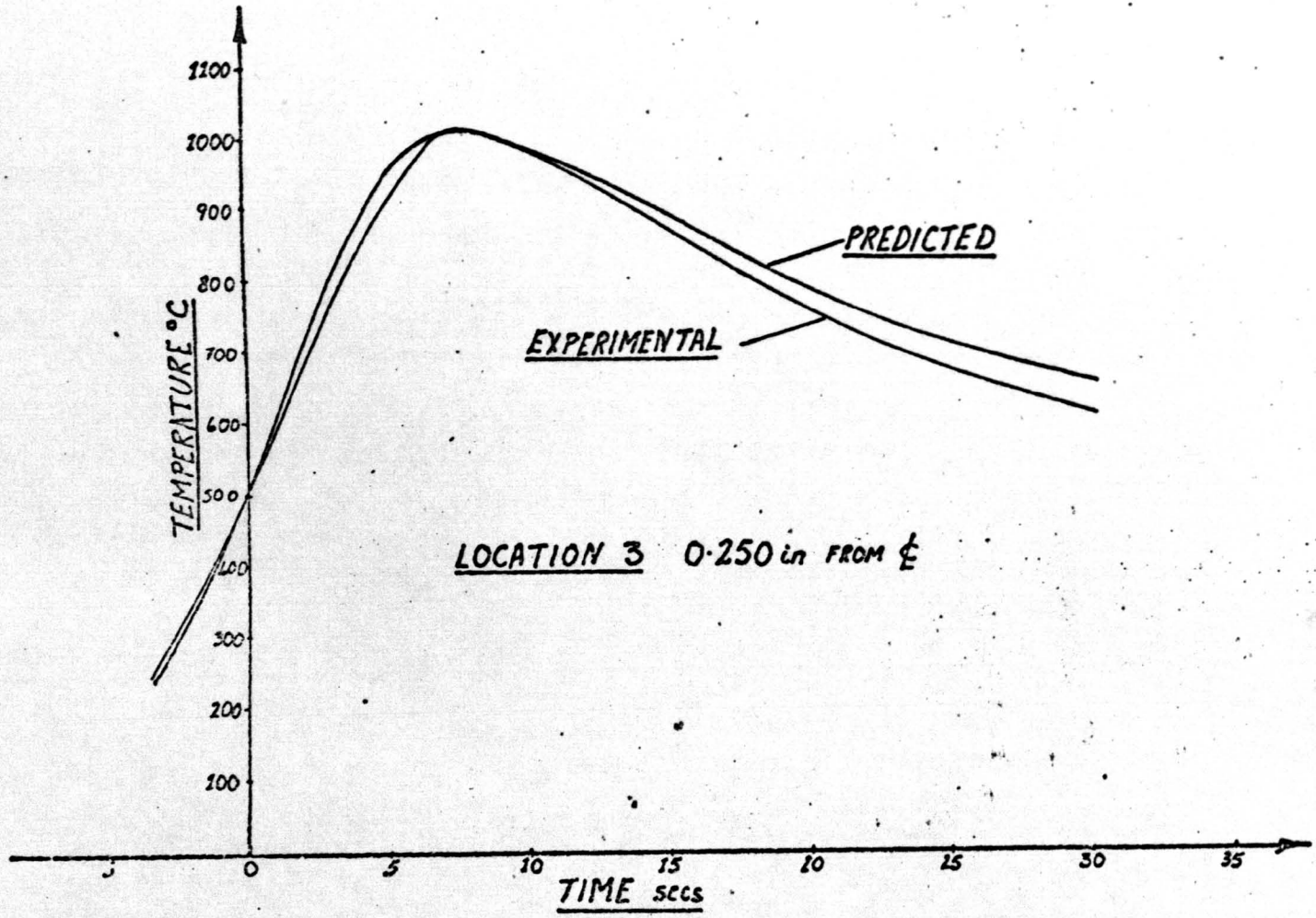

FIG 6·8 TEST A COMPARISON 3

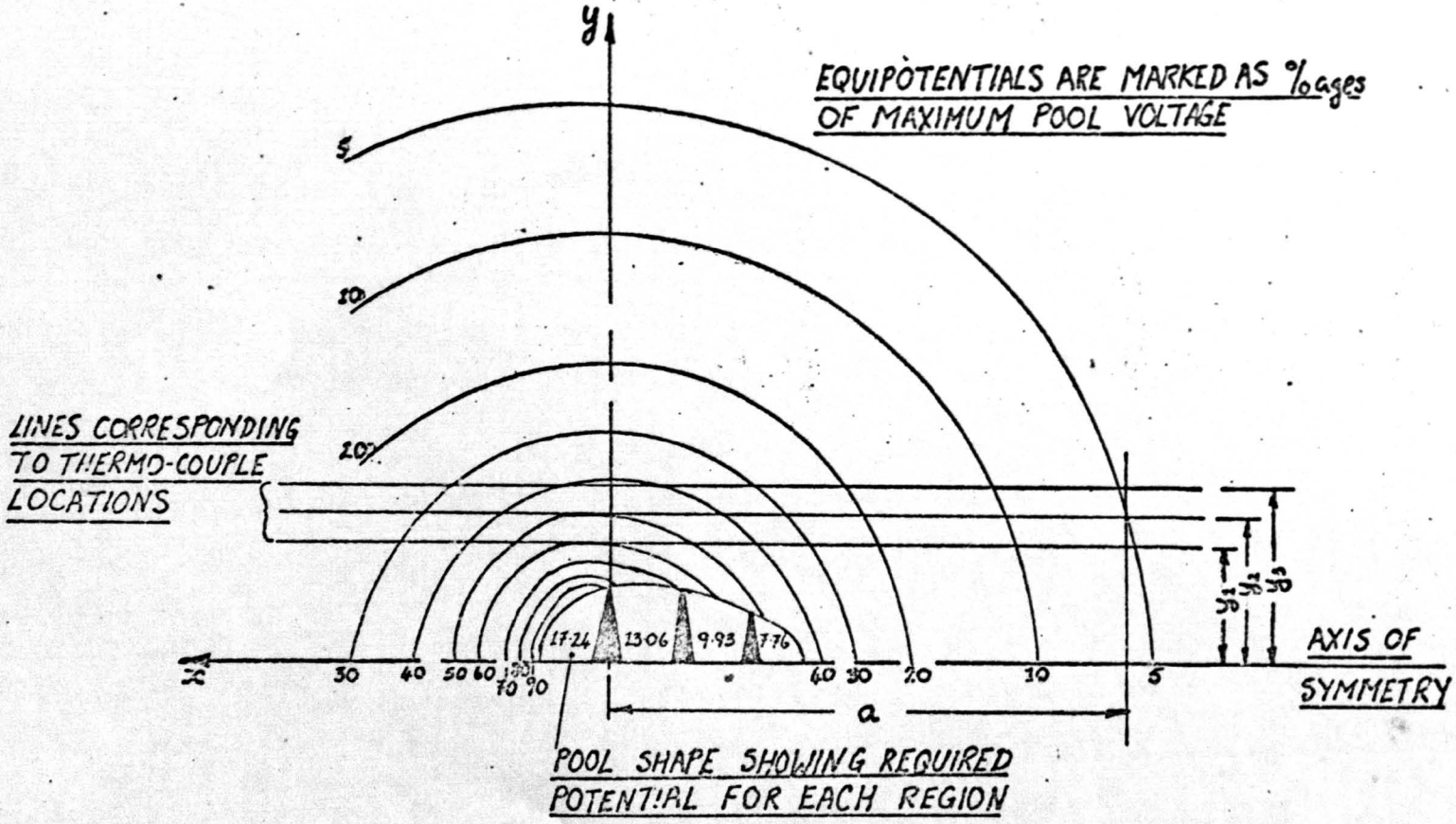

FIG 6·9 TEST A EQUIPOTENTIAL PLOT

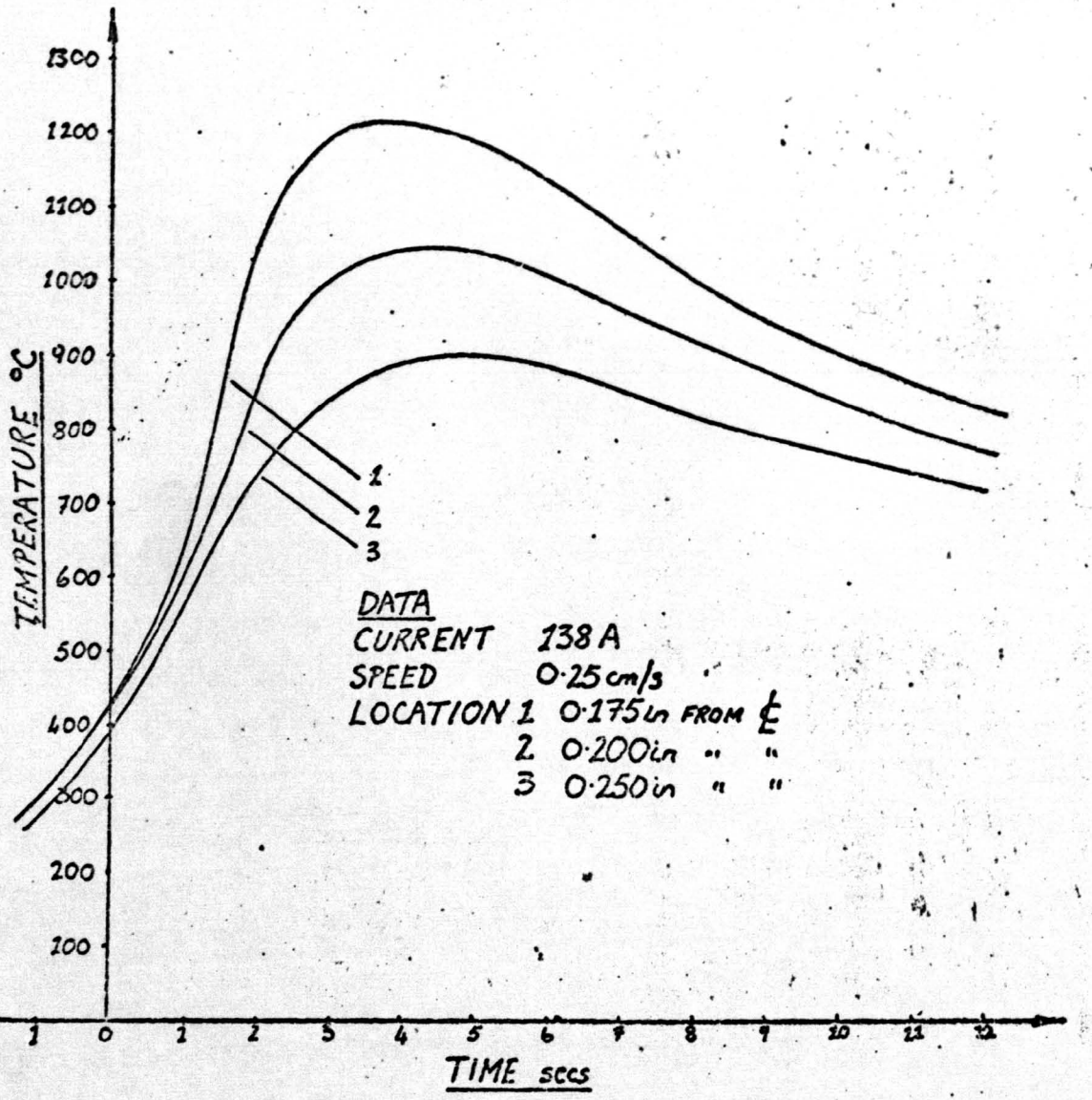

FIG 6·10 TEST B EXPERIMENTAL RESULTS

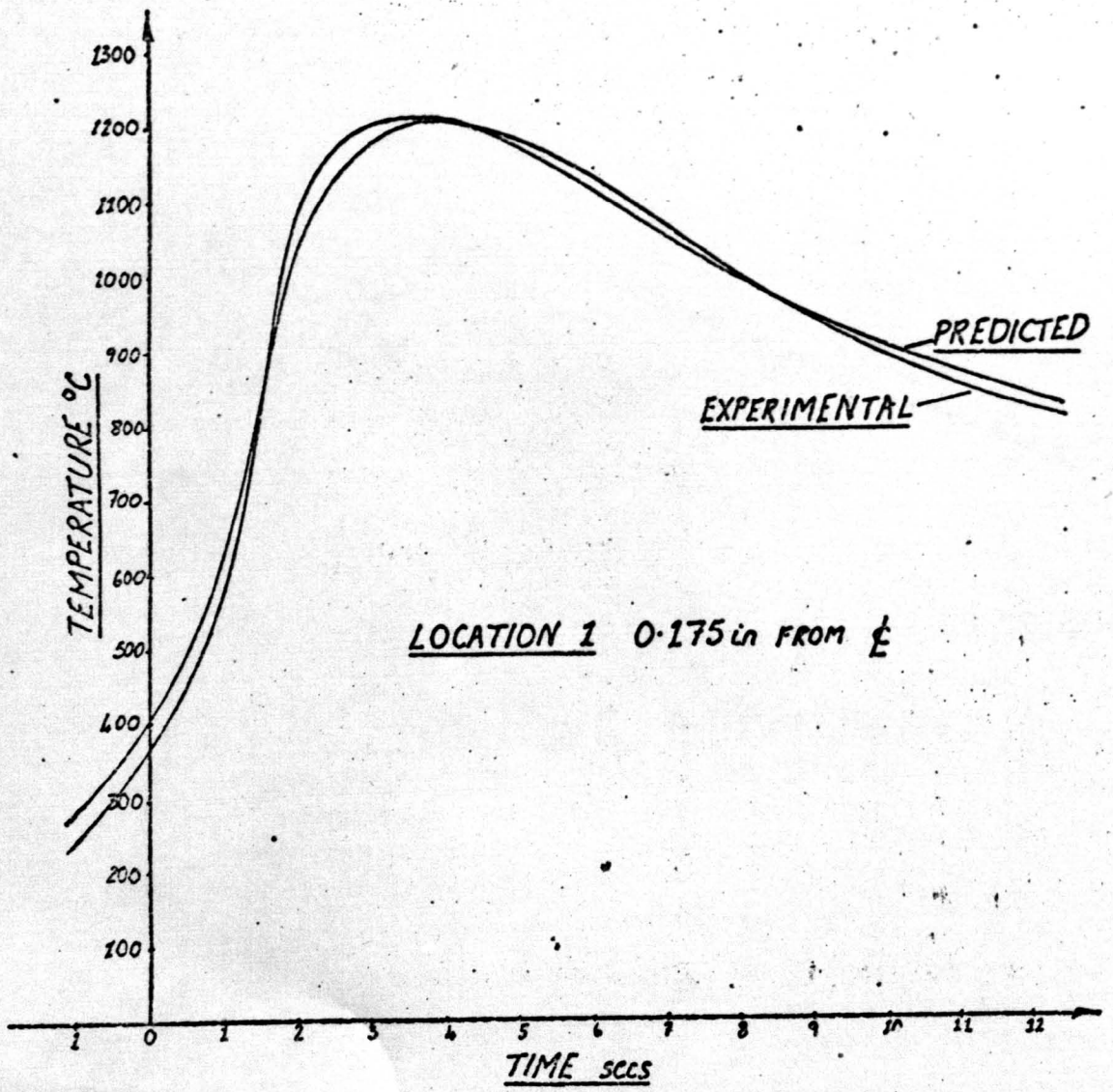

FIG 6·11 TEST B COMPARISON 1

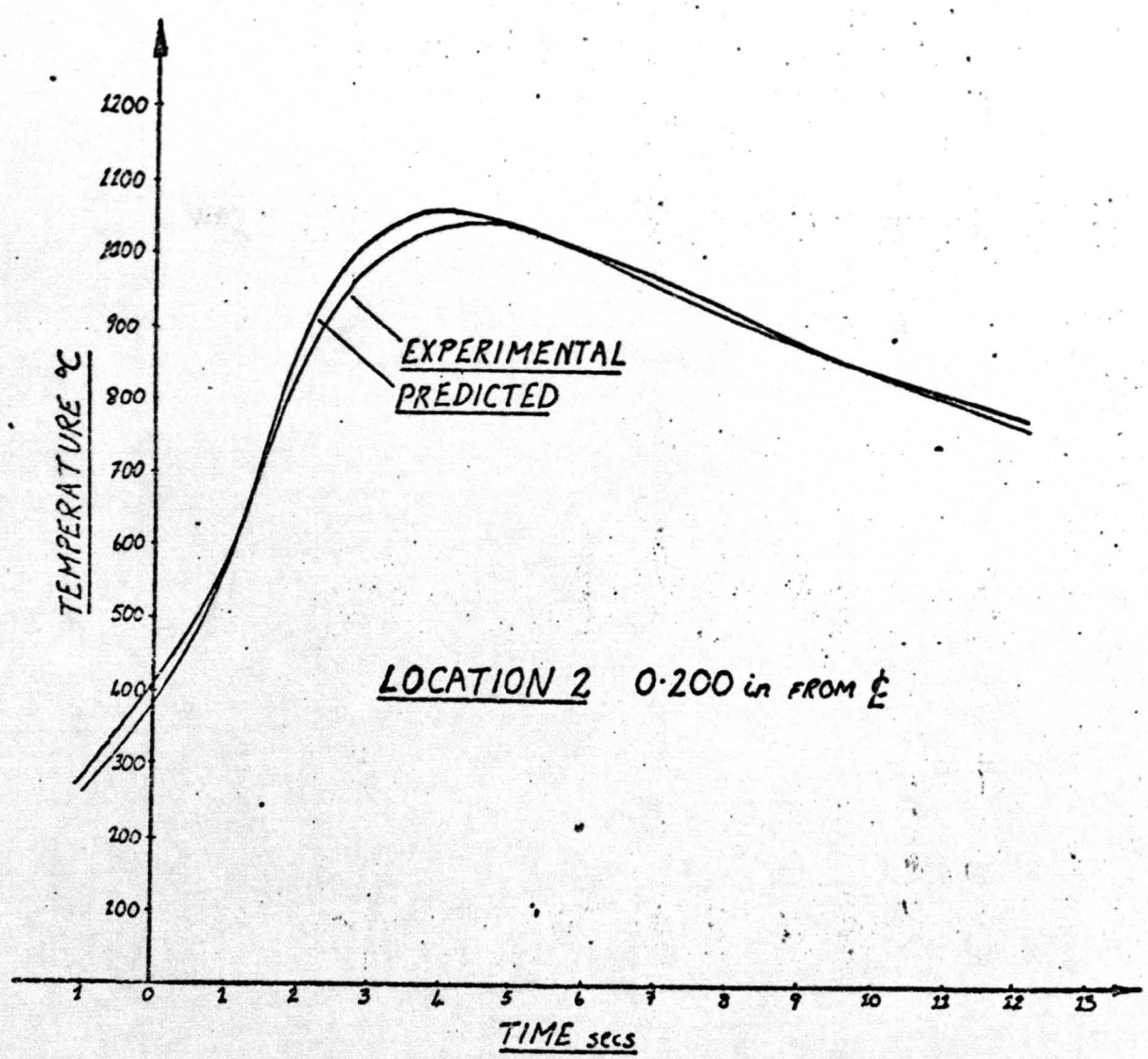

FIG 6·12 TEST B COMPARISON 2

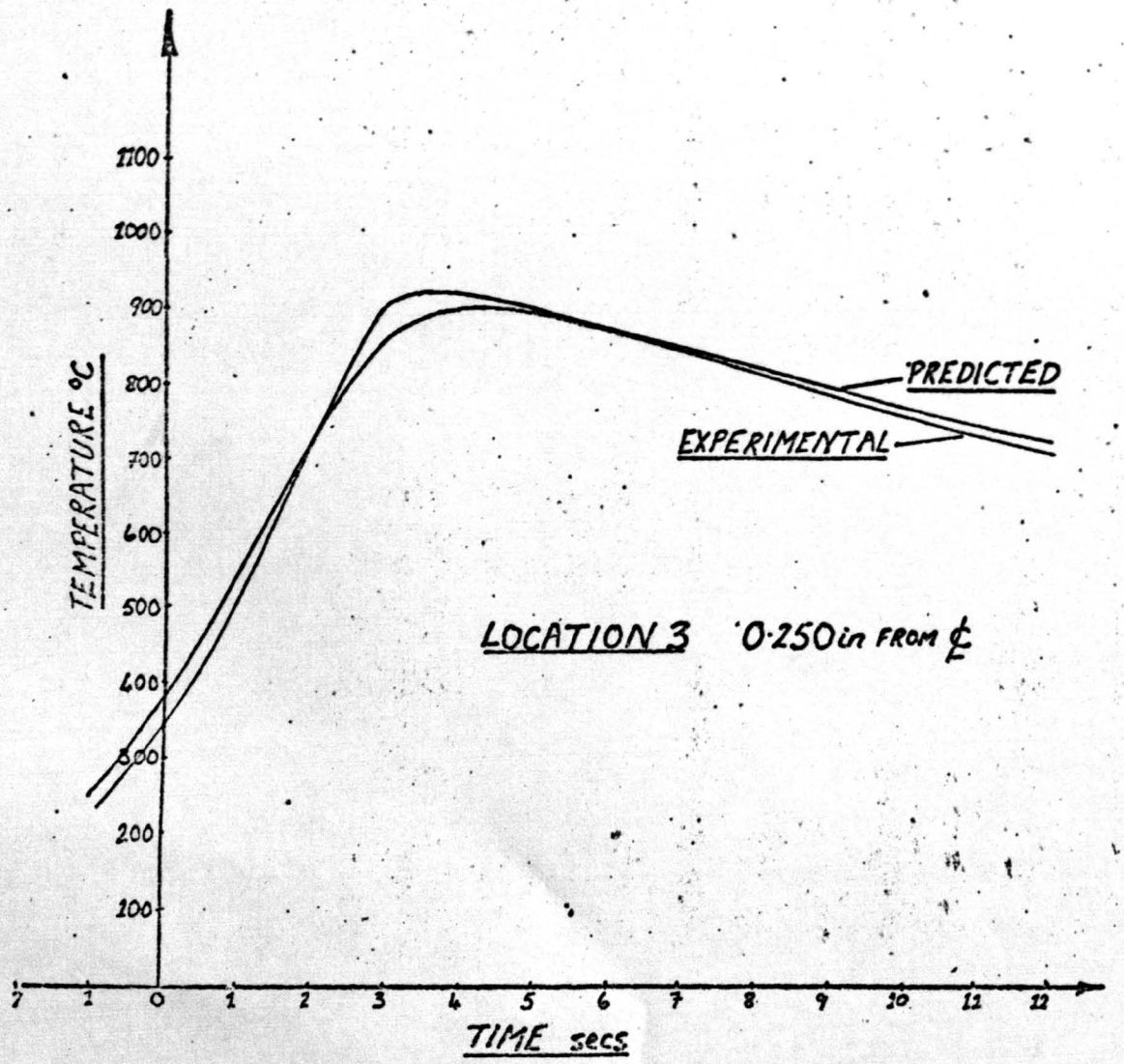

FIG 6·13 TEST B COMPARISON 3

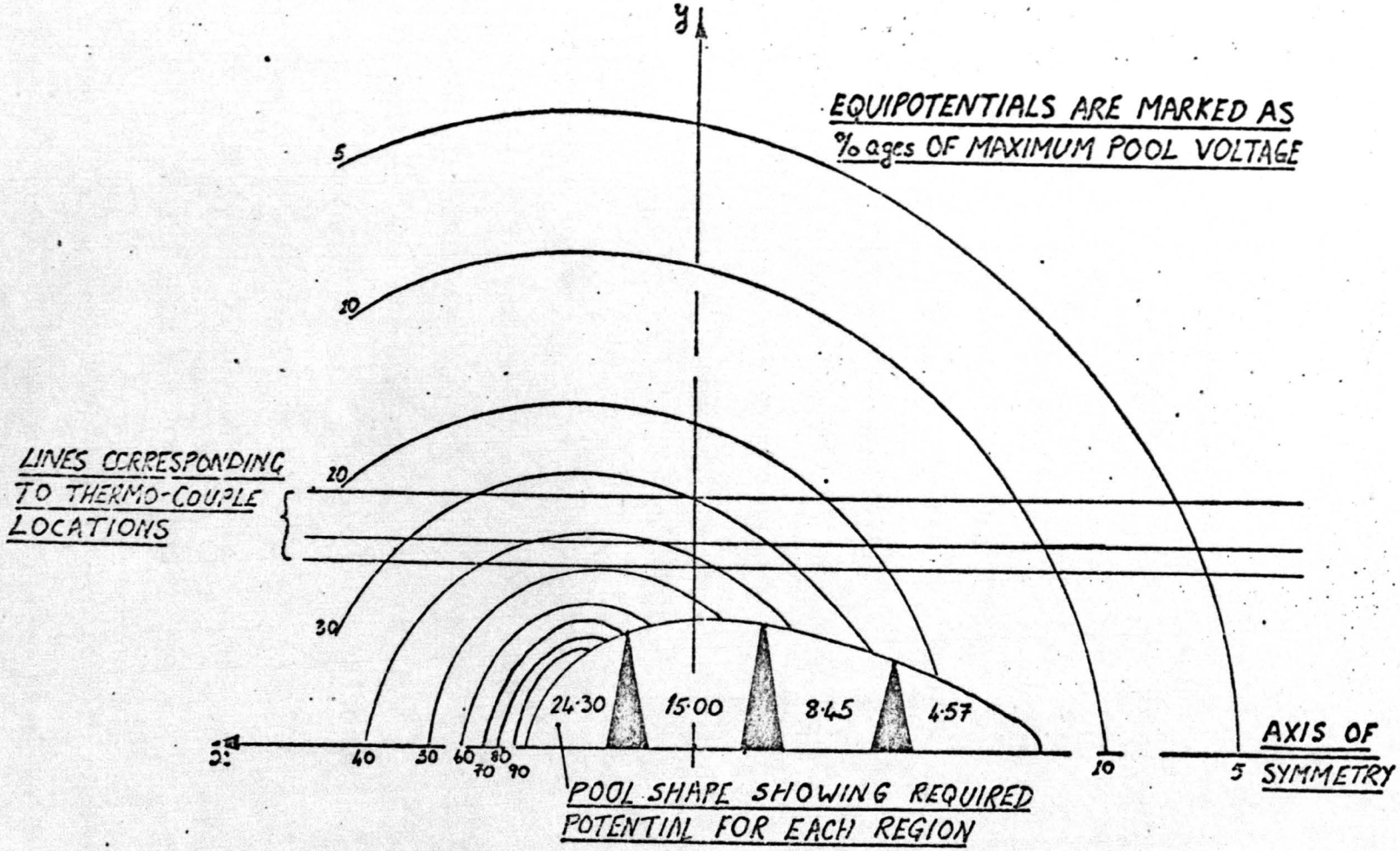

FIG 6·14 TEST B EQUIPOTENTIAL PLOT

6.4) Discussion

As can be judged from the graphs (Figs. 6.6 - 6.8 and 6.11 - 6.13), the results of the comparative tests showed good agreement between the analogue predicted and experimentally measured temperature histories. From the summary of these results given in Table 6.2, it can be seen that the agreement between peak temperatures was better than 3%. This was well within the error range expected of either the analogue or the experimental technique. However, this excellent agreement was not maintained throughout the temperature-time range considered. As the graphs show, the analogue results consistently predicted a slower cooling rate than that observed experimentally. The extent of this divergence for the time ranges considered can be judged from the figures quoted in Table 6.2 which compare the results 25s after zero for Test A and 10s after zero for Test B.

The peak temperature comparisons are considerably better than those reported by Tanbakuchi (12) and are comparable with those reported by Pavelic (5) using finite difference analysis. Pavelic's numerical approach accounted for the spread of arc plasma onto the parent metal beyond the pool boundary. The excellent agreement for the peak temperatures achieved with the analogue, therefore, suggested that, for the test conditions considered, there was little or no arc spread beyond the pool boundary.

This hypothesis was tested by photographing stationary arcs and measuring the arc spread at the surface of the test plate. One such photograph is shown in Plate 6.4. This shows a negative print

TEST A		DISTANCE FROM ℄ (in)		
		0.200	0.225	0.250
PEAK	PREDICTED EXPERIMENTAL	1267 1255	1178 1180	1024 1024
25s AFTER PEAK	PREDICTED	712 685	704 695	690 700
TEST B		DISTANCE FROM ℄ (in)		
		0.175	0.200	0.250
PEAK	PREDICTED EXPERIMENTAL	1220 1212	1055 1049	922 902
10s AFTER PEAK	PREDICTED EXPERIMENTAL	902 891	840 840	772 765

TABLE 6.2 COMPARATIVE TEST RESULTS

PLATE 6.4 NEGATIVE PRINT SHOWING A 100A ARC

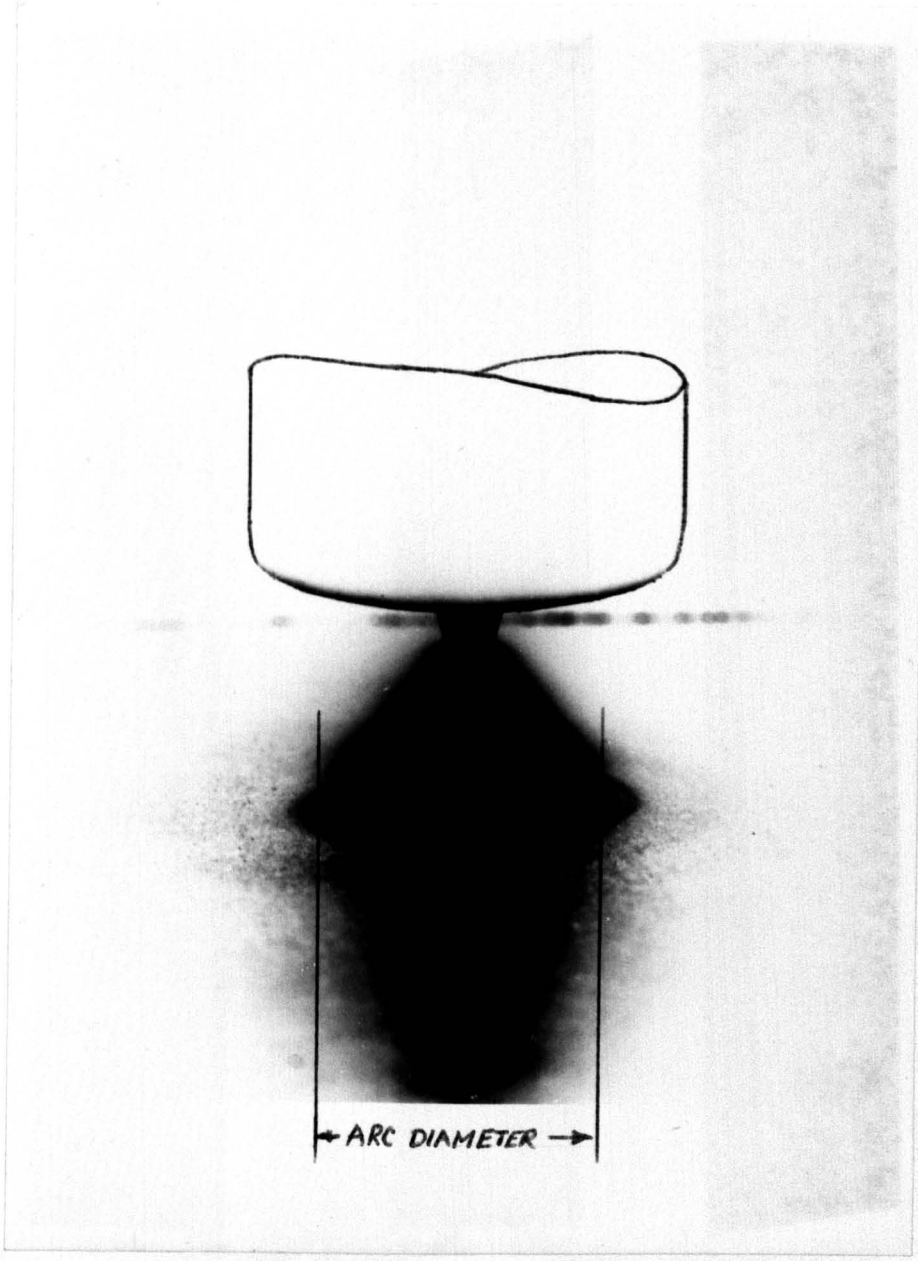
ARC DIAMETER

of a 100A arc (arc height 3.5 mm., gas flow 8.0 ft^3/hr) with the ceramic nozzle and electrode superimposed to show their position relative to the arc. Using this technique, measurements of the arc spread at the plate surface indicated that at 100A, the arc spread was less than 1 mm. beyond the maximum width of the weld pool recorded for Test A for a 106A arc (see Fig. 6.5, Test A). While this weld pool relates to a moving arc, the actual welding speed is very slow and experience suggests that the effect of movement on the arc shape is to make it longer and somewhat narrower (5). The estimates of arc spread obtained from stationary arcs are therefore somewhat greater than the actual spread for a moving arc. Although the arc spread increases with arc current, a similar result was obtained for a 140A arc, the arc spread in this case being only slightly more than 1 mm. greater than the maximum pool width. (see Fig. 6.5, Test B). The agreement in peak temperatures, therefore, suggests that provided the arc spread does not extend significantly beyond the pool boundary, the peak temperatures experienced by points close to the molten zone are primarily dependent upon the conduction of heat across the molten pool boundary into the parent metal.

In applying the Mk II analogue to the welding problem, no account was made of either the heat loss from the surface of the test plate by radiation and convection or of the variation with temperature of the plate's thermal properties (i.e. conductivity, specific heat and density). While it is not too unreasonable to assume that for the range of temperatures considered the variation in the thermal properties had only a second order effect on the

temperature histories, the divergence of the analogue and experimental cooling curves could be attributed to the failure of the analogue to account for the heat loss from the surface of the plate. Since the analogue is essentially a linear model of the linear Rosenthal system, it is not possible to account for the non-linear heat loss by radiation. However, as shown in Appendix 2a, it is possible to account for the linear heat loss by convection (i.e. heat loss proportional to temperature) on the ϕ field analogue simply by altering the scaling factor. If certain assumptions are made about the variation of the thermal properties with temperature, it is also possible to account for this variation in a somewhat similar manner. This is discussed in Appendix 2b. Accounting for these two effects will certainly be important if the analogue predictions were extended beyond the temperature ranges considered in the above tests.

However, the major disadvantage of the Mk II analogue for this application arises from its fixed leakage resistor construction. Having constructed an analogue with fixed resistance values, it can be appreciated from section 6.2 that the scale factor will be directly proportional to the welding speed. This has a somewhat unfortunate "double-edged" effect. Increasing the welding speed and thus the scale factor results in a larger analogue representation of the pool shape. While this may be advantageous for accurate determinations of potential close to the pool boundary, it also has the effect of reducing the area of real space (or space-time) represented by the finite area of the analogue. This effect is clearly demonstrated by comparing the ϕ field plots for Tests A and B

(Figs. 6.9 and 6.14). These are both 1:1 representations of the actual plots obtained on the Mk II analogue. Comparison of the sizes of the pool shapes in these plots with the actual pool profiles shown in Fig. 6.5, demonstrates the effect of the difference in scale factor (3.224 for Test A and 6.017 for Test B). The greater resolution obtained for the Test B plot (Fig. 6.14) is gained at the expense of a reduction in the area of real space represented by the analogue. It is for this reason that the Test B comparative results (Figs. 6.11 - 6.13) stop 12s after zero (c.f. 30s after zero for the Test A results), this being the limit allowed by the finite size of the Mk II analogue. Since the value of the analogue parameter $\sqrt{\frac{\rho}{R}}$ was essentially the same for both tests (0.365 for Test A and 0.358 for Test B), the difference in scale factor is due to the difference in welding speed (0.14 cm/s for Test A and 0.25 cm/s for Test B).

There are two obvious design changes which could be made to overcome this problem. The first is to simply increase the size of the analogue field, particularly in the x direction. The second is to devise a construction with variable leakage resistances (or interchangeable resistance values) so that the value of the analogue parameter $\sqrt{\frac{\rho}{R}}$ can be changed to compensate for different welding speeds (see the design formula, equation 6.1).

It is also recommended that closer tolerance resistors be used to improve the accuracy of the ϕ field distribution. It was found that although the evaluation tests (section 4.6) showed excellent agreement with theory and the ϕ distributions around the weld pools appeared perfectly smooth, there were, in fact, small random errors

in the measured ϕ values due to the small variations in the leakage resistance values ($\pm$ 2% of nominal value). From the nature of the Rosenthal transformation, these errors were magnified when the $\phi(x)$ distributions were transformed to the T(t) distributions with the result that the T(t) plots were not perfectly smooth, the calculated points being scattered in a random fashion about the mean curve. While only the mean curves have been shown compared with the experimental histories (Figs. 6.6 - 6.8 and 6.11 - 6.13), Fig. 6.15 shows one such mean curve with the actual calculated values shown by the crosses. The calculated values, however, were never more than $\pm$ 20°C from the mean curve. This variation can be completely accounted for by a $\pm$ 2% error in resistance value and could, therefore, be removed by using better quality resistors in the analogue construction. This is particularly recommended if a larger analogue field is to be constructed since better resolution in ϕ values will be required for these points more remote from the pool boundary.

Despite these shortcomings, the Mk II analogue has been shown to predict the thermal field during welding extremely well for the range of test conditions considered. While it is not possible for the analogue technique to provide as detailed an analysis as is possible using a numerical approach, it is felt that the analogue approach could be usefully employed for the welding application. Since the whole of the ϕ field (and, hence, the corresponding temperature field) for any number of welds (provided the heat flow remains 2-D) can be readily determined, hypotheses can be quickly tested and trends observed experimentallly investigated. Particular zones of

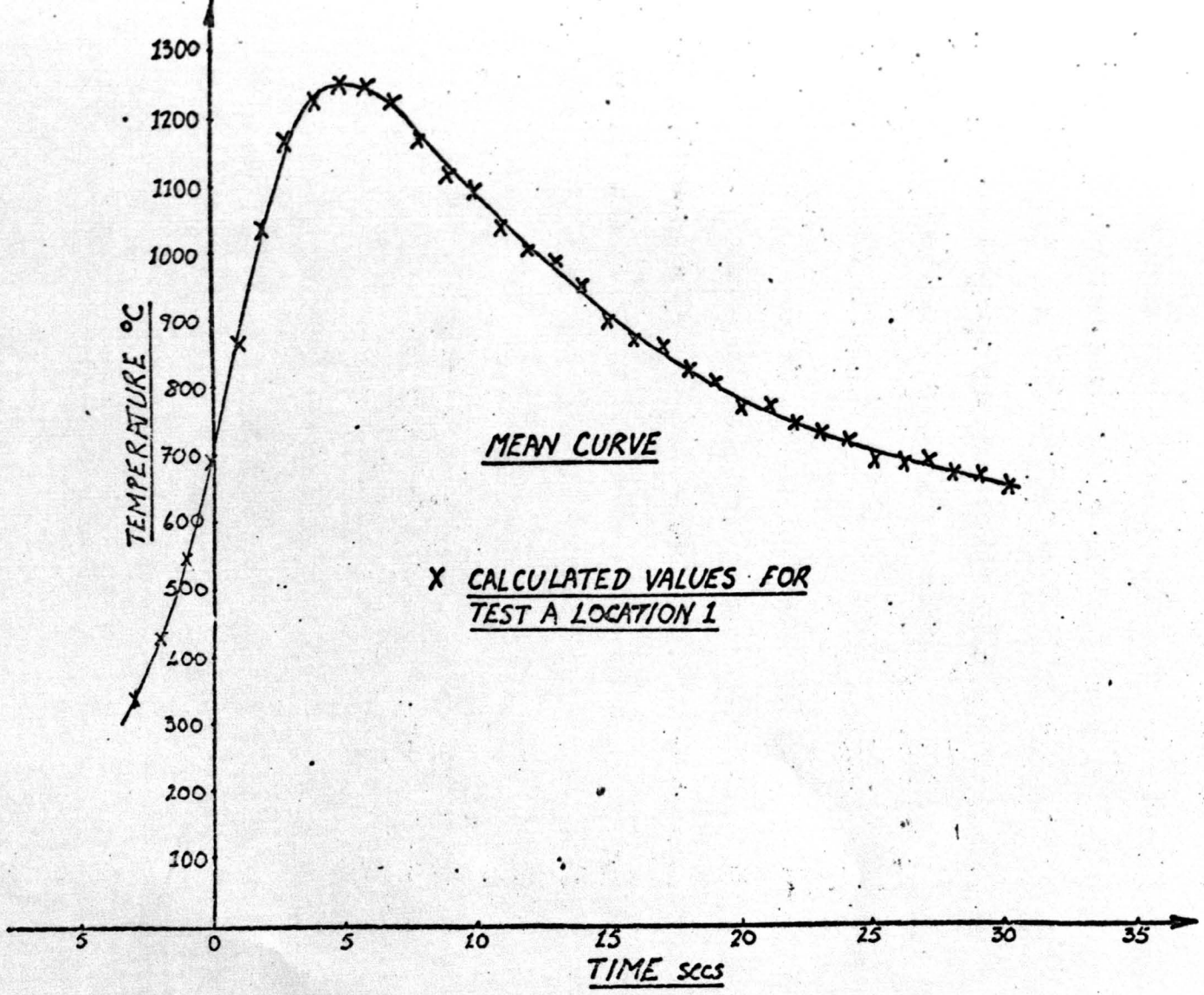

FIG 6·15 CALCULATED VALUES OF TEMPERATURE

interest could then be identified for more detailed examination using a numerical approach.

As a demonstration of the way in which the analogue may be employed, consider the three experimental recordings for Test A shown in Fig. 6.4. It will be observed that the three temperature curves are decaying at substantially the same rate despite the obvious difference in the peak temperatures. Indeed, it would seem that the three cooling curves tend to converge to a single curve.

This trend can be explained by studying the nature of the ϕ field distribution at increasing distances from the pool shape as shown in Fig. 6.9. It can be seen that the equipotentials rapidly become circular in nature with increasing distance from the pool shape. It can therefore be appreciated that the $\phi(x)$ distributions along each of the lines shown (corresponding to the thermocouple locations) tend to become identical with increasing distance from the pool shape.

Consider the three values of ϕ at $|x| = a$, $y = y_1, y_2, y_3$ as shown in Fig. 6.9. Due to the almost vertical nature of the equipotentials in the neighbourhood of $|x| = a$, it can be appreciated that the three ϕ potentials will be almost identical and that this will become increasingly true with increasing $|x|$

i.e. $$\phi(x,y_1) \rightleftharpoons \phi(x,y_2) \rightleftharpoons \phi(x,y_3)$$

with increasing $|x|$.

Since the Rosenthal transformation operates only on the x-axis, it is independent of y, being given by equation 4.1,

$$T(x,y) = e^{-\frac{v}{2\alpha}.x} \phi(x,y)$$

it follows that

$$T(x,y_1) \rightleftharpoons T(x,y_2) \rightleftharpoons T(x,y_3)$$

with increasing $|x|$.

Since x is simply proportional to t, it can be concluded that

$$T(t,y_1) \rightleftharpoons T(t,y_2) \rightleftharpoons T(t,y_3)$$

with increasing t.

This is in agreement with the experimental observation that the cooling curves shown in Fig. 6.4 tend to converge. For points located at greater distances from the welding axis, it is evident that the same effect would be observed but only after a longer time and at a lower temperature. Incidentally, it is also the circular nature of the ϕ field distribution which indicates how quickly the ϕ field becomes independent of the actual pool shape.

To summarise, the comparative tests showed the good agreement between the analogue predicted and experimentally measured temperature histories. While this, of course, can only be said to be true for the welding conditions adopted in the tests, it is felt that these conditions were not too far removed from standard procedure (19) and that the analogue technique could be equally applied to a wide range of welding conditions found in practice. Although it is not possible for the analogue approach to provide as detailed an analysis as has been shown to be possible using a numerical approach (5), its simplicity and flexibility make it

an extremely useful tool for at least an initial investigation of quasi-static 2-D thermal fields during welding.

CONCLUSIONS

1) A study of the modal characteristics of Rosenthal fields indicates the possibility of using a simple analogue for the analysis of heat flow during welding. From this initial study, it is demonstrated that the modal characteristics of non-uniform systems can be related to the characteristics of the corresponding uniform system. In particular, it is shown in Appendix 1 that the longitudinal vibration characteristics of a uniform cross-section beam are only a special case of a more generalised set of characteristics relating to a variable cross-section. It is also shown that, in general, the eigenvectors for such variable cross-section systems are orthogonal with respect to a weighting function identical to the function defining the variation in cross-section.

2) It is shown that a potential field having an exponential variation in conductivity can be identified as a Rosenthal field and that a direct electrical analogue based on this principle could be designed. However, owing to the very large variation in resistance required, this approach is impractical for most welding heat flow studies. The feasibility study for the direct analogue does reveal that to obtain the same temperature distribution in the welding of materials of the same geometry under different welding conditions, it is only necessary that the ratios $\frac{v}{\alpha}$ and $\frac{q}{k}$ remain the same. While this conclusion is subject to the basic assumptions of Rosenthal's analysis and, consequently, that control of these two ratios alone may be insufficient to completely control the thermal field, particularly in the HAZ, they are, nevertheless, important parameters. Since $\frac{v}{\alpha}$ is independent of the exact nature of q, it is

expected that it has a particular significance in the determination of temperature gradients.

3) By employing a transformation of Rosenthal's equation a simple electrical analogue can be constructed which is not restricted by the variation in resistance required by direct analogues. This analogue has the advantage of having a continuous surface which makes it particularly suitable for 2-D heat flow studies based on the pool shape model proposed by Apps and Milner (7). Comparative tests between analogue predicted and experimentally measured temperature histories in the HAZ for continuous DC TIG welding show that the thermal field in the HAZ can be successfully simulated using this type of analogue. Peak temperatures are particularly well predicted and while consistent divergence in cooling curves is shown, this can be attributed to heat losses from the plate which were not accounted for. A simple procedure for making allowance for such losses is, however, demonstrated in Appendix 2a. Although the application of the analogue is restricted to 2-D quasi-static analysis, it is especially valuable in that the thermal field in the HAZ can be simulated on a continuous analogue field. Provided single pass, full penetration welding is considered, there is no apparent reason why this analogue approach may not be applied to other welding processes. Until the mechanisms by which heat is transported through the arc and weld pool are completely understood, it is anticipated that the ϕ field analogue will prove to be a useful experimental tool in analysing welding heat flow.

Appendix 1

Longitudinal vibrations of some variable cross-section beams

As noted in Chapter 2, it was of some interest to explore the way in which the eigenvectors of a uniform system change when one of the properties of the system is allowed to vary. For example, it is shown in Chapter 3, that an exponential variation in conductivity can result in the same governing equation (and hence the same eigenvectors) as Fourier's equation of conduction in a homogeneous medium but referred to a Rosenthal co-ordinate system. To develop this idea further, consider the longitudinal vibrations $u(x,t)$ of a beam whose cross-sectional area $A(x)$ varies along the length of the beam. It is readily established that $u(x,t)$ obeys the governing equation

$$\frac{\partial^2 u}{\partial x^2} + \frac{1}{A}\cdot\frac{\partial A}{\partial x}\cdot\frac{\partial u}{\partial x} = \frac{\rho}{E}\cdot\frac{\partial^2 u}{\partial t^2} \qquad \text{(A1.1)}$$

where ρ is the density and E the Young's Modulus of the material of the beam (both assumed constant). In establishing this equation, the usual assumptions that during its motion, plane sections of the beam remain plane and that Poisson's ratio effects are negligible, have been made. The only conditions to be imposed upon $A(x)$ are that it be continuous, differentiable at least once and have no zeros in the range of x.

Provided the boundary conditions imposed on the beam are linear, solutions to equation A1.1 may be sought by separating the variables i.e. consider a solution of the form

$$u(x,t) = \phi(x).\Omega(t)$$

Substituting for $u(x,t)$ in equation A1.1 and re-arranging gives the two separated equations

$$\frac{\partial^2 \phi}{\partial x^2} + \frac{1}{A}.\frac{\partial A}{\partial x}.\frac{\partial \phi}{\partial x} + \lambda^2 \phi = 0 \qquad \text{(A 1.2)}$$

and

$$\frac{\partial^2 \Omega}{\partial t^2} + \lambda^2.\frac{E}{\rho}.\Omega = 0 \qquad \text{(A1.3)}$$

where λ is the separation constant.

The solutions $\phi(x)$ to equation A1.2 will define the eigenvectors of the system while the solutions $\Omega(t)$ to equation A1.3 will define the behaviour of the system with time. However, since the solutions (i.e. the eigenvectors) of equation A1.2 are obviously dependent upon $A(x)$, it is this equation which is of particular interest.

Consider, for example, the case where $A(x)$ is a linear function of the form

$$A(x) = a + bx$$

where a and b are non zero constants.

Substituting in equation A1.2 yields

$$\frac{\partial^2 \phi}{\partial x^2} + \frac{b}{(a+bx)}.\frac{\partial \phi}{\partial x} + \lambda^2 \phi = 0$$

It is convenient to transform the independent variable to $\omega = a + bx$ in the above equation, reducing it to

$$\frac{\partial^2 \phi}{\partial \omega^2} + \frac{1}{\omega} \cdot \frac{\partial \phi}{\partial \omega} + \left(\frac{\lambda}{b}\right)^2 . \phi = 0$$

This equation is readily recognised as a zero order Bessel equation whose solution is given by

$$\phi(\omega) = c_1 J_o\left(\frac{\lambda}{b} \cdot \omega\right) + c_2 Y_o\left(\frac{\lambda}{b} \cdot \omega\right)$$

where c_1 *and* c_2 *are constants and* J_o *and* Y_o *are zero order Bessel* functions of the first and second kind respectively.

This solution defines the eigenvectors (or normal modes) of this system. The eigenvectors λ would be determined by the particular boundary conditions imposed on the beam.

The corresponding solution to equation A1.3 is simply

$$\Omega(t) = c_3 \sin \lambda \sqrt{\frac{\rho}{E}} \cdot t + c_4 \cos \lambda \sqrt{\frac{\rho}{E}} \cdot t$$

and it can be seen that the natural frequencies would be given by $\lambda . \sqrt{\frac{\rho}{E}}$.

It is interesting to note that the simple linear variation in cross-section has produced eigenvectors in the form of Bessel functions. This should be compared with the pure sinusoidal eigenvectors for uniform cross-sections.

Consider now the case of a circular rod whose radius of cross section r is varying such that

$$r = a + bx$$

The cross-sectional area A(x) is, therefore, given by

$$A(x) = \pi (a + bx)^2$$

Substituting for A(x) in equation A1.2 gives

$$\frac{\partial^2 \phi}{\partial x^2} + \frac{2b}{(a+bx)} \cdot \frac{\partial \phi}{\partial x} + \lambda^2 \phi = 0$$

Again, transforming the independent variable to

$$\omega = a + bx$$

reduces this equation to the form

$$\frac{\partial^2 \phi}{\partial \omega^2} + \frac{2}{\omega} \cdot \frac{\partial \phi}{\partial \omega} + \left(\frac{\lambda}{b}\right)^2 \phi = 0$$

This is another Bessel equation whose solutions are of the form

$$\phi(\omega) = \omega^{-\frac{1}{2}} \cdot \left[c_1 J_{\frac{1}{2}}\left(\frac{\lambda}{b} \cdot \omega\right) + c_2 Y_{\frac{1}{2}}\left(\frac{\lambda}{b} \cdot \omega\right) \right]$$

where c_1 and c_2 are constants.

Again the eigenvectors appear as Bessel functions but from the theory of such functions, it can be shown that

$$Y_{\frac{1}{2}}(x) = -J_{-\frac{1}{2}}(x),$$

$$J_{\frac{1}{2}}(x) = \left(\frac{2}{\pi x}\right)^{\frac{1}{2}} \sin x$$

and

$$J_{-\frac{1}{2}}(x) = \left(\frac{2}{\pi x}\right)^{\frac{1}{2}} \cos x$$

Using these relations in the above expression for $\phi(\omega)$, it can readily be shown that

$$\phi(\omega) = \frac{1}{\omega} \left[c_1' \sin\left(\frac{\lambda}{b} \cdot \omega\right) + c_2' \cos\left(\frac{\lambda}{b} \cdot \omega\right) \right]$$

From the boundary conditions, the eigenvalues λ and hence the natural frequencies can be determined in the usual way.

It is interesting to note that in this last case, the sinusoidal

PAGE
MISSING
IN
ORIGINAL

functions have re-appeared, qualified by the factor $\frac{1}{\omega}$. It can in fact be shown from the solutions to generalised Bessel equations (20) that, if A(x) has the form

$$A(x) = ax^{\alpha},$$

the eigenvectors can be expressed as

$$\phi(x) = x^{\frac{1}{2}(1-\alpha)} \cdot \left[c_1 J_n(\lambda x) + c_2 Y_n(\lambda x) \right]$$

where $n^2 = \frac{1}{4}(1-\alpha)^2$ and c_1 and c_2 are constants. If α is zero i.e. a uniform beam, then using the Bessel function relations for $J_{\pm\frac{1}{2}}(x)$ and $Y_{\pm\frac{1}{2}}(x)$ already stated, this "general" eigenvector will reduce to the simple trigonometric functions $\sin\lambda x$ and $\cos\lambda x$ as indeed it must.

It would, therefore, seem that in considering the response of non-uniform systems similar to those described above, the eigenvectors are likely to be Bessel functions and that where sinusoidal eigenvectors are observed, they are, in fact degenerate Bessel functions.

The variation in area A(x) can, however, be shown to have a completely general relationship with the eigenvectors.

Consider the nth eigenvector $\phi_n(x)$ whose governing equation (or characteristic equation) has the form

$$\frac{\partial^2 \phi_n}{\partial x^2} + \frac{1}{A} \cdot \frac{\partial A}{\partial x} \cdot \frac{\partial \phi_n}{\partial x} + \lambda_n^2 \phi_n(x) = 0$$

(i.e. equation A1.2).

Multiplying this equation by $A(x)$ and re-arranging yields

$$\frac{\partial}{\partial x}\left[A.\frac{\partial \phi_n}{\partial x}\right] + \lambda_n^2 A(x).\phi_n(x) = 0 \qquad \text{A1.3}$$

Similarly, if $\phi_n(x)$ is the eigenvector corresponding to the mth eigenvalue λ_m, then

$$\frac{\partial}{\partial x}\left[A.\frac{\partial \phi_m}{\partial x}\right] + \lambda_m^2 A(x).\phi_m(x) = 0 \qquad \text{A1.4}$$

Multiplying equation A1.3 by ϕ_m and equation A1.4 by ϕ_n and subtracting yields

$$\frac{\partial}{\partial x}\left[A.\left(\phi_m.\frac{\partial \phi_n}{\partial x} - \phi_n.\frac{\partial \phi_m}{\partial x}\right]\right. + A\phi_n.\phi_m\left[\lambda_n^2 - \lambda_m^2\right] = 0$$

Integrating this equation with respect to x over the range of x (say a:b) yields,

$$\left[A.\left(\phi_m \frac{\partial \phi_n}{\partial x} - \phi_n.\frac{\partial \phi_m}{\partial x}\right)\right]_a^b = \left[\lambda_m^2 - \lambda_n^2\right].\int_a^b A.\phi_n.\phi_m dx \qquad \text{A1.5}$$

Whatever the exact nature of ϕ_m and ϕ_n, they must satisfy the boundary conditions at x = a,b. Boundary conditions for a wide range of systems will have the general form

$$a_1\,\phi(a) + a_2\,\phi'(a) = c_1$$

and

$$b_1\,\phi(b) + b_2\,\phi'(b) = c_2$$

where a_1, a_2, b_1, b_2, c_1 and c_2 are constants. It can be seen that, under these conditions, the left hand side of equation A1.5 must always vanish.

i.e. $$\left[\lambda_m^2 - \lambda_n^2\right]\int_a^b A.\phi_m.\phi_n dx = 0$$

Provided $m \neq n$ i.e. $\lambda_m^2 \neq \lambda_n^2$, then

$$\int_a^b A.\phi_m.\phi_n dx = 0 \qquad \text{A1.6}$$

This result indicates that the eigenvectors $\phi_m(x)$ and $\phi_n(x)$ are orthogonal on the interval a:b with respect to the weighting function A(x).

N.B. The approach outlined above is generally attributed to Sturm and Liouville and may be found in standard texts describing orthogonal functions. e.g. (22).

The variation of cross-section A(x) will, therefore, always appear as the weighting function to which the eigenvectors of the system will be orthogonal. It should, however, be noted that the eigenvectors will not necessarily be one of the fundamental orthogonal functions.

From the previous discussion, it has been shown that if A(x) has the form

$$A(x) = ax^{\alpha},$$

the eignevectors $\phi_n(x)$ can be written as

$$\phi_n(x) = x^{\frac{1}{2}(1-\alpha)}J_n(\lambda_n x) \qquad \text{or} \left[x^{\frac{1}{2}(1-\alpha)}Y_n(x)\right]$$

Substituting for A(x), $\phi_n(x)$ and $\phi_m(x)$ in the orthogonality condition (equation A1.6) gives

$$\int_a^b x.\ J_m(\lambda_m x).J_n(\lambda_n x)dx = 0$$

This is, of course, the orthogonality condition for Bessel functions which are all orthogonal with respect to a weighting function of x. Thus, although the eigenvectors

$$\phi_n(x) = x^{\frac{1}{2}(1-\alpha)} J_n(\lambda_n x)$$

are orthogonal to the weighting factor

$$A(x) = ax^{\alpha},$$

the basic orthogonal function involved $J_n(\lambda_n x)$ has a weighting factor of x.

Although this discussion has been restricted to a simple vibration system, the above results apply to a large number of problems in a diverse number of fields. Consider, for example, the variable conductivity form of Fourier's equation (equation 3.2) used in Chapter 3 to establish the direct analogue principle. Although this is a 2-D equation, its form is not dissimilar to equation A1.1. Indeed, the eigenvector equation in the x direction would be identical in form to equation A1.2 and the above discussion would apply equally to that heat conduction system.

Appendix 2

a) Thin plates with heat loss by convection.

The well established (22) form of Fourier's equation for the 2-D conduction of heat in a thin plate losing heat by convection from its major surfaces, is given in Cartesian co-ordinates by

$$\nabla^2 T - \left(\frac{2H}{kd}\right) T = \frac{1}{\alpha} \frac{\partial T}{\partial t} \qquad \text{(A2.1)}$$

where the temperature T of the plate is measured relative to the ambient temperature of the surroundings, H is the coefficient of convective heat transfer from the surfaces of the plate to the surroundings and d is the thickness of the plate (other symbols having their usual meaning).

Transforming equation A2.1 to Rosenthal co-ordinates (see Chapter 1) and making the quasi-static assumption that, with respect to these co-ordinates, $\frac{\partial T}{\partial t} = 0$ gives,

$$\nabla^2 T + \frac{v}{\alpha} \frac{\partial T}{\partial x} - \left(\frac{2H}{kd}\right) T(x, y) = 0 \qquad \text{(A2.2)}$$

If the dependent variable T(x, y) is now transformed by the Rosenthal transformation

i.e. $$T(x, y) = \bar{e}^{\frac{vx}{2\alpha}} . \phi(x, y);$$

equation A2.2 becomes

$$\nabla^2 \phi - \left[\left(\frac{v}{2\alpha}\right)^2 + \left(\frac{2H}{kd}\right)\right] \phi = 0 \qquad \text{(A2.3)}$$

Comparing this equation with the governing equation for the ϕ field analogue (equation 4.7)

i.e. $$\nabla^2 V - \frac{\rho}{Rh^2} V = 0$$

shows that, for the ϕ-field to be an analogue of equation A2.3,

$$h = \left[\left(\frac{v}{2\alpha}\right)^2 + \left(\frac{2H}{kd}\right) \right]^{-1/2} \sqrt{\frac{\rho}{R}} \qquad \text{(A2.4)}$$

This is the required analogue design formula and it is comparable with equation 6.1.

It can be seen that the effect of the convective loss is to reduce the value of h i.e. the distance of real space represented by the analogue resistor spacing. Since the analogue scale factor is inversely proportional to h (see section 6.2), the effect of the convective loss is to increase the scale factor. In fact, the effect is similar to increasing $\frac{v}{\alpha}$ which as discussed in section 3.2, has the effect of increasing the thermal gradients (both with respect to space and time) around the weld pool.

b) Thin plates with variable thermal properties

Fourier's equation governing the conduction of heat in a 2-D medium whose thermal properties (i.e. conductivity, density and specific heat) are functions of temperature, takes the form (22),

$$\nabla (k \nabla T) = \rho c \frac{\partial T}{\partial t} \qquad \text{(A2.5)}$$

Again transforming to Rosenthal co-ordinates and assuming quasi-static conditions yields

$$\nabla (k \nabla T) + \rho c v \frac{\partial T}{\partial x} = 0 \qquad \text{(A2.6)}$$

Solutions to equation A2.6 have been investigated (by Grosh et al (23) and Kazimirov et al (24)) for Rosenthal's line source model of the welding heat imput. The particular relevance to this work, however, lies in the transformation of the dependent variable which was used by both the authors cited above.

If it is assumed that both the thermal conductivity $k(T)$ and the volumetric heat capacity $\rho c(T)$ are the same functions of temperature then it is convenient to write

$$k(T) = k_o f'(T) \qquad \text{(A2.7)}$$

and

$$\rho c(T) = (\rho c)_o f'(t) \qquad \text{(A2.8)}$$

where $f'(t)$ is the temperature derivative of some function of temperature $f(T)$. It is assumed that both $f(T)$ and $f'(T)$ are differentiable (and are non-zero in the range of T).

From equation A2.7, it can be seen that

$$\frac{\partial f(T)}{\partial x} = f'(T)\frac{\partial T}{\partial x}$$

and equation A2.6 may, therefore, be re-written as

$$\frac{\partial^2 f(T)}{\partial x^2} + \frac{\partial^2 f(T)}{\partial y^2} + \frac{v}{\alpha}\frac{\partial f(T)}{\partial x} = 0 \qquad \text{(A2.9)}$$

where $$\alpha = \frac{k_o}{(\rho c)_o}$$

This equation can be seen to have the same form as a Rosenthal equation (equation 1.2). Again employing the Rosenthal transformation which in this case takes the form

$$f(T) = e^{-\frac{v}{2\alpha}x}\,\phi(x,y)$$

transforms equation A2.9 to the standard ϕ equation

i.e. $$\nabla^2\phi - \left(\frac{v}{2\alpha}\right)^2 \phi(x,y) = 0$$

This, of course, may be solved directly on the ϕ field analogue.

The nature of the relationship between $\phi(x,y)$ and $T(x,y)$ does, however, depend upon the nature of $f(T)$. If for example, $f(T)$ is such that

$$f'(T) = (1 + mT),$$

then it can be readily shown that

$$T(x,y) = \frac{1}{m}\left\{\left[2m\, e^{-\frac{v}{2\alpha}x} \cdot \phi(x,y)\right]^{\frac{1}{2}} - 1\right\} \qquad \text{(A2.10)}$$

while this relationship is not as simple as the standard Rosenthal transformation

i.e. $$T(x,y) = e^{-\frac{v}{2\alpha}x} \cdot \phi(x,y),$$

there would be no real difficulty in applying equation A2.10 for a particular problem. The required variation in ϕ along the pool length would, for example, be given by

$$\phi(x) = e^{\frac{v}{2\alpha}x} (1 + mT_m)^2$$

where T_m is the melting point of the material under consideration.

Whether or not the assumption that the thermal conductivity and the volumetric heat capacity have the same temperature dependence (i.e. a constant thermal diffusivity) would depend on the particular material but it would seem not to be too unreasonable for most metals (24).

It is interesting to note from the above analysis that the variation in thermal properties is handled by a transformation of the dependent variable T(x,y). This is somewhat in keeping with the discussion of section 3, where it is shown that a change in the ratio $\frac{q}{k}$ results directly in a change in T(x,y).

This discussion has shown how both convective heat loss from and variable thermal properties of the welded plate may be incorporated into the ϕ field analogue approach. Unfortunately, it does not seem possible to incorporate both effects simultaneously to form a single ϕ equation. This is due to the non-linear nature of f(T). However, it is felt that both these techniques may be used with the ϕ field analogue to some advantage to determine, for example, what significance each has on the thermal field in particular cases.

References

(1) Rosenthal, D. : "The Theory of Moving Sources of Heat and its Application to Metal Treatments", ASME Trans., 849-866 (Nov. 1946).

(2) Wells, A.A. : "Heat Flow in Welding", Welding Journal, 31(5), Research Suppl., 263-267 (May, 1952).

(3) Myers, P.S. et al.: "Fundamentals of Heat Flow in Welding", Welding Research Council Bulletin 123 (July 1967).

(4) Christensen, N. et al.: "Distribution of Temperatures in Arc Welding", British Welding Journal 54-75 (Feb. 1965).

(5) Pavelic, V. : "Temperature Histories in a Thin Steel Plate Welded with Tungsten Inert Gas Process", Ph.D. Thesis, University of Wisconsin (1968).

(6) Quigley, M.B.C. : "Heat Flow to the Workpiece from a TIG Welding Arc", Journal of Physics: D Applied Physics, Vol. 6 (2250-2258) (Sept. 1973).

(7) Milner, D.R. et al.: "Arc Characteristics and their Significance in Welding", British Welding Journal 73-88 (Feb. 1960).

(8) Pavelic, V. et al. : "Experimental and Computed Temperature Histories in Gas Tungsten-Arc Welding of Thin Plates", Welding Journal Research Suppl., 295-305 (July 1969).

(9) Apps, R.L. and Milner, D.R. : "Heat Flow in Argon-Arc Welding", British Welding Journal, 2, 475-485 (Oct. 1955).

(10) Dobrotina, Z.Z. : "Influence of Welding Current and Speed (at Constant Linear Heat Input) on Weld Geometry and Properties of the Zone near the Weld", Svar. Proiz., 8, 33-34 (1972).

(11) Demyantsevich, V.P.: "Characteristics of the Movement of Molten Metal in the Weld Pool during Welding with a Non-Consumable Electrode", Svar. Proiz., 10, 1-3 (1972).

(12) Tanbakuchi, R. : "Comparison of Measured Metal Temperatures During Arc Welding with Temperatures Calculated Using a Finite Heat Source", Ph.D. Thesis, University of Wisconsin (1967).

(13) Boughton, P. : "An Analysis of the Thermal Situation in Welding using an Electrical Analogue", Welding Research International, Vol. 3 no. 4 (1973).

(14) Vitkovich, D. (ed): "Field Analysis", publ. by Van Norstrand and Co. Ltd.

(15) Karplus, W.J. and Soroka, W.W.: "Analog Methods", 2nd ed. publ. McGraw Hill (1959).

(16) "Tables of the Exponential Function", Federal Works Agency, Work Project Administration for the City of New York (National Bureau of Standards, 1939).

(17) Simmons, W.R. : "An Analogue for the Solution of Heat Conduction Problems", Chem. Eng. Progress Symp. 52, 123 (1956).

(18) Roberts, D.K. and Wells, A.A. : "Fusion Welding of Aluminium Alloys", Pt. V "A Mathematical Examination of the Effect of Bounding Planes on the Temperature Distribution due to Welding", British Welding Journal, 553-560 (Dec. 1954).

(19) Davies, A.C. : "The Science and Practice of Welding", 6th ed. publ. Cambridge University Press.

(20) Myers, G.E. : "Analytical Methods in Conduction Heat Transfer", publ. McGraw Hill (1971).

(21) Artley, J. : "Fields and Configurations", publ. Holt, Rinehart and Winston.

(22) Carslaw, H.S. and Jaeger, J.C. : "Conduction of Heat in Solids", publ. Oxford University Press.

(23) Grosh, R.J. et al. : "Temperature Distribution in Solids of Variable Thermal Properties Heated by Moving Heat Sources", Quart. Appl. Math., 13(2), 161-167 (1955).

(24) Kazimirov, A.A. et al.: "Calculating the Distribution of Heat during the Butt Welding of Plates Allowing for the Effect of Temperature on their Physical Properties", Avt. Svarka, 11, 28-30 (1973).

LIST OF FIGURES AND TABLES

LIST OF PLATES

LIST OF ENGINEERING DRAWINGS

(contained at the end of the Thesis)

DRAWING 5.1 Assembly of Top Plate

DRAWING 5.2 Top Plate Assemblies

DRAWING 5.3 Blow Out Valve Layout

DRAWING 5.1 ASSEMBLY OF TOP PLATE

DRAWING NUMBER
3040269

DO NOT SCALE DRAWING
IF IN DOUBT - ASK

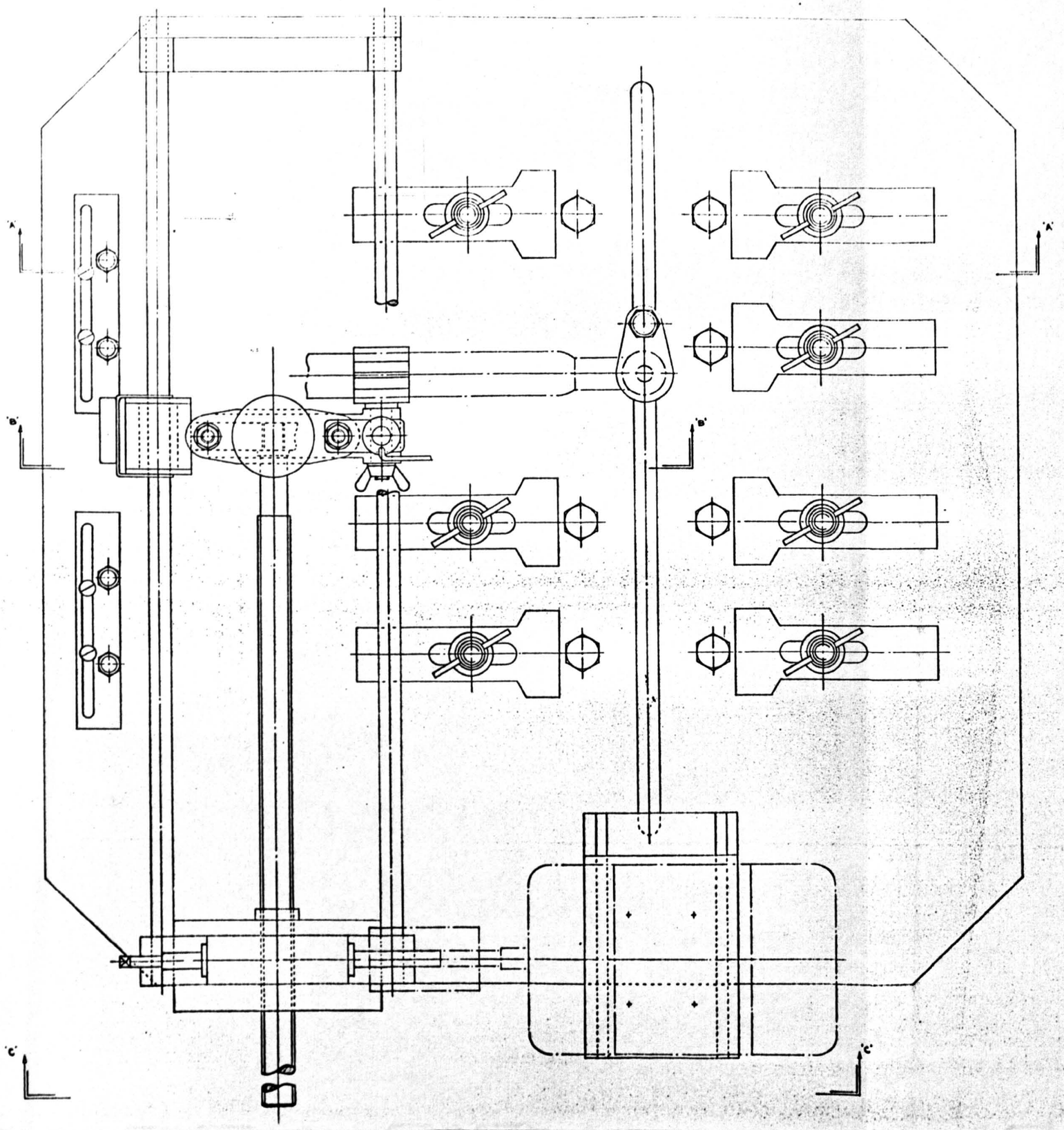

ITEM	No.OFF	DESCRIPTION	MATL.	REMARKS

UNIVERSITY GLASGOW
ENGINEERING LABORATORIES

TITLE OF DRAWING:- ASSEMBLY OF TOP PLATE.			
TITLE OF PROJECT:- WELDING TEST RIG.			
DEPARTMENT:- MECHANICS & MECHANISMS.			
PROJECT No.	COST No.	WHEN QUOTING DRWG. PLEASE QUOTE LETTER OF ISSUE	
		SCALE: FULL SIZE	
DRAWN BY	A. M.	3040269/B	
TRACED BY			
CHECKED BY			
APPROVED BY			
DATE DRAWN	6 3 75	No. OF SHEETS 3	SHEET No. 1

NOTE: THIS DRAWING IS A PRIVATE AND CONFIDENTIAL COMMUNICATION AND THE PROPERTY OF THE UNIVERSITY OF GLASGOW IT MUST NOT BE COPIED OR LOANED WITHOUT THE WRITTEN CONSENT OF THE UNIVERSITY AND MUST BE RETURNED IMMEDIATELY ON COMPLETION OF TENDER OR CONTRACT.

A ORIGINAL LETTER OF ISSUE

DIMENSIONS MUST NOT BE TAKEN OFF THIS DRAWING BUT FIGURED DIMENSIONS ONLY TO BE WORKED TO. FINISHED DIMENSION GIVEN IN ALL CASES. MACHINE SYMBOLS NAMED THUS:- ∛ MACHINE ∛ ROUGH MACHINE ∛ SMOOTH MACHINE ∛ GROUND FINISH

ALL UNTOLERANCED DIMENSIONS IN DECIMALS TO BE WITHIN THE FOLLOWING LIMITS:- HOLES AND INTERNAL SURFACES + .010" SHAFTS AND EXTERNAL SURFACES - .010" CENTRES OF HOLES AND CENTRES TO FACES + .005" PRACTICAL DIMENSIONS ± 1/64"

1 2 3 4 5 6 7 8 9 10 11 12 13 14 15 16 17 18 19 20 21

DRAWING 5.2 TOP PLATE ASSEMBLIES

3040269

DO NOT SCALE DRAWING
IF IN DOUBT - ASK

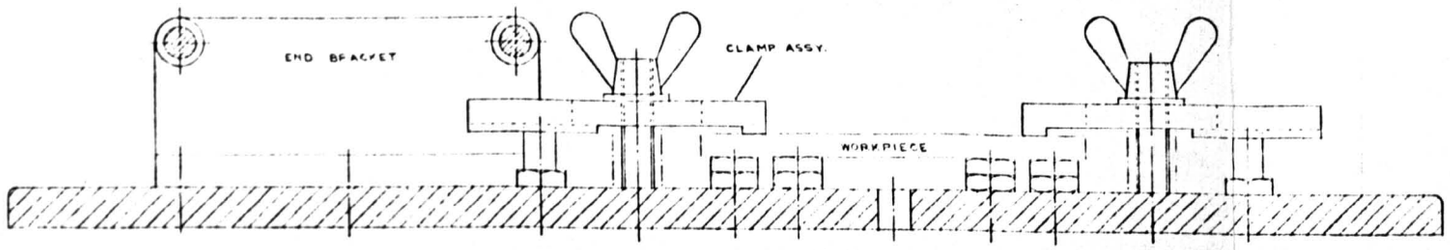

ELEVATION ON 'A-A'
SHOWING BRACKET & CLAMP ASSY.

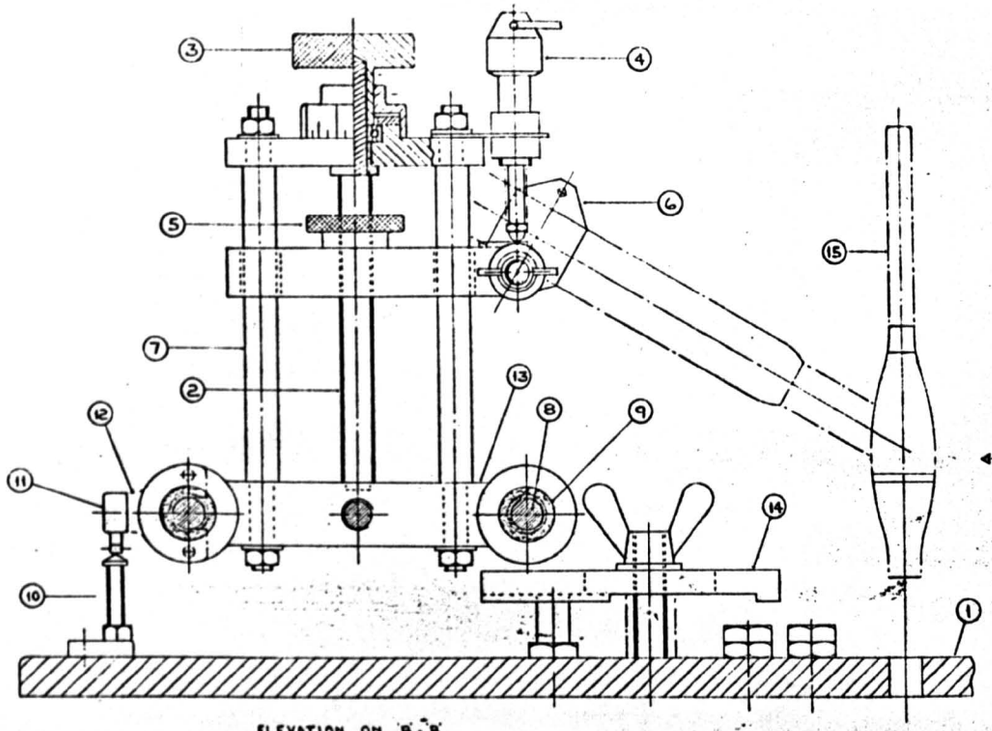

ELEVATION ON 'B-B'
SHOWING H.S.V. LEADSCREW ASSY.

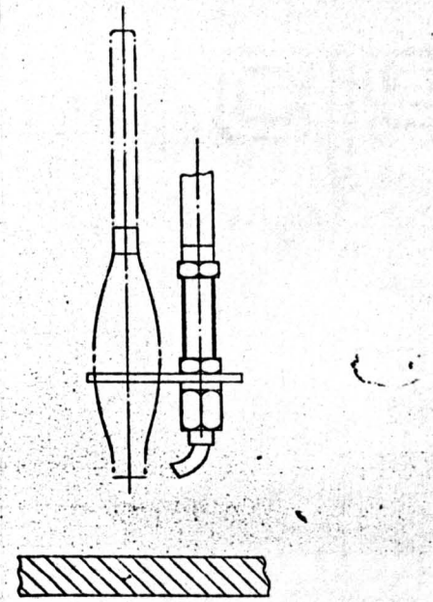

PART VIEW ON 'X'

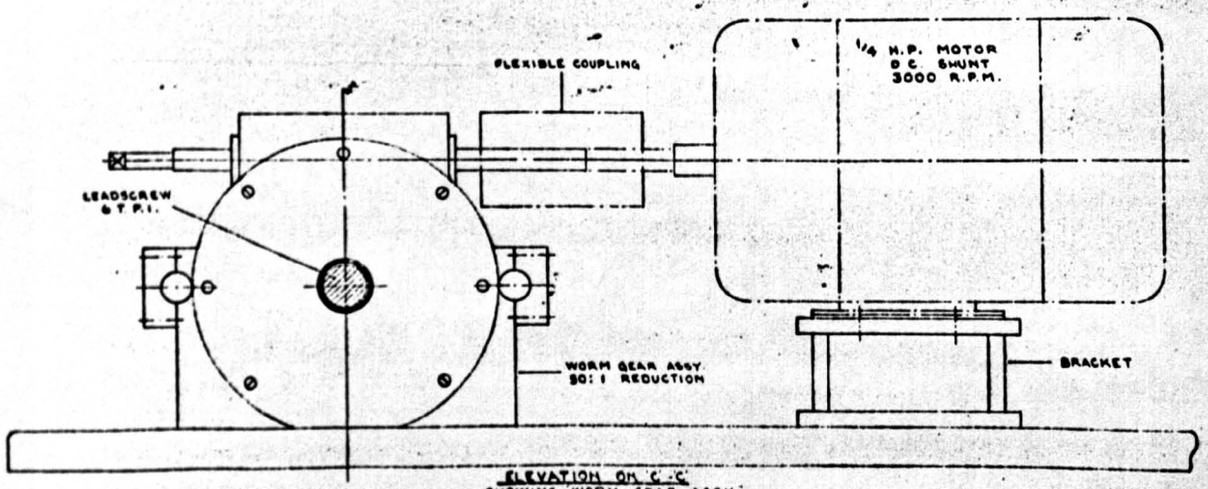

ELEVATION ON 'C-C'
SHOWING WORM GEAR ASSY.

ITEM	No.OFF	DESCRIPTION	MATL.	REMARKS
15		WELDING TORCH		
14		CLAMP ASSY.		
13		CROSSHEAD		
12		BRACKET		
11		ROLLER OPER MICRO-SWITCH		
10		ACTIVATING PIN		
9		LINEAR BALL BUSHING		
8		GUIDE ROD		
7		GUIDE ROD		
6		TORCH CLAMP ASSY		
5		LOCKNUT		
4		ARC HEIGHT DISPLACEMENT TRANSDUCER		
3		ADJUSTMENT SCREW ASSY.		
2		HEIGHT ADJ. SCREW		2 m m PITCH
1		BASEPLATE		

UNIVERSITY GLASGOW
ENGINEERING LABORATORIES

TITLE OF DRAWING:- TOP PLATE ASSEMBLIES.
TITLE OF PROJECT:- WELDING TEST RIG.
DEPARTMENT:- MECHANICS & MECHANISMS

PROJECT No.	COST No.	WHEN QUOTING DRWG. PLEASE QUOTE LETTER OF ISSUE
		SCALE: FULL SIZE
DRAWN BY	A.M.	
TRACED BY		3040269/B
CHECKED BY		
APPROVED BY		
DATE DRAWN	6.3.75	No. OF SHEETS 3 SHEET No. 2

NOTE: THIS DRAWING IS A PRIVATE AND CONFIDENTIAL COMMUNICATION AND THE PROPERTY OF THE UNIVERSITY OF GLASGOW IT MUST NOT BE COPIED OR LOANED WITHOUT THE WRITTEN CONSENT OF THE UNIVERSITY AND MUST BE RETURNED IMMEDIATELY ON COMPLETION OF TENDER OR CONTRACT.

A ORIGINAL LETTER OF ISSUE

DIMENSIONS MUST NOT BE TAKEN OFF THIS DRAWING BUT FIGURED DIMENSIONS ONLY TO BE WORKED TO. FINISHED DIMENSION GIVEN IN ALL CASES. MACHINE SPINDLES MARKED THUS:- √ MACHINE √ ROUGH MACHINE √ SMOOTH MACHINE √ GROUND FINISH

ALL UNTOLERANCED DIMENSIONS IN DECIMALS TO BE WITHIN THE FOLLOWING LIMITS:- HOLES AND INTERNAL SURFACES ± .010" SHAFTS AND EXTERNAL SURFACES ± .010" CENTRES OF HOLES AND CENTRES TO FACES ± .020" FRACTIONAL DIMENSIONS ± 1/64"

DRAWING 5.3 BLOW OUT VALVE LAYOUT

DRAWING NUMBER
3040269

DO NOT SCALE DRAWING
IF IN DOUBT—ASK.

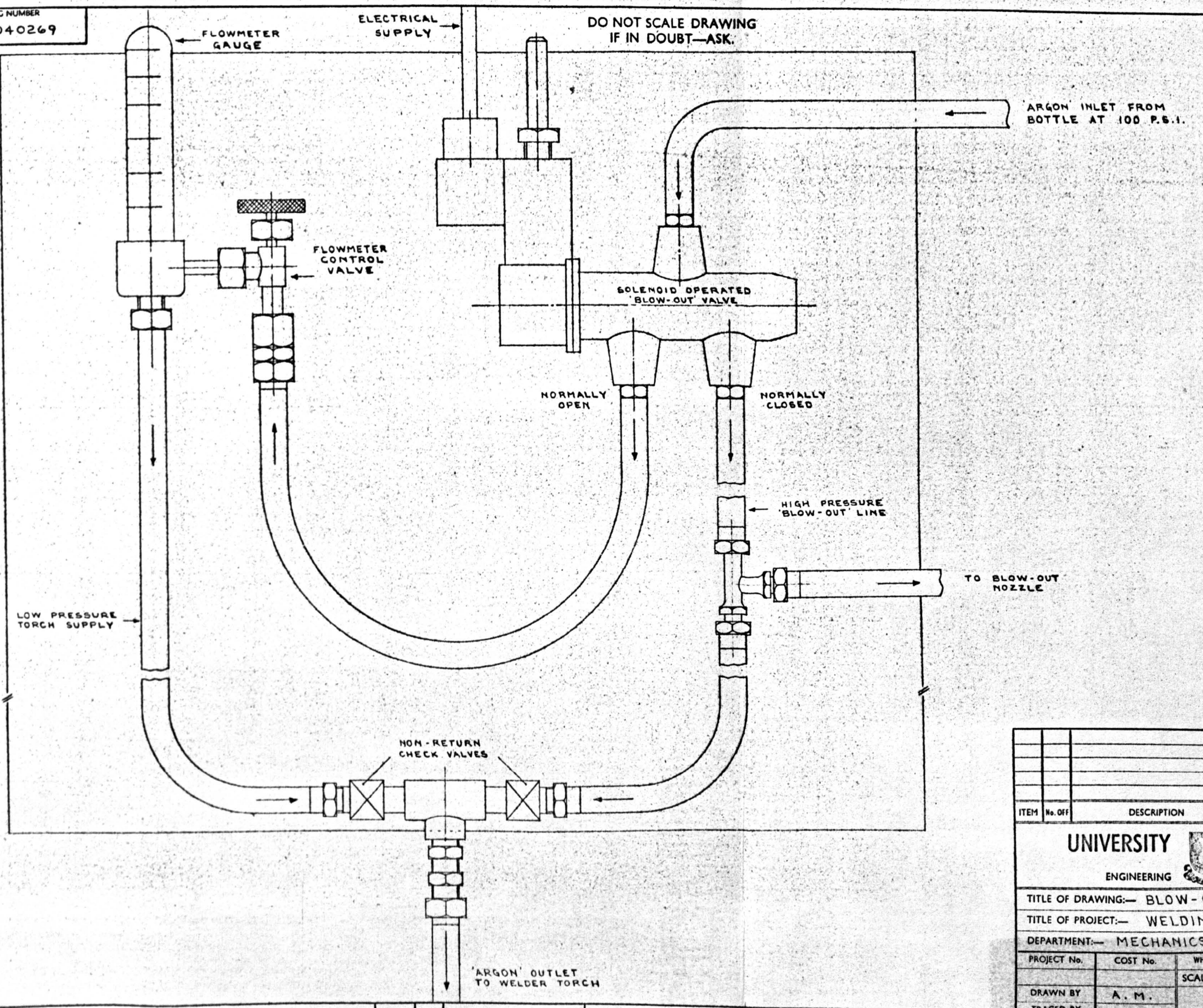

ITEM	No. OFF	DESCRIPTION	MATL.	REMARKS

UNIVERSITY GLASGOW
ENGINEERING LABORATORIES

TITLE OF DRAWING:— BLOW-OUT VALVE LAYOUT.
TITLE OF PROJECT:— WELDING TEST RIG.
DEPARTMENT:— MECHANICS & MECHANISMS.

PROJECT No.	COST No.	WHEN QUOTING DRWG. PLEASE QUOTE LETTER OF ISSUE
		SCALE:- FULL SIZE
DRAWN BY	A. M.	
TRACED BY		3040269/B
CHECKED BY		
APPROVED BY		
DATE DRAWN	6.3.75	No. OF SHEETS 3 / SHEET No. 3

A ORIGL LETTER OF ISSUE

DIMENSIONS MUST NOT BE TAKEN OFF THIS DRAWING BUT FIGURED DIMENSIONS ONLY TO BE WORKED TO FINISHED DIMENSIONS GIVEN IN ALL CASES.
MACHINE SYMBOLS MARKED THUS:-
√ MACHINE √ SMOOTH MACHINE
√ ROUGH MACHINE √ GROUND FINISH

ALL UNTOLERANCED DIMENSIONS IN DECIMALS TO BE WITHIN THE FOLLOWING LIMITS.
HOLES AND INTERNAL SURFACES + .010"
SHAFTS AND EXTERNAL SURFACES — .010"
CENTRES OF HOLES AND CENTRES TO FACE + .005"
FRACTIONAL DIMENSIONS + 1/64"